Patient-derived antibodies reveal the subcellular distribution and heterogeneous interactome of LGI1

Jorge Ramirez-Franco, Kévin Debreux, Johanna Extremet, Yves Maulet, Maya Belghazi, Claude Villard, Marion Sangiardi, Fahamoe Youssouf, Lara El Far, Christian Lévêque, et al.

Patient-derived antibodies reveal the subcellular distribution and heterogeneous interactome of LGI1

Jorge Ramirez-Franco, Kévin Debreux, Johanna Extremet, Yves Maulet, Maya Belghazi, Claude Villard, Marion Sangiardi, Fahamoe Youssouf, Lara El Far, Christian Lévêque, et al.

Patient-derived antibodies reveal the subcellular distribution and heterogeneous interactome of LGI1

Jorge Ramirez-Franco,[1,†] Kévin Debreux,[1,†] Johanna Extremet,[1] Yves Maulet,[1] Maya Belghazi,[2] Claude Villard,[2] Marion Sangiardi,[1] Fahamoe Youssouf,[1] Lara El Far,[1] Christian Lévêque,[1] Claire Debarnot,[3] Pascale Marchot,[3] Sofija Paneva,[4] Dominique Debanne,[1] Michael Russier,[1] Michael Seagar,[1] Sarosh R Irani,[4,5] & Oussama El Far[1]

[†]These authors contributed equally to this work.

Abstract

Autoantibodies against leucine-rich glioma-inactivated 1 occur in patients with encephalitis who present with frequent focal seizures and a pattern of amnesia consistent with focal hippocampal damage. To investigate whether the cellular and subcellular distribution of LGI1 may explain the localisation of these features, and hence gain broader insights into LGI1's neurobiology, we analysed the detailed localisation of LGI1, and the diversity of its protein interactome, in mouse brains using patients-derived recombinant monoclonal LGI1-antibodies. Combined immunofluorescence and mass spectrometry analyses showed that LGI1 is enriched in excitatory and inhibitory synaptic contact sites, most densely within CA3 regions of the hippocampus. LGI1 is secreted in both neuronal somatodendritic and axonal compartments, and occurs in oligodendrocytic, neuro-oligodendrocytic and astro-microglial protein complexes. Proteomic data support the presence of LGI1 / Kv1 / MAGUK complexes, but did not reveal LGI1 complexes with postsynaptic glutamate receptors. Our results extend our understanding of regional, cellular and subcellular LGI1 expression profiles and reveal novel LGI1-associated complexes, thus providing insights into the complex biology of LGI1 and its relationship to seizures and memory loss.

Author affiliations:

1 UMR 1072, INSERM, Unité de Neurobiologie des canaux Ioniques et de la Synapse, (UNIS) Aix-Marseille Université, 13015 Marseille, France

2 Aix-Marseille Univ, CNRS, Institute of Neurophysiopathology (INP), PINT, PFNT, 13385 Marseille cedex 5, France.

3 Lab 'Architecture et Fonction des Macromolécules Biologiques (AFMB)', CNRS, Aix-Marseille Université, 13288 Marseille cedex 09, France.
4 Oxford Autoimmune Neurology Group, Nuffield Department of Clinical Neurosciences, John Radcliffe Hospital, University of Oxford, Oxford, UK
5 Department of Neurology, Oxford University Hospitals, Oxford, UK

Correspondence to: Oussama El Far
Aix-Marseille University, INSERM,
UNIS, UMR_S 1072
51 Bvd Pierre Dramard
13015 Marseille
E-mail: oussama.el-far@inserm.fr

Running title: Distribution and interactome of LGI1

Keywords: Leucine-rich Glioma Inactivated 1 (LGI1); Auto-antibodies; Limbic Encephalitis; Autosomal-dominant lateral temporal lobe epilepsy (ADLTE); Kv1 channels

Abbreviations: ADLTE = Autosomal-dominant lateral temporal lobe epilepsy; AIS = axonal initial segment; DG = dentate gyrus DG; EPTP = Epitempin; GCL = Granule Cell Layer; LGI1 = Leucine-rich Glioma Inactivated 1; LRR= Leucine-rich repeat; MF = mossy fibres; SL = Stratum Lucidum; SO = Stratum Oriens; SP = Stratum Pyramidale; SR = Stratum Radiatum;

Introduction

LGI1 (Leucine-rich Glioma Inactivated 1) is a secreted glycoprotein predominantly expressed within neurons in the central nervous system. It is composed of an N-terminal leucine-rich repeat (LRR) and a C-terminal epitempin (EPTP) domains. Through the latter it interacts with the ectodomains of ADAM22, 23 and 11 which are catalytically-inactive members of the ADAM family of metalloproteases. [1-4] It has been suggested that LGI1 plays an essential role in the formation of a functional trans-synaptic complex linking presynaptic Kv1 channels to postsynaptic AMPA/NMDA receptors and PSD95 through interaction with ADAM 22/23 .[2,5,6,7]

LGI1 owes its name to its downregulated expression in malignant gliomas, its first involvement in a human disease.[8] Point mutations in LGI1, the majority of which lead to an inhibition of LGI1 secretion,[9-11] have been linked to inherited, autosomal-dominant lateral temporal lobe

epilepsy (ADLTE)[12,13] and neuronal hyperexcitability.[14-16] In ADLTE, the few secreted LGI1 mutants show impaired ADAM22 binding,[17,18] suggesting that hypofunction of the ADAM22-LGI1 interaction may account for the phenotype associated with these human LGI1 mutations.[7] In mice, LGI1 deletion results in lethal seizures accompanied by a reduction in the AMPA / NMDA receptor ratio and a decrease in AMPA receptor-mediated synaptic transmission.[5,6,19] However, whether these modifications account for the observed neuronal hyperexcitability is unclear.[14-16] We recently showed that downregulation of Kv1 channels in axonal initial segments (AIS) may also contribute to epileptogenesis in *Lgi1*$^{-/-}$ mice, through an increase in the intrinsic excitability of CA3 neurons,[20] and suggested that the decrease in AMPA receptors may be a consequence of neuronal hyperexcitability. Furthermore, hypomyelination[21] and alterations in dendritic pruning and spine development[16,22] have been described in *Lgi1*$^{-/-}$ mice. More recently, a novel missense LGI1 mutation was shown to impair oligodendrocyte differentiation and induce white matter abnormalities.[23] Collectively, these findings suggest that LGI1 is differentially involved at distinct developmental stages, in a cell and context-specific manner.[24]

The link between LGI1 and Kv1 channels has been supported by immunoprecipitation studies using anti Kv1.2 antibodies[25] and human LGI1-autoantibodies.[26-28] Upon passive transfer to rodents, LGI1 antibodies modulate both Kv1 function and expression and AMPAR function, akin to genetic paradigms.[29,30] Furthermore, when administrated in animal models, these antibodies reproduce key cognitive features of the patients from which they were derived – namely a marked, and partially reversible amnesia likely related to the CA3-predominant, hippocampal damage observed in patients with LGI1-antibody encephalitis[29,31-33].

Throughout these studies, examining the role of native LGI1 has been challenging, partly because available commercial and custom made LGI1-antibodies are of poor quality[15,34,35] and rarely validated on knockout tissues. Thus, they represent unreliable tools to define the native LGI1 interactome or its brain distribution. To date, the search for native partners of LGI1 has been addressed using recombinant, tagged LGI1 either by incubating it with brain extracts[36] or by generating knock-in mice.[5] These approaches have shown an association of LGI1 with synapse-related protein complexes. Also, aspects of LGI1 neurobiology have been partially addressed in dissociated hippocampal cultures[37] but not in structured tissues such as organotypic slices. Furthermore, different methodological approaches have resulted in contradictory results regarding LGI1's expression pattern. For example, using GFP-expressing cells under the control of a cis-regulatory element of LGI1 in mice, a widespread distribution

of LGI1 from embryonic to late postnatal stages has been determined.[34,38] Whereas, analysis of mRNA distribution in adult mice brains, and other approaches, showed that LGI1 is highly enriched in the hippocampal circuitry with strong expression in CA3 and the dentate gyrus (DG).[39-41]

The most accurate and specific staining of native LGI1 to date has been achieved using patient-derived LGI1-antibodies, which are directly pathogenic *in vivo*.[27,29,42] However, these studies mainly addressed regional LGI1 distribution and did not focus on potential enrichment in subcellular domains and pre- or post-synaptic processes.

Recently, we isolated and characterized several monoclonal antibodies from two patients with LGI1-antibody encephalitis, which targeted either its native LRR or EPTP domains[30]. In the present study, we used these patient-derived domain-specific monoclonal-antibodies along with WT and *Lgi1*$^{-/-}$ animal tissues, as well as exogenously expressed fluorescent LGI1, to characterize, in the murine hippocampus, the detailed subcellular distribution and secretion pattern of LGI1. Furthermore, by immunoprecipitation and mass spectrometry from WT and *Lgi1*$^{-/-}$ brain extracts, we identified a series of distinct molecular complexes which constitute the native LGI1 interactome. Our findings reconcile a large number of contradictory findings concerning the functional consequences of LGI1 depletion and offer insights into the localisation and function of this enigmatic protein, whose dysfunction is increasingly implicated in human diseases.

Materials and methods

Methods are described below, briefly. Further details are available online as Electronic Supplementary Materials.

Plasmids

A smaller version (pIND-IRES-EGFP) of the pINDUCER11 (miR-RUG) plasmid[43] was first generated and pIND-LGI1-IRES-EGFP and pIND-ΔIRES-Dendra2-LGI1 were constructed as described in the Electronic Supplementary Materials.

LGI1 knock-out mice

Heterozygous *Lgi1*$^{+/-}$ mice[41] were inter-crossed to generate *Lgi1*$^{-/-}$ and *Lgi1*$^{+/+}$ littermates. All experiments were carried out according to the European and Institutional guidelines for the care

and use of laboratory animals (Council Directive 86/609/EEC and French National Research Council) and were approved by the local animal health authority (# D 13 055 08, Préfecture des Bouches-du-Rhône, Marseille). This study does not involve experiments on live animals.

Antibodies

A set of recombinant monoclonal anti-IgG IgGs consisting in three LRR-directed (herein referred to as LRR1-3; mAb01, 02 and 07 respectively in Ramberger et al.[30]) and two non-previously described EPTP-directed (referred to as EPTP1-2) was generated from two encephalitis patients, as previously described.[30] Two LRR-directed (LRR1 and 2) mAbs were previously found to cross-compete (Group 1 in Ramberger et al.); LRR3 is from Group 2.[30] In contrast to EPTP2, EPTP1 recognized the surface of live hippocampal neurons although more weakly than LRR antibodies. Other antibodies used in this study are described in Electronic Supplementary Materials.

Surface Plasmon Resonance

Using a Biacore T200 and a CM5_sensor chip (Cytiva), purified His-tagged recombinant LGI1[20] (about 1-2 fmoles) was captured on covalently coupled EPTP2. EPTP1, EPTP2, LRR1, or healthy control (HC) human IgGs were then injected at 1 µl/min for 5 min at different concentrations. Background signals were subtracted from flow cells in which irrelevant human IgGs were immobilized.

Immunohistofluorescence of fixed brains

P14-P16 C57BL/6 wild-type mice or *Lgi1*$^{-/-}$ littermates of either sex were used and prepared as described in the Electronic Supplementary Materials.

Hippocampal slice cultures and transfection of hippocampal neurons

Hippocampal organotypic slices were prepared as previously described.[44] Details and the transfection procedure are described in the Electronic Supplementary Materials.

Immunofluorescence of organotypic slices and image analysis

For the immunolabeling of organotypic slices, we adapted the protocol described in.[45] Images were analyzed with ImageJ (NIH). Details are described in the Electronic Supplementary Materials.

Statistics

Statistical analysis was performed with Origin 8.0 and the specific test is indicated in the figure legends. One-way ANOVA followed by Bonferroni's post-hoc test was used for multiple comparisons. Comparisons were considered significant when p-value<0.05. Figures were prepared for presentation using Adobe Illustrator.

Immunoprecipitations

Wild type and *Lgi1*$^{-/-}$ brains were extracted, snap-frozen in liquid nitrogen and kept at -80°C until use. Brains were homogenised in HB buffer (20 mM NaP pH 7.4, 30 mM NaCl containing phosphatase inhibitors (Pierce^{TM}) and protease inhibitors (Complete, Roche Diagnostics GmbH)). Each brain was homogenised using 1 ml of HB and nuclei were eliminated by 900 x g centrifugation. Supernatants were solubilized in HB supplemented with 1% CHAPS at 5 mg/ml and subjected to 100.000 x g ultracentrifugation. The solubilised material from both wildtype and LGI1 knockout samples were precleared with rProtein A Sepharose Fast Flow (Cytiva) and immunoprecipitated in triplicates using the human autoimmune IgGs (LRR1; LRR3, EPTP1; EPTP2) (3-5 µg / immunoprecipitated sample). Immunoprecipitated samples were washed three times with HB containing 0.5% CHAPS before denaturation. Samples were then analysed either by SDS-PAGE and Western blot or by mass spectrometry.

Mass spectrometry analysis and data processing

Samples were analyzed by mass spectrometry using a hybrid Q-Orbitrap mass spectrometer as described in[44] (Q-Exactive, Thermo Fisher Scientific, United States) coupled to a nanoliquid chromatography (LC) Dionex RSLC Ultimate 3000 system (Thermo Fisher Scientific, United States). For details see the Electronic Supplementary Materials.

Data availability

Data supporting this manuscript are available in the Electronic Supplementary Materials. Mass spectrometry proteomics data have been deposited in the ProteomeXchange Consortium

(http://proteomecentral.proteomexchange.org) via the PRIDE partner repository[46] with the dataset identifier PXD032712.

Results

Native LGI1 distribution in mouse brain

To characterize the expression pattern of native LGI1 in mice brain, we used three patient-derived LRR-directed antibodies of which two are competing (LRR1 & LRR2).[30] Similar to mRNA distribution,[39] immunofluorescence in coronal telencephalic slices revealed equivalent staining patterns with all three LRR-antibodies which was abrogated in *Lgi1*$^{-/-}$ sections (Supplementary Fig. 1A-B). LGI1 expression intensities, displayed as a Look Up Table (LUT) for each antibody and normalized to hippocampal levels, showed that LGI1 is most concentrated in the hippocampus and caudate-putamen complex, with far lower expression intensities in other cortical regions and basal ganglia / diencephalic regions (Supplementary Fig. 1B-C). An intra-hippocampal, analysis showed ~50% less LGI1 expression in ventral versus dorsal CA3 (Fig. 1A and B)**.** Further analysis of sub-regional distribution of LGI1 in the dorsal hippocampus revealed its prominent expression in CA1, CA3 and DG but barely detectable levels in the Stratum Pyramidale (SP) and Granule Cell Layer (GCL) (Fig 1). Normalized immunoreactivity (Fig. 1B-E) shows a pattern of dorsal expression where CA3 = DG > CA1, with the highest LGI1 density found at the level of the CA3 stratum radiatum (CA3_SR), where afferents from contralateral CA3 and recurrent collaterals of ipsilateral CA3 pyramidal neurons establish synapses with the distal apical dendrites of CA3 pyramidal neurons. Among the three main CA3 strata, LGI1 expression was lower in CA3 Stratum Lucidum (CA3_SL) where mossy fibres (MF) meet the proximal apical dendrites and thorny excrescences of CA3 pyramidal neurons. Furthermore, these differential regional expression levels were also observed when the punctate LGI1 cluster densities were studied (Fig. 1D, F), with significantly higher cluster densities in CA3_SR and DG ML versus CA1 subsectors.

A closer observation of the stratum oriens (SO) of both CA1 and CA3, as well as the DG granule cell layer, showed that LGI1 clusters are often attached to ankyrin-G-dense axonal initial segments (AIS) (Fig. 2). This is well-demonstrated in the three-dimensional reconstruction of AIS (Fig. 2B) with a CA3 >DG > CA1 gradient of LGI1 expression (Fig. 2C). In order to address whether LGI1 staining in CA3_SL and CA3_SR corresponded to postsynaptic dendritic staining of CA3 pyramidal neurons or to presynaptically expressed LGI1, we co-stained both

LGI1 and the presynaptic synaptic vesicle marker synaptophysin. Partial colocalization between LGI1 and synaptophysin was observed in all hippocampal strata (Supplementary Fig. 2) with a slight but significant reduction of this colocalization seen in CA3_SL when compared to CA3_SR or DG_ML (Supplementary Fig. 2B). The strong immunoreactivity of CA3_SR and the partial co-localization with synaptophysin suggest LGI1 staining in the CA3_SR is, at least partially, attributable to the dendritic expression of LGI1 in CA3 pyramidal cells. Therefore, we evaluated the colocalization of LGI1 with the postsynaptic marker PSD93 in CA1, CA3 and DG layers. As shown in Supplementary Figs 2A and 3A, Manders' overlap coefficients (Supplementary Fig. 2B and 3B) indicate a limited however more prominent LGI1::PSD93 colocalization index compared to LGI1::synaptophysin. This finding corroborates the presence of a significant postsynaptic LGI1 pool.

Astrocytic expression of LGI1

While LGI1 has been almost exclusively considered as a trans-synaptic protein, it was first described in astrocytic gliomas. Also, strong LGI1 mRNA expression was reported in astrocytes (The human protein atlas database; www.proteinatlas.org). Therefore, we investigated the expression of LGI1 in hippocampal astrocytes with a focus on the CA3 hippocampal subregion (Fig. 3A and B). As shown in Fig. 3A (CA3) and B (CA3_SO), GFAP-expressing astrocytes in CA3 mainly populate CA3_SO and CA3_SR and, consequently, are present in the CA3 strata enriched for LGI1. Given the widespread punctate staining of LGI1 in all CA3 strata, maximal projections of the z-stacks required to fully cover the span of astrocytes (>20 optical slices; 0.38 µm/slice) were inappropriate to resolve the precise localization of LGI1 within astrocytic processes (Fig. 3C, top). Reduced z-stacks (3 optical slices which focus on the span of specific astrocytic processes) show LGI1 immunoreactive puncta that can be ascribed to some of the single astrocytic processes (Fig. 3C, bottom). Also, AnkG co-staining showed occasional astrocytic juxtaposition to the AIS of CA3 pyramidal neurons, forming astrocyte-AIS contact points (Figs. 3B and D). While its sporadic nature ruled out a detailed quantitative analysis, in the CA3_SO, LGI1 was consistently observed at astrocytes-AIS contact points (Fig. 3E and F).

Subcellular distribution of secreted LGI1

To observe LGI1 secretion from neurons, we transfected by Gene Gun rat hippocampal organotypic slices with Dendra2-fused LGI1 (D2::LGI1), and used an anti-dendra2 antibody to visualise intracellular and secreted LGI1 5-7 days post-transfection (Fig. 4A). LGI1 was observed across neuronal arborisations (Fig. 4B), including the axon, AIS and dendrites of the

CA1 (Fig. 4C), CA3 (Fig. 4D) and DG (Fig. 4E) transfected neurons. In the DG, a differential subregional expression was observed within dendrites ≥ AIS > axon (Fig. 4E). The AIS LGI1 punctae were often observed in AnkG gap-like microdomains (Fig. 4F), previously shown to express GABAaα2 receptor clusters at axo-axonal synapses.[47,48] Indeed, we also identified GABAaα2 subunits adjacent to LGI1 (Fig. 4G).

Next, as Gene Gun transfection can be stochastic, we electroporated D2-tagged (D2::LGI1) LGI1 into selected CA3 pyramidal neurons in organotypic slices to dissect LGI1 distribution versus secretion in CA3 neurons. The identical appearances of D2::LGI1 distribution in mice and rat cultures (Supplementary Fig. 4) justified use of this system to profile secreted D2::LGI1 by applying anti-dendra antibodies to live cultures before fixation. As shown in Fig. 5B, this procedure robustly labelled punctae of secreted LGI1 surrounding the electroporated neuron, around the cell body, proximal apical dendrites, the AIS and a distal axonal region of the transfected neurons (Fig. 5C). Several D2::LGI clusters colocalized with PSD93 at the AIS of transfected neurons (Fig. 6 and Supplementary Fig. 5), as well as in thorny excrescences and proximal apical dendrites of CA3 pyramidal neurons (Supplementary Fig. 5). Colocalisation of secreted D2::LGI1 with PSD93 was similar in all analysed regions of the transfected neurons (Fig. 6C, D).

To confirm the specificity of this distribution, we electroporated and followed untagged LGI1 immunostaining in *Lgi1*$^{-/-}$ slices, using LRR1. The observed subcellular distribution of LGI1 closely resembled that of D2::LGI1 (Fig. 7, inset 1) with LGI1 clusters colocalized with AnkG in the AIS, and also in dendritic branches and at the tip of individual dendritic spines (Fig. 7, Inset 2). These findings confirm an important cis-enrichment of LGI1 in dendrites and postsynaptic compartments.

LGI1-associated proteome

In order to identify protein complexes in which native LGI1 is expressed and, at the molecular level, address the potential heterogeneity in LGI1-associated protein complexes suggested by its immunolocalization, we performed immunoprecipitation and mass spectrometry analysis of wild type and *Lgi1*$^{-/-}$ rodent brain homogenates using the non-competing antibodies (LRR1 & 3[30]) and also EPTP1 & 2. EPTP1 & 2 specifically recognized the LGI1-EPTP domain (Supplementary Fig. 6 A, B, C) through non-overlapping epitopes (Supplementary Fig. 6 D). Full string networks for the LGI1 interactome associated with all antibodies were generated using string-db.org and are represented in Supplementary Figs. 8, 9, 10, 11 & 12. As expected,

LGI1 was efficiently recovered by all antibodies (Fig. 8 and Spreadsheet). Each antibody showed a specific interactome (Fig. 8, Supplementary Table 1 and Spreadsheet) with common partners immunoprecipitated by either two (Supplementary Table 2) or three different antibodies (Supplementary Table 3). Our data confirm the presence of several previously reported proteins such as ADAM proteins, pre and postsynaptic scaffolds as well as potassium channel subunits[5,36,49] and uncovers several novel partnerships, showing the existence of different LGI1 complexes selectively identified by different patient-derived antibodies. These partners are principally neuronal but glial-associated proteins were also identified and their subcellular distributions are presented hereafter within a cell-specific context.

Neurons: axonal, dendritic and synaptic

Our immunofluorescence results indicate that LGI1 is not targeted to a specific neuronal compartment, however its significant colocalization with PSD93 suggests a relative enrichment at synaptic contact sites. Besides previously recognized partners such as ADAM11, 22 and 23, Kv1 channel subunits and pre/post-synaptic MAGUKs, LRR3 immunoprecipitated the calcium-dependent phospholipid-binding protein annexin 2 (ANXA2) that is known to be associated, in GABAergic interneurons,[50] with the extracellular leaflet of plasma membranes at cell-cell contact sites.[51] LRR1 also recognised LGI1-associated complexes in axon-terminals, since it efficiently immunoprecipitated neuromodulin (GAP43). This palmitoylated phosphoprotein is involved in synaptic function modulation[52] and is enriched in axon terminals, where it regulates actin cytoskeleton dynamics and participates in signalling pathways by promoting $PI(_{4.5})P_2$ clustering in cholesterol rich domains.[53] Presynaptic complexes were highlighted by the efficient immunoprecipitation by EPTP1 of the effector protein rabphilin-3A, the presynaptic CASK-binding scaffolding proteins Lin7A (Veli1) and 7C (Veli3). A unique link with G-protein signalling is also highlighted by this antibody since it co-immunoprecipitated LANC2 (LanC-like protein 2), a myristoylated peripheral phosphoinositide-phosphate binding protein that activates adenylate cyclase through interaction with G-proteins.[54] The strong staining of LGI1 in dendritic structures is corroborated by a significant association with neurogranin and with several postsynaptic scaffold proteins such as PSD93, PSD95, SAP97 and SAP102 (Supplementary Table 3, Supplementary Fig. 7 and Spreadsheet). The postsynaptic MTAP2 as well as the axonal STOP protein MAP6[55] were also

efficiently retained by LRR1, LRR3 and EPTP1 confirming the immunofluorescent identification of LGI1 in stable dendritic and axonal compartments.

Cytoskeletal

Immunoprecipitation of microtubule-associated proteins (LRR1, LRR3 and EPTP1) (Fig. 8 and Supplementary Table 3), tubulins (LRR1 and EPTP1) (Supplementary Table 2) and the axonal marker tau (EPTP1) (Supplementary Table 1 and Spreadsheet) as well as the cytoskeletal GTPase Septin-11 show that, although intra-vesicular, LGI1 coimmunoprecipitates with cytoskeletal proteins most likely via vesicle membrane-partners.[56]

Axo-glial junctions

EPTP antibodies selectively captured potential juxtaparanodal protein complexes. EPTP1 immunoprecipitated contactin 1 (CNTN1), TAG1 (CNTN2) and Caspr2 (CNTNAP2) while EPTP2 coimmunoprecipitated only CNTN1.

Neurons: vesicular trafficking

LRR1, LRR3 and EPTP1 highlighted common and distinct links of LGI1 to vesicular trafficking pathways. While LRR1 co-immunoprecipitated Rab3a, an effector of exocytosis implicated in fine tuning synaptic vesicle release and synaptic plasticity,[57,58] LRR3 was associated with synaptic vesicle glycoprotein 2A (SV2A) known to be particularly involved in GABAergic synaptic transmission.[59] EPTP1 was the only IgG that enriched VAPA, (Vesicle-associated membrane protein-associated protein A. This protein mediates ER / plasma membrane contact sites[60] through its interaction with oxysterol-binding protein-related protein 3 and is involved in several cellular functions such as lipid transport, Kv2 exocytosis, membrane trafficking and microtubule reorganisation.[61] AP2 complex subunits as well as syntaxin1 and synaptotagmin1 were co-immunoprecipitated by several antibodies (Supplementary Table 2).

Kinases and other enzymes

Alongside the neuron-specific PKCγ (KPCG)[62] immunoprecipitated by LRR1, LRR3 and EPTP1 (Supplementary Table 3), several kinases such as casein kinase 1ε, 1δ, doublecortin-

like kinase 1 (DCLK1) and other enzymes were also immunoprecipitated by different LGI1 antibodies (Supplementary Tables 1, 2 & 3). This is in line with the fact that several phosphorylation pathways are involved in Kv1 targeting[63] and that Kv1 expression is perturbed in *Lgi1*$^{-/-}$ mice.

Rafts

Despite the diversity of the observed protein complexes, all antibodies recovered proteins previously described as part of the lipid raft proteome[64] (Supplementary Tables 1, 2 and 3). LRR1, 3 and EPTP2 recovered a considerable amount of the antiporter ADP/ATP translocase 2 (ADT2 / SLC25A5), a master regulator of mitochondrial energy enriched in microglia and endothelial cells.[65] LRR1 immunoprecipitated neuromodulin (GAP-43), a major component of growth cones involved in long term potentiation and synaptic function.[52] Other proteins enriched in lipid rafts were immunoprecipitated by several antibodies like tubulin beta subunits, microtubule associated protein 1A as well as the Na/K ATPase subunit α1 and the ATP synthase β subunit of the mitochondrial ATP synthase (Spreadsheet). Other lipid raft-enriched partners with specific characteristics are mentioned within the corresponding compartmental classification.

Oligodendrocytes

All LGI1-antibodies immunoprecipitated proteins known to be part of the myelin proteome[66] (Spreadsheet and Supplementary Tables 1, 2 & 3). LRR1, LRR3 and EPTP1 uncovered a strong and specific enrichment of CN37 (2',3'-cyclic-nucleotide 3'-phosphodiesterase), a marker for non-myelinating oligodendrocytes[67,68] (Supplementary Table 3). LRR1 selectively captured Bcas1, which defines an oligodendrocytic population involved in active myelin formation.[69] EPTP1 also enriched tubulin polymerization-promoting protein (TPPP), a crucial actor in myelin sheath elongation in oligodendrocytes.[70]

Astrocytes

A limited number of partners suggesting an astrocytic association were recovered. EPTP1 immunoprecipitated the astrocytic excitatory amino acid transporters EAA1 (GLAST-1) and

EAA2 (GLT-1) and LRR3 specifically immunoprecipitated Glutathione S-transferase Mu 1 (GSTM1) implicated in proinflammatory astrocyte-microglia communication.[71]

Other

Partly because of their ubiquitous expression, the enrichment of some proteins was not straightforward to interpret. Alpha-enolase (ENOA1), stratifin (14-3-3 S) and peptidyl-prolyl cis-trans isomerase B (PPIB) were recovered by LRR3 and the mitochondrial proteins creatine kinase KCRU and amino acid transporter GHC1 (Slc25a22) were recovered by EPTP2 and LRR1 respectively (Fig. 8 and Supplementary Table 1). It is interesting however to mention that 14-3-3 proteins were reported to stabilize LGI1/ADAM22 interaction[72] and that ENO1 was recently shown to protect against cerebral ischemia-induced neuronal injury.[73] Although specific, the co-association of the plasma membrane calcium-transporting ATPase2 (AT2B2) is very weak and awaits further confirmation.

Discussion

In this study, we used a set of recombinant LGI1-autoantibodies, derived from two patients with LGI1-antibody encephalitis, to address the precise localisation of native LGI1 and its interactome. Our immunofluorescent and immunoprecipitation data converge, expanding the known synaptic localisation of LGI1 to include somatodendritic and axonal subcellular localisations and to highlight diverse oligodendrocytic, neuro-oligodendrocytic and astro-microglial complexes containing LGI1. These, and the cytoskeletal, vesicular, enzyme and membrane raft-enriched proteins complexed with LGI1, provide focussed pathways to study LGI1's functions in basic neurobiology and in the context of multiple human diseases.

Three LRR-antibodies (LRR1, LRR2 and LRR3) were used on fixed brain or organotypic slices to investigate the detailed distribution of native LGI1 throughout mice forebrain and hippocampal structures, and to follow its secretion profile. Both LRR- and EPTP-antibodies were used to dissect the composition of LGI1-associated protein complexes. Two of the three antibodies (LRR1 and 2) used for immunostaining have overlapping epitopes [30] which do not overlap with LRR3. All three antibodies generated very similar signals and were specific with respect to not staining *Lgi1*$^{-/-}$ tissue. We found that LGI1 is differentially expressed in brain regions with sub-regional profiles that correlate with observed dysregulations in LGI1-antibody limbic encephalitis patients. These include the relatively prominent atrophy of CA3 subfield in these patients (although all hippocampal subfields are also reported as reduced). [31,32,74,75];

abnormal caudate and putamen imaging often observed in the ~60% of LGI1-antibody patients displaying faciobrachial dystonic seizures; and the serum hyponatraemia which may relate to dysregulation of hypothalamic structures.[76,77]

LGI1 is predominantly expressed in hippocampus, thalamus and hypothalamus with a lower expression in the cortical and subcortical regions. In the hippocampus, the CA3 and the DG were the most intensely labelled regions and LGI1 was equally distributed in somatodendritic and axonal projections. Interestingly, normalized immunoreactivities indicated that the CA3_SR was the most intensely labelled zone. This region is highly interconnected, receiving perforant-path inputs. Mossy fibers synapse onto local inhibitory interneurons in CA3_SR and onto the proximal apical dendrites of excitatory pyramidal cells at thorny excrescences in CA3_SL. Of note, all hippocampal subfields as well as the subiculum were shown to be atrophied in patients with anti-LGI1 encephalitis.[74,75] In CA1, CA3 and DG, LGI1 immunoreactive puncta were highly enriched at axonal initial segments (AIS), and partially overlapped with the synaptic vesicle marker synaptophysin. The presence of LGI1 at the AIS is in agreement with the observed increase in intrinsic excitability in *Lgi1* $^{-/-}$ mice.[14,20,78] Also, the presynaptic effects in *Lgi1*$^{-/-}$ mice[14,15] or in an LGI1 secretion mutant[16] are in agreement with the observed presynaptic expression and immunoprecipitated complexes. Although pre- and postsynaptic effects in *Lgi1*$^{-/-}$ mice have been reported,[14] exclusive pre- or postsynaptic effects have also been described. Reported postsynaptic effects in *Lgi1*$^{-/-}$ mice[5,6,42] are in agreement with the dendritic expression of this protein and the presence of postsynaptic LGI1-associated protein complexes. Considering the prominent expression of LGI1 in the DG, the reduced staining of LGI1 in CA3_SL and its limited co-localization with synaptophysin, our data imply LGI1 is not solely enriched in mossy fibres from the granule cells but may have a major postsynaptic localisation. We corroborated this by showing a significant colocalization with the postsynaptic marker PSD93.

LGI1 association with vesicular trafficking pathways and the enrichment of VAPA by EPTP1 as well as the presence of LGI1 at Ankyrin G deficient regions adjacent to GABAα2 clusters at the AIS suggest that LGI1 may be important in the organization and dynamics of neuronal signalling pathways[47] that contribute to control of AIS excitability. LRR1, LRR3 and EPTP1 immunoprecipitation profiles highlighted common and distinct links of LGI1 to vesicular trafficking pathways. While LRR1 co-immunoprecipitated Rab3a, an effector of exocytosis implicated in fine tuning synaptic vesicle release and synaptic plasticity, LRR3 was associated with synaptic vesicle glycoprotein 2A (SV2A) known to be particularly involved in GABAergic

synaptic transmission. EPTP1 was the only IgG that enriched VAPA, (Vesicle-associated membrane protein-associated protein A. This protein mediates ER / plasma membrane contact sites through its interaction with oxysterol-binding protein-related protein 3 and is involved in several cellular functions such as lipid transport, Kv2 exocytosis, membrane trafficking and microtubule reorganisation. AP2 complex subunits as well as syntaxin1 and synaptotagmin1 were co-immunoprecipitated by several LGI1 antibodies (Supplementary Table 2).

Fluorescent recombinant LGI1 transfection in CA3 pyramidal neurons allowed us to address its secretion profile. LGI1 did not show preferential exocytic sites and was found to be similarly secreted from axonal and somatodendritic regions. Of note, in addition to its expression at the AIS, somatodendritic expression of LGI1 was also reported in mature cultured hippocampal neurons.[37] The diffuse distribution of LGI1 in native tissue suggests that depending on its localisation, LGI1 participates in multiple distinct functional protein complexes and that its role may not be restricted to trans-synaptic complexes. While no major structural changes in neurons were identified in *Lgi1* $^{-/-}$ mice,[15] an increase in dendritic arborization and a decrease in dendritic pruning were reported.[16] However, no aberrant dendritic sprouting or synaptic pruning defects were observed in mice infused with anti-LGI1.[29] This may indicate that despite traces of neuronal damage in LGI1-dependent limbic encephalitis patients,[79] either some LGI1 protein complexes are not accessible to patient-derived autoantibodies or that despite the presence of antibodies, LGI1 molecules are still able to modulate dendritic pruning. Also, LGI1 involvement in dendritic sprouting and synaptic pruning may be purely developmental and thus not observed during antibody application in mature animals.

In contrast to previous reports of relatively restricted LGI1-associated complexes,[5,36] mass spectrometry analysis of immunoprecipitated proteins uncovered an intriguingly rich and complex LGI1 interactome, which converged on specific cell types and pathways. Together with GFAP co-labelling, the presence of LGI1 (of neuronal or astrocytic origin) at neuron-astrocyte contact points and the enrichment of juxtaparanodal protein complexes (contactin1, TAG1 and Caspr2) with some LGI1-antibodies, may have functional implications for its role in glial biology.[80,81] Although we cannot conclude that LGI1 is systematically enriched in hippocampal astrocytes, some astrocytic processes clearly show the presence of immunoreactive LGI1 clusters. It is tempting to hypothesize that EPTP1 may recognize LGI1-associated complexes in non-neuronal cells. These complexes may offer EPTP1 epitope accessibility through the previously described multimeric LGI1 complexes.[1] An interaction of LGI1 with astrocytic cell adhesion molecules[82] cannot be excluded and needs further

investigation. The neuronal and oligodendrocytic GPI-anchored TAG1 is a crucial determinant of axo-glial interactions[83] and is involved in Caspr2 and Kv1 channel complexes at juxtaparanodes.[84] It is also enriched with Kv1.2 in the axonal initial segment.[85] The single transmembrane domain protein Caspr2 is an axonal protein that interacts extracellularly with TAG1 and binds MPP2 and CASK[86] that were co-immunoprecipitated in this study. These observations may concur with phenotypic overlaps observed in patients who have Caspr2-directed antibodies[87] and provide a molecular link to hypomyelination reported in *Lgi1*$^{-/-}$ mice.[21] Our data also suggest that Caspr2/ADAM22/23 complexes[37] as well as LGI1/ADAM22/23 occur in association with Kv1 at the AIS and/or glutamatergic synapses. The constant presence of ADAM proteins, MAGUKs and Kv1 subunits in the interactomes is consistent with the hypothesis that LGI1-antibodies destabilize membrane Kv1 channels leading to hyperexcitability, however the precise mechanisms involved await elucidation. Interestingly, the glial protein CNPase was unambiguously identified by three distinct antibodies and, the molecular link mediating LGI1 interaction with this multifunctional intracellular protein[88] deserves additional investigation.

Although our data do not allow us to determine to what extent LGI1 participates in trans synaptic complexes, the observed localisation of native LGI1 as well as the diversity of LGI1-linked complexes are not in favour of a major implication of LGI1 as trans-synaptic linker proteins. Of particular note, no AMPA or NMDA receptor-associated subunits were immunoprecipitated with any of the autoantibodies. This suggests that, if such interactions resist our mild solubilisation conditions, AMPAR/NMDAR/LGI1 complexes may not be recognized by the LGI1-antibodies or that all our antibodies specifically dissociated from these complexes. These assumptions seem unlikely since three of the antibodies efficiently enriched proteins containing PDZ domains, especially PSD95 (DLG4), known to independently co-associate with ADAM22[2] and AMPA receptor subunits.[89] Indeed, it is interesting to note that LGI1 was not reported in an AMPA receptor interactome, nor AMPARs in LGI1 complexes.[5,36,90] A decrease in total and synaptic Kv1.1 precedes AMPA receptor downregulation in mice infused with patient-derived whole LGI1-IgGs.[29] Taken together, these results question a molecular link between LGI1 and AMPA receptors. To reconcile these findings with the literature, the observed downregulation of these postsynaptic receptors in LGI1-linked pathologies may be a homeostatic response to hyperexcitability induced by a reduction in Kv1 expression.[20,29] Additional research is needed to clarify this issue.

Consistent with the hypothesis that anti-LGI1 antibodies may initiate Kv1 channel downregulation, we identified Kv1.1, 1.2, 1.4 and 1.6 subunits as well as Kv beta subunits (KCAB1 & 2) associated with LGI1, in agreement with previous reports.[5] Presumably ADAM22/11 and MAGUKs provide the predominant link between Kv1 and LGI1. A direct association between ADAM23 and Kv1 is unlikely since ADAM23 lacks a PDZ interaction domain. LGI1 mRNA expression levels in astrocytes, neurons, microglial cells and oligodendrocytes show an important heterogeneity (www.proteinatlas.org) and therefore, providing a relatively stable mRNA/protein ratio and similar secretion profile from one cell type to the other, the abundance of certain LGI1 associated protein complexes may differentially depend on the nature of each antibody and the LGI1 secretion point.

In conclusion, our immunostaining and mass spectrometry results indicate strong regional expression of LGI1 that is consistent with imaging of hippocampal damage in patients with LGI1-antibody encephalitis. Subcellular localisation supports a role for LGI1 in regulating intrinsic excitability and synaptic transmission. Our data reconcile a large number of contradictory reports regarding the neurobiology of LGI1, notably by demonstrating LGI1 secretion in both axonal and somatodendritic compartments and highlighting LGI1 expression at glial contact sites and its association with glial proteins. Our findings support the hypothesis that LGI1 antibodies in patients with limbic encephalitis induce hyperexcitability by destabilizing Kv1 channels, notably at axonal initial segments. However, the precise mechanisms by which these antibodies trigger downregulation require further investigation.

Acknowledgements

The facility for recombinant protein production in eukaryotic cell systems of the AFMB laboratory is supported by the French Infrastructure for Integrated Structural Biology (FRISBI) (grant ANR-10-INSB-05-01). Acquisition of the mass spectrometer was financially supported by the "Fédération de Recherche pour le Cerveau" (FRC) through the Rotary operation "Espoir en tête". We thank Stephanie Baulac for sharing the *Lgi1*$^{-/-}$ mice_ENREF_41 and the pcDNA3.1-FLAG-LGI1 plasmid. We also thank Stephen Elledge for providing the pINDUCER11 (miR-RUG) plasmid. We are grateful for UCB Pharma, 208-216 Bath Road, Berkshire, UK who generated and purified human recombinant monoclonal anti-LGI1 IgGs. We thank Faivre-Sarrailh for critically reading the manuscript.

Funding

This work was supported by the Institut National pour la Science et la Recherche Médicale (INSERM), Aix-Marseille Université (AMU) and the Agence Nationale de la Recherche (ANR) (grant ANR-17-CE16-0022). The postdoctoral financial support of J.R.F. and the PhD thesis support of J.E. were from the ANR (grant ANR-17-CE16-0022). The PhD thesis of K.D. was supported by a fellowship from the French Ministry of Research (MESRI).

Competing interests

The authors report no competing interests.

Supplementary material

Supplementary material is available at *Brain* online

Figure legends

Figure 1 Characterization of the hippocampal pattern of expression and distribution of LGI1. (**A**) LGI1 (LRR2) immunostaining in different rostro-caudal levels through the mouse brain showing a differential expression of LGI1 in the dorsal and the ventral hippocampus. WT dorsal hippocampus (Bregma approx. -1.80mm, top panels). *Lgi1*$^{-/-}$ dorsal hippocampus (Bregma approx. -1.80mm, middle panels). WT ventral hippocampus (Bregma approx. -3.00 mm, top panels). LGI1 signal is shown in green, AnkG in red, and DAPI in blue. Scale bar = 1mm. (**B**) Quantification of LGI1 expression at different hippocampal levels. n = 4 animals (LRR1 n = 1; LRR2 n = 2; LRR3 n = 1). For the sake of clarity only non-significant comparisons are shown. Any other comparison is $^{**}P < 0.01$. n CA1 Dorsal = 140 ROIs; n CA1 Ventral = 110 ROIs; n CA3 Dorsal = 210 ROIs; n CA3 ventral = 195 ROIs; n DG Dorsal = 210 ROIs; n DG Ventral = 165 ROIs. Data obtained with different antibodies were normalized to DG Dorsal levels in each experiment and pooled thereafter. (**C**) LGI1 (LRR1) immunostaining throughout different dorsal hippocampal regions showing specific immunolabelling of LGI1 in CA1 (top panels), CA3 (middle panels), and DG (bottom panels). LGI1 signal is shown in green, AnkG is in red, and DAPI is in blue. Scale bar = 50 µm. (**D**) High-magnification pictures showing a punctate pattern of staining with anti-LGI1 (LRR1) in the different hippocampal strata analysed. LGI1 is shown in green, and DAPI is in blue. Scale bar = 10 µm**.** (**E**) Quantification

of LGI1 expression in different hippocampal subregions within the dorsal hippocampus. *n* = 4 animals (LRR1 *n* = 1; LRR2 *n* = 2; LRR3 *n* = 1). For the sake of clarity only non-significant comparisons are shown. Any other comparison is $^{**}P < 0.01$. *n* CA1 Str. Oriens = 70 ROIs; *n* CA1 Str. Radiatum = 70 ROIs; *n* CA3 Str. Oriens = 70 ROIs; *n* CA3 Str. Lucidum = 70 ROIs; *n* CA3 Str. Radiatum = 70 ROIs; *n* DG Molecular Layer = 140 ROIs; *n* DG Hilum = 70 ROIs. Data obtained with different antibodies was normalized to CA3 Stratum Radiatum levels in each experiment and pooled thereafter. (**F**) Quantification of LGI1 puncta densities (number of clusters/μm^3) in the different hippocampal strata within the dorsal hippocampus. *n* = 2 independent experiments (WT vs *Lgi1*$^{-/-}$, LRR1 *n* = 1; LRR2 *n* = 1). For the sake of clarity only significant comparisons are shown. $^{*}P < 0.05$; $^{**}P < 0.01$. Any other comparison is non-significant. *n* CA1 Str. Oriens = 8 Fields of view; ROIs; *n* CA1 Str. Radiatum = 8 Fields of view; *n* CA3 Str. Oriens = 8 Fields of view; *n* CA3 Str. Lucidum = 8 Fields of view; *n* CA3 Str. Radiatum = 8 Fields of view; *n* DG Molecular Layer = 8 Fields of view. Data in B, E and F are presented as box-plots of immuonoreactivity levels. The box ranges from the lower (Q1) to the upper (Q3) quartiles; Median is indicated as a horizontal bar within the box, and Mean is indicated as a filled square. Crosses outside the box indicate 1% and 99% of the distribution, and horizontal bars outside the box indicate the limits of the distribution. One-way ANOVA followed by Bonferroni's test was applied.

Figure 2 LGI1 is differentially expressed at the AIS of distinct hippocampal neurons. (**A**) High-magnification pictures showing specific LGI1 (LRR1) immunostaining at the AIS of CA1 pyramidal cells (top panels), CA3 pyramidal cells (middle panels), and DG granule cells (bottom panels). LGI1 signal is shown in green, AnkG is in red, and DAPI is in blue. Scale bar = 10 µm. (**B**) Orthogonal views (left columns) and surface reconstruction (right columns) of LGI1 signal (LRR1, green) restricted to the AIS (AnkG, red) of CA1 pyramidal cells (top panels), CA3 pyramidal cells (middle panels), and DG granule cells (bottom panels). (**C**) Quantification of LGI1 immunoreactivity at the AIS of different hippocampal neuronal subtypes. *n* = 2 independent experiments (WT vs *Lgi1*$^{-/-}$; LRR1 *n* = 1; LRR2 *n* = 1). Data are shown as box-plots of immuonoreactivity levels. The box ranges from the lower (Q1) to the upper (Q3) quartiles; Median is indicated as a horizontal bar within the box, and Mean is indicated as an open square. Horizontal bars outside the box indicate the limits of the distribution. One way ANOVA followed by Bonferroni's test was applied to data in panel C. For the sake of clarity only comparisons within the WT genotype are shown. $^{*}P < 0.05$; $^{**}P <$

0.01. *n* CA1 WT= 260 AIS; *n* CA1 *Lgi1*$^{-/-}$ =126 AIS; *n* CA3 WT = 425 AIS; *n* CA3 *Lgi1*$^{-/-}$ = 156 AIS; *n* DG WT = 427 AIS; *n* DG *Lgi1*$^{-/-}$ = 191 AIS. Data obtained with different antibodies were normalized to CA3-AIS levels in each experiment, and pooled thereafter

Figure 3 LGI1 is expressed by hippocampal astrocytes. (**A, B**) LGI1 (LRR2, yellow), AnkG (cyan), GFAP (magenta), and DAPI (gray) staining in CA3 mouse hippocampus at low magnification (**A**) and at high magnification (**B**) in the Stratum Oriens of CA3. Scale bars = 100 µm (**A**) and 10 µm (**B**). (**C**) Maximal projections and 3D projections of a Z-stack spanning a CA3-hippocampal astrocyte showing LGI1 (LRR1, yellow), GFAP (magenta), and DAPI (gray) staining (top) and reduced Z-stack of the two astrocytic processes corresponding to the insets (1, 2) outlined in the top rows (bottom). Arrowheads indicate LGI1 puncta over the astrocytic processes. Scale bars = 5 µm. (**D**) LGI1 (LRR2, yellow), AnkG (cyan), GFAP (magenta), and DAPI (gray) staining in the Stratum Oriens of CA3 showing an astrocytic process in close contact with an axon initial segment stained with GFAP and AnkG, respectively. (**E**) Orthogonal views of the region boxed in (**D**) showing that LGI1 (LRR2, yellow) is precisely located between the astrocytic process (GFAP, magenta) and the axonal initial segment (AnkG, cyan). Scale bar = 5 µm. (**F**) Volume reconstruction of the region boxed in (**E**). Images are representative of 3 independent experiments (WT vs *Lgi1*$^{-/-}$; LRR2 *n* = 2; LRR1 *n* = 1)

Figure 4 Subcellular distribution of total DENDRA2::LGI1 studied by gene-gun transfection and immunohistofluorescence in rat organotypic slices. (**A**) Schematic of the experimental protocol used for gene-gun transfection and immunostaining. (**B**) Top panels, CA3 pyramidal cells transfected with DENDRA2::LGI1 and labelled with anti-DENDRA2 (green), anti-AnkG (red), and DAPI (blue). Arrowheads point towards the axonal initial segment. Arrows show dendritic branches. Scale bar = 25 µm. Bottom panels, high-magnification picture showing the expression of LGI1 at axonal initial segment (arrowheads) and surrounding dendrites. Scale bar = 5 µm. (**C**)**,** (**D**)**,** (**E**) Quantification of the relative immunoreactivity levels of DENDRA2::LGI1 at the AIS, axon, and dendrites of transfected neurons in CA1 (**C**), CA3 (**D**), and DG (**E**). Data are presented as box-plots of immuonoreactivity levels. The box ranges from the lower (Q1) to the upper (Q3) quartiles; Median is indicated as a horizontal bar within the box, and Mean is indicated as a filled square. Crosses outside the box indicate 1% and 99% of the distribution, and horizontal bars outside the box indicate the limits of the distribution. One way ANOVA followed by Bonferroni's test

was applied to data in panels C, D, and E. *n* = 2 independent organotypic cultures. *n* CA1 = 3 cells; *n* CA3 = 3 cells; *n* DG = 5 cells. n.s. non-significant; * $P < 0.05$; ** $P < 0.01$. (**F**) Left columns, High-magnification picture of two axonal initial segments from two transfected cells showing prominent expression of DENDRA2::LGI1 at the AIS. DENDRA2::LGI1 is shown in green, AnkG is in red. Scale bar = 5 µm. Right columns, detail of the outlined inset showing that DENDRA2::LGI1 is partially distributed in the AnkG gap-like microdomains at the AIS (top panel). Normalized immunoreactivity levels for DENDRA2::LGI1 and AnkG (green and red traces, respectively) of the lines depicted in the inset (bottom panels). **G** Immunostaining of DENDRA2::LGI1 (green), AnkG (gray), and GABAaα2 (magenta), at the AIS of a CA3 transfected neuron (top panels). Scale bar = 5 µm. Traces for DENDRA2::LGI1 and GABA aα2 normalized immunoreactivity (green and magenta, respectively) of the lines shown in the inset (bottom panels)

Figure 5 DENDRA2::LGI1 is reliably secreted by CA3 pyramidal cells after single cell electroporation. (**A**) Schematic of the experimental protocol used for single cell electroporation and immunostaining for extracellular detection of DENDRA2::LGI1. (**B**) Extracellular (secreted) DENDRA2::LGI1 revealed by anti-DENDRA2 (green) in an electroporated CA3 pyramidal cell. AnkG is shown in red, and DAPI is in blue. Scale bar = 10 µm. (**C**) High-magnification reconstruction of the electroporated neuron shown in (**B**). Outlined insets are shown in the right panels where inset 1 corresponds to the axon (arrowheads indicate axonal secretion spots of DENDRA2::LGI1), inset 2 correspond to the axonal initial segment, and inset 3 corresponds to the proximal apical dendrite. Images are representative of 3 CA3 pyramidal neurons from 2 independent cultures. Scale bars = 5 µm in all panels

Figure 6 Secreted DENDRA2::LGI1 colocalizes with AnkG and PSD93 after single cell electroporation in mouse hippocampal slices. (**A**) Schematic of the experimental protocol used for single cell electroporation and immunostaining. (**B**) Low-magnification picture of two individual CA3 pyramidal neurons electroporated with DENDRA2::LGI1 and immunostained against secreted DENDRA2::LGI1 with anti-DENDRA2 (yellow), anti-AnkG (cyan), anti-PSD93 (magenta), and DAPI (gray). Scale bar = 10 µm. **C** High magnification detail of the inset 1 outlined in panel (**B**) showing colocalization of secreted DENDRA2::LGI1 (yellow) with the AIS marker AnkG (cyan), and PSD93 clusters (magenta) at the AIS. Dashed lines

indicate the edges of the AIS taking AnkG signal as a reference. Line traces (1,2) correspond to the line traces depicted in the bottom left panel. Scale bar = 5 µm. (**D**) High magnification detail of the inset 2 outlined in panel (**B**) showing colocalization of secreted DENDRA2::LGI1 (yellow) with PSD93 clusters (magenta) at the dendrites of CA3 pyramidal neurons. Maximal projections (left panels) and orthogonal views (right panels) of the basal dendrites of CA3 pyramidal neurons shown in (**B**). Scale bars = 5 µm

Figure 7 WT LGI1 localizes to the AIS and dendrites of CA3 pyramidal neurons after single cell electroporation in mouse *Lgi1*$^{-/-}$ hippocampal slices. (**A**) Schematic of the experimental protocol used for single cell electroporation and immunostaining. (**B**) CA3 pyramidal cell transfected with WT LGI1 and soluble GFP and labelled with anti-LGI1 (Yellow), anti-AnkG (cyan), anti-GFP (magenta) and DAPI (grey). Scale bars = 10 µm. (**C**) Detailed view of the region outlined in b (1) corresponding to the AIS of the electroporated neuron showing the appearance of LGI1 clusters at the AIS (left panels) and 90° rotated view (right panels). Scale bars = 5 µm. (**D**) Detailed view of the region outlined in b (2) showing LGI1 clusters at the proximal basal dendrites of the electroporated neurons. Arrowheads point towards individual dendritic spines in which LGI1 clusters were identified (top panels). Volume reconstruction of the regions 1 and 2 boxed in the top panels (bottom panels). Scale bars = 5 µm

Figure 8 Histograms of specific LGI1 partners immunoprecipitated by the recombinant patient-derived anti-LGI1 antibodies. Absolute mean emPAI values of LGI1 partners immunoprecipitated by LRR1 (**A**), LRR3 (**B**), EPTP1 (**C**) and EPTP2 (**D**) illustrates their relative enrichment. Partners exclusively immunoprecipitated by a specific antibody are represented by open histograms. For clarity, tubulins are not represented in these histograms and are listed in Spreadsheet. Data are shown as mean ± SD. Individual data points are superimposed on the histograms. Each shape (square, triangle, circle) represents a different experiment. A Venn Diagram (**E**) shows the number of overlapping LGI1 partners immunoprecipitated by the antibodies used. Immunoprecipitated partners are classified by functional classes (Partially from http://www.pantherdb.org/)

References

1. Yamagata A, Miyazaki Y, Yokoi N, et al. Structural basis of epilepsy-related ligand-receptor complex LGI1-ADAM22. *Nat Commun*. Apr 18 2018;9(1):1546. doi:10.1038/s41467-018-03947-w

2. Fukata Y, Adesnik H, Iwanaga T, Bredt DS, Nicoll RA, Fukata M. Epilepsy-related ligand/receptor complex LGI1 and ADAM22 regulate synaptic transmission. *Science*. Sep 22 2006;313(5794):1792-5. doi:10.1126/science.1129947
3. Sagane K, Ishihama Y, Sugimoto H. LGI1 and LGI4 bind to ADAM22, ADAM23 and ADAM11. *Int J Biol Sci*. 2008;4(6):387-96. doi:10.7150/ijbs.4.387
4. Owuor K, Harel NY, Englot DJ, Hisama F, Blumenfeld H, Strittmatter SM. LGI1-associated epilepsy through altered ADAM23-dependent neuronal morphology. *Mol Cell Neurosci*. Dec 2009;42(4):448-57. doi:10.1016/j.mcn.2009.09.008
5. Fukata Y, Lovero KL, Iwanaga T, et al. Disruption of LGI1-linked synaptic complex causes abnormal synaptic transmission and epilepsy. *Proc Natl Acad Sci U S A*. Feb 23 2010;107(8):3799-804. doi:10.1073/pnas.0914537107
6. Lovero KL, Fukata Y, Granger AJ, Fukata M, Nicoll RA. The LGI1-ADAM22 protein complex directs synapse maturation through regulation of PSD-95 function. *Proc Natl Acad Sci U S A*. Jul 28 2015;112(30):E4129-37. doi:10.1073/pnas.1511910112
7. Fukata Y, Hirano Y, Miyazaki Y, Yokoi N, Fukata M. Trans-synaptic LGI1-ADAM22-MAGUK in AMPA and NMDA receptor regulation. *Neuropharmacology*. Jun 2 2021:108628. doi:10.1016/j.neuropharm.2021.108628
8. Chernova OB, Somerville RP, Cowell JK. A novel gene, LGI1, from 10q24 is rearranged and downregulated in malignant brain tumors. *Oncogene*. Dec 3 1998;17(22):2873-81. doi:10.1038/sj.onc.1202481
9. Senechal KR, Thaller C, Noebels JL. ADPEAF mutations reduce levels of secreted LGI1, a putative tumor suppressor protein linked to epilepsy. *Hum Mol Genet*. Jun 15 2005;14(12):1613-20. doi:10.1093/hmg/ddi169
10. Nobile C, Michelucci R, Andreazza S, Pasini E, Tosatto SC, Striano P. LGI1 mutations in autosomal dominant and sporadic lateral temporal epilepsy. Review. *Hum Mutat*. Apr 2009;30(4):530-6. doi:10.1002/humu.20925
11. Leonardi E, Andreazza S, Vanin S, Busolin G, Nobile C, Tosatto SC. A computational model of the LGI1 protein suggests a common binding site for ADAM proteins. *PLoS One*. Mar 29 2011;6(3):e18142. doi:10.1371/journal.pone.0018142
12. Morante-Redolat JM, Gorostidi-Pagola A, Piquer-Sirerol S, et al. Mutations in the LGI1/Epitempin gene on 10q24 cause autosomal dominant lateral temporal epilepsy. *Hum Mol Genet*. May 1 2002;11(9):1119-28.
13. Kalachikov S, Evgrafov O, Ross B, et al. Mutations in LGI1 cause autosomal-dominant partial epilepsy with auditory features. *Nat Genet*. Mar 2002;30(3):335-41. doi:10.1038/ng832
14. Yu YE, Wen L, Silva J, et al. Lgi1 null mutant mice exhibit myoclonic seizures and CA1 neuronal hyperexcitability. *Hum Mol Genet*. May 1 2010;19(9):1702-11. doi:10.1093/hmg/ddq047
15. Boillot M, Lee CY, Allene C, Leguern E, Baulac S, Rouach N. LGI1 acts presynaptically to regulate excitatory synaptic transmission during early postnatal development. *Sci Rep*. 2016;6:21769. doi:10.1038/srep21769
16. Zhou YD, Lee S, Jin Z, Wright M, Smith SE, Anderson MP. Arrested maturation of excitatory synapses in autosomal dominant lateral temporal lobe epilepsy. *Nat Med*. Oct 2009;15(10):1208-14. doi:10.1038/nm.2019
17. Dazzo E, Leonardi E, Belluzzi E, et al. Secretion-Positive LGI1 Mutations Linked to Lateral Temporal Epilepsy Impair Binding to ADAM22 and ADAM23 Receptors. *PLoS Genet*. Oct 2016;12(10):e1006376. doi:10.1371/journal.pgen.1006376
18. Yokoi N, Fukata Y, Kase D, et al. Chemical corrector treatment ameliorates increased seizure susceptibility in a mouse model of familial epilepsy. *Nat Med*. Jan 2015;21(1):19-26. doi:10.1038/nm.3759
19. Fukata Y, Yokoi N, Miyazaki Y, Fukata M. The LGI1–ADAM22 protein complex in synaptic transmission and synaptic disorders. *Neurosci Res*. 2016;doi:http://dx.doi.org/10.1016/j.neures.2016.09.011

20. Seagar M, Russier M, Caillard O, et al. LGI1 tunes intrinsic excitability by regulating the density of axonal Kv1 channels. *Proc Natl Acad Sci U S A*. Jul 18 2017;114(29):7719-7724. doi:10.1073/pnas.1618656114
21. Silva J, Sharma S, Hughes B, Yu YE, Cowell JK. Homozygous inactivation of the LGI1 gene results in hypomyelination in the peripheral and central nervous systems. Research Support, N.I.H., Extramural. *J Neurosci Res*. Nov 15 2010;88(15):3328-36. doi:10.1002/jnr.22496
22. Thomas RA, Gibon J, Chen CXQ, et al. The Nogo Receptor Ligand LGI1 Regulates Synapse Number and Synaptic Activity in Hippocampal and Cortical Neurons. *eNeuro*. Jul-Aug 2018;5(4)doi:10.1523/ENEURO.0185-18.2018
23. Teng XY, Hu P, Chen Y, et al. A novel Lgi1 mutation causes white matter abnormalities and impairs motor coordination in mice. *FASEB journal : official publication of the Federation of American Societies for Experimental Biology*. Mar 2022;36(3):e22212. doi:10.1096/fj.202101652R
24. Cowell JK. LGI1: from zebrafish to human epilepsy. Review. *Prog Brain Res*. 2014;213:159-79. doi:10.1016/B978-0-444-63326-2.00009-0
25. Ogawa Y, Oses-Prieto J, Kim MY, et al. ADAM22, a Kv1 channel-interacting protein, recruits membrane-associated guanylate kinases to juxtaparanodes of myelinated axons. *J Neurosci*. Jan 20 2010;30(3):1038-48. doi:10.1523/JNEUROSCI.4661-09.2010
26. Irani SR, Alexander S, Waters P, et al. Antibodies to Kv1 potassium channel-complex proteins leucine-rich, glioma inactivated 1 protein and contactin-associated protein-2 in limbic encephalitis, Morvan's syndrome and acquired neuromyotonia. *Brain : a journal of neurology*. Sep 2010;133(9):2734-48. doi:10.1093/brain/awq213
27. Lai M, Huijbers MG, Lancaster E, et al. Investigation of LGI1 as the antigen in limbic encephalitis previously attributed to potassium channels: a case series. *Lancet Neurol*. Aug 2010;9(8):776-85. doi:10.1016/S1474-4422(10)70137-X
28. Michael S, Waters P, Irani SR. Stop testing for autoantibodies to the VGKC-complex: only request LGI1 and CASPR2. Review. *Pract Neurol*. Oct 2020;20(5):377-384. doi:10.1136/practneurol-2019-002494
29. Petit-Pedrol M, Sell J, Planaguma J, et al. LGI1 antibodies alter Kv1.1 and AMPA receptors changing synaptic excitability, plasticity and memory. *Brain : a journal of neurology*. Nov 1 2018;141(11):3144-3159. doi:10.1093/brain/awy253
30. Ramberger M, Berretta A, Tan JMM, et al. Distinctive binding properties of human monoclonal LGI1 autoantibodies determine pathogenic mechanisms. *Brain : a journal of neurology*. Jun 1 2020;143(6):1731-1745. doi:10.1093/brain/awaa104
31. Miller TD, Chong TT, Aimola Davies AM, et al. Human hippocampal CA3 damage disrupts both recent and remote episodic memories. *Elife*. Jan 24 2020;9doi:10.7554/eLife.41836
32. Miller TD, Chong TT, Aimola Davies AM, et al. Focal CA3 hippocampal subfield atrophy following LGI1 VGKC-complex antibody limbic encephalitis. *Brain : a journal of neurology*. May 1 2017;140(5):1212-1219. doi:10.1093/brain/awx070
33. Thompson J, Bi M, Murchison AG, et al. The importance of early immunotherapy in patients with faciobrachial dystonic seizures. *Brain : a journal of neurology*. Feb 1 2018;141(2):348-356. doi:10.1093/brain/awx323
34. Head K, Gong S, Joseph S, et al. Defining the expression pattern of the LGI1 gene in BAC transgenic mice. Research Support, N.I.H., Extramural. *Mamm Genome*. May 2007;18(5):328-37. doi:10.1007/s00335-007-9024-6
35. Boillot M, Huneau C, Marsan E, et al. Glutamatergic neuron-targeted loss of LGI1 epilepsy gene results in seizures. *Brain : a journal of neurology*. Nov 2014;137(Pt 11):2984-96. doi:10.1093/brain/awu259
36. Kunapuli P, Jang GF, Kazim L, Cowell JK. Mass spectrometry identifies LGI1-interacting proteins that are involved in synaptic vesicle function in the human brain. *J Mol Neurosci*. Sep 2009;39(1-2):137-43. doi:10.1007/s12031-009-9202-y

37. Hivert B, Marien L, Agbam KN, Faivre-Sarrailh C. ADAM22 and ADAM23 modulate the targeting of the Kv1 channel-associated protein LGI1 to the axon initial segment. *J Cell Sci*. Jan 16 2019;132(2)doi:10.1242/jcs.219774
38. Silva J, Wang G, Cowell JK. The temporal and spatial expression pattern of the LGI1 epilepsy predisposition gene during mouse embryonic cranial development. *BMC Neurosci*. May 13 2011;12:43. doi:10.1186/1471-2202-12-43
39. Herranz-Perez V, Olucha-Bordonau FE, Morante-Redolat JM, Perez-Tur J. Regional distribution of the leucine-rich glioma inactivated (LGI) gene family transcripts in the adult mouse brain. *Brain Res*. Jan 11 2010;1307:177-94. doi:10.1016/j.brainres.2009.10.013
40. Ribeiro PA, Sbragia L, Gilioli R, Langone F, Conte FF, Lopes-Cendes I. Expression profile of Lgi1 gene in mouse brain during development. *J Mol Neurosci*. Jul 2008;35(3):323-9. doi:10.1007/s12031-008-9096-0
41. Chabrol E, Navarro V, Provenzano G, et al. Electroclinical characterization of epileptic seizures in leucine-rich, glioma-inactivated 1-deficient mice. *Brain : a journal of neurology*. Sep 2010;133(9):2749-62. doi:10.1093/brain/awq171
42. Ohkawa T, Fukata Y, Yamasaki M, et al. Autoantibodies to epilepsy-related LGI1 in limbic encephalitis neutralize LGI1-ADAM22 interaction and reduce synaptic AMPA receptors. *J Neurosci*. Nov 13 2013;33(46):18161-74. doi:10.1523/JNEUROSCI.3506-13.2013
43. Meerbrey KL, Hu G, Kessler JD, et al. The pINDUCER lentiviral toolkit for inducible RNA interference in vitro and in vivo. *Proc Natl Acad Sci U S A*. Mar 01 2011;108(9):3665-70. doi:10.1073/pnas.1019736108
44. Rama S, Boumedine-Guignon N, Sangiardi M, et al. Chromophore-Assisted Light Inactivation of the V-ATPase V0c Subunit Inhibits Neurotransmitter Release Downstream of Synaptic Vesicle Acidification. journal article. *Mol Neurobiol*. August 28 2018;doi:10.1007/s12035-018-1324-1
45. Gogolla N, Galimberti I, DePaola V, Caroni P. Staining protocol for organotypic hippocampal slice cultures. *Nat Protoc*. 2006;1(5):2452-6. doi:10.1038/nprot.2006.180
46. Perez-Riverol Y, Csordas A, Bai J, et al. The PRIDE database and related tools and resources in 2019: improving support for quantification data. *Nucleic Acids Res*. Jan 8 2019;47(D1):D442-D450. doi:10.1093/nar/gky1106
47. King AN, Manning CF, Trimmer JS. A unique ion channel clustering domain on the axon initial segment of mammalian neurons. *J Comp Neurol*. Aug 1 2014;522(11):2594-608. doi:10.1002/cne.23551
48. Wefelmeyer W, Cattaert D, Burrone J. Activity-dependent mismatch between axo-axonic synapses and the axon initial segment controls neuronal output. *Proc Natl Acad Sci U S A*. Aug 4 2015;112(31):9757-62. doi:10.1073/pnas.1502902112
49. Schulte U, Thumfart JO, Klocker N, et al. The epilepsy-linked Lgi1 protein assembles into presynaptic Kv1 channels and inhibits inactivation by Kvbeta1. *Neuron*. Mar 2 2006;49(5):697-706. doi:10.1016/j.neuron.2006.01.033
50. Zhao WQ, Lu B. Expression of annexin A2 in GABAergic interneurons in the normal rat brain. *J Neurochem*. Mar 2007;100(5):1211-23. doi:10.1111/j.1471-4159.2006.04311.x
51. Zhao WQ, Waisman DM, Grimaldi M. Specific localization of the annexin II heterotetramer in brain lipid raft fractions and its changes in spatial learning. *J Neurochem*. Aug 2004;90(3):609-20. doi:10.1111/j.1471-4159.2004.02509.x
52. Pereira JB, Janelidze S, Ossenkoppele R, et al. Untangling the association of amyloid-beta and tau with synaptic and axonal loss in Alzheimer's disease. *Brain : a journal of neurology*. Feb 12 2021;144(1):310-324. doi:10.1093/brain/awaa395
53. Chung D, Shum A, Caraveo G. GAP-43 and BASP1 in Axon Regeneration: Implications for the Treatment of Neurodegenerative Diseases. Review. *Front Cell Dev Biol*. 2020;8:567537. doi:10.3389/fcell.2020.567537
54. Fresia C, Vigliarolo T, Guida L, et al. G-protein coupling and nuclear translocation of the human abscisic acid receptor LANCL2. *Sci Rep*. May 25 2016;6:26658. doi:10.1038/srep26658

55. Huang CY, Rasband MN. Axon initial segments: structure, function, and disease. *Ann N Y Acad Sci*. May 2018;1420(1):46-61. doi:10.1111/nyas.13718
56. Kunapuli P, Lo K, Hawthorn L, Cowell JK. Reexpression of LGI1 in glioma cells results in dysregulation of genes implicated in the canonical axon guidance pathway. *Genomics*. Feb 2010;95(2):93-100. doi:10.1016/j.ygeno.2009.10.001
57. Lang T, Jahn R. Core proteins of the secretory machinery. Review. *Handb Exp Pharmacol*. 2008;(184):107-27. doi:10.1007/978-3-540-74805-2_5
58. Ferrer-Orta C, Perez-Sanchez MD, Coronado-Parra T, et al. Structural characterization of the Rabphilin-3A-SNAP25 interaction. *Proc Natl Acad Sci U S A*. Jul 3 2017;114(27):E5343-E5351. doi:10.1073/pnas.1702542114
59. Ohno Y, Tokudome K. Therapeutic Role of Synaptic Vesicle Glycoprotein 2A (SV2A) in Modulating Epileptogenesis. Review. *CNS Neurol Disord Drug Targets*. 2017;16(4):463-471. doi:10.2174/1871527316666170404115027
60. Kamemura K, Chihara T. Multiple functions of the ER-resident VAP and its extracellular role in neural development and disease. Review. *J Biochem*. May 1 2019;165(5):391-400. doi:10.1093/jb/mvz011
61. Sun EW, De Camilli P. Kv2 potassium channels meet VAP. *Proc Natl Acad Sci U S A*. Jul 31 2018;115(31):7849-7851. doi:10.1073/pnas.1810059115
62. Saito N, Shirai Y. Protein kinase C gamma (PKC gamma): function of neuron specific isotype. Review. *J Biochem*. Nov 2002;132(5):683-7. doi:10.1093/oxfordjournals.jbchem.a003274
63. Vacher H, Trimmer JS. Diverse roles for auxiliary subunits in phosphorylation-dependent regulation of mammalian brain voltage-gated potassium channels. *Pflugers Arch*. Nov 2011;462(5):631-43. doi:10.1007/s00424-011-1004-8
64. Kalinowska M, Castillo C, Francesconi A. Quantitative profiling of brain lipid raft proteome in a mouse model of fragile X syndrome. *PLoS One*. 2015;10(4):e0121464. doi:10.1371/journal.pone.0121464
65. Babenko VN, Smagin DA, Galyamina AG, Kovalenko IL, Kudryavtseva NN. Altered Slc25 family gene expression as markers of mitochondrial dysfunction in brain regions under experimental mixed anxiety/depression-like disorder. *BMC Neurosci*. Dec 11 2018;19(1):79. doi:10.1186/s12868-018-0480-6
66. Jahn O, Tenzer S, Werner HB. Myelin proteomics: molecular anatomy of an insulating sheath. *Mol Neurobiol*. Aug 2009;40(1):55-72. doi:10.1007/s12035-009-8071-2
67. Bifulco M, Laezza C, Stingo S, Wolff J. 2',3'-Cyclic nucleotide 3'-phosphodiesterase: a membrane-bound, microtubule-associated protein and membrane anchor for tubulin. *Proc Natl Acad Sci U S A*. Feb 19 2002;99(4):1807-12. doi:10.1073/pnas.042678799
68. Lee J, Gravel M, Zhang R, Thibault P, Braun PE. Process outgrowth in oligodendrocytes is mediated by CNP, a novel microtubule assembly myelin protein. *J Cell Biol*. Aug 15 2005;170(4):661-73. doi:10.1083/jcb.200411047
69. Fard MK, van der Meer F, Sanchez P, et al. BCAS1 expression defines a population of early myelinating oligodendrocytes in multiple sclerosis lesions. *Sci Transl Med*. Dec 6 2017;9(419)doi:10.1126/scitranslmed.aam7816
70. Fu MM, McAlear TS, Nguyen H, et al. The Golgi Outpost Protein TPPP Nucleates Microtubules and Is Critical for Myelination. *Cell*. Sep 19 2019;179(1):132-146 e14. doi:10.1016/j.cell.2019.08.025
71. Kano SI, Choi EY, Dohi E, et al. Glutathione S-transferases promote proinflammatory astrocyte-microglia communication during brain inflammation. *Sci Signal*. Feb 19 2019;12(569)doi:10.1126/scisignal.aar2124
72. Yokoi N, Fukata Y, Okatsu K, et al. 14-3-3 proteins stabilize LGI1-ADAM22 levels to regulate seizure thresholds in mice. *Cell Rep*. Dec 14 2021;37(11):110107. doi:10.1016/j.celrep.2021.110107
73. Jiang W, Tian X, Yang P, et al. Enolase1 Alleviates Cerebral Ischemia-Induced Neuronal Injury via Its Enzymatic Product Phosphoenolpyruvate. *ACS Chem Neurosci*. Jun 19 2019;10(6):2877-2889. doi:10.1021/acschemneuro.9b00103

74. Finke C, Pruss H, Heine J, et al. Evaluation of Cognitive Deficits and Structural Hippocampal Damage in Encephalitis With Leucine-Rich, Glioma-Inactivated 1 Antibodies. Multicenter Study. *JAMA neurology*. Jan 1 2017;74(1):50-59. doi:10.1001/jamaneurol.2016.4226
75. Heine J, Pruss H, Scheel M, et al. Transdiagnostic hippocampal damage patterns in neuroimmunological disorders. *Neuroimage Clin*. 2020;28:102515. doi:10.1016/j.nicl.2020.102515
76. Irani SR, Michell AW, Lang B, et al. Faciobrachial dystonic seizures precede Lgi1 antibody limbic encephalitis. *Ann Neurol*. May 2011;69(5):892-900. doi:10.1002/ana.22307
77. Flanagan EP, Kotsenas AL, Britton JW, et al. Basal ganglia T1 hyperintensity in LGI1-autoantibody faciobrachial dystonic seizures. *Neurology(R) neuroimmunology & neuroinflammation*. Dec 2015;2(6):e161. doi:10.1212/NXI.0000000000000161
78. Zhou L, Su LD, Cao SL, et al. Celecoxib Ameliorates Seizure Susceptibility in Autosomal Dominant Lateral Temporal Epilepsy. *J Neurosci*. Mar 28 2018;38(13):3346-3357. doi:10.1523/JNEUROSCI.3245-17.2018
79. Lardeux P, Fourier A, Peter E, et al. Core cerebrospinal fluid biomarker profile in anti-LGI1 encephalitis. *J Neurol*. Jun 8 2021;doi:10.1007/s00415-021-10642-2
80. Farhy-Tselnicker I, Allen NJ. Astrocytes, neurons, synapses: a tripartite view on cortical circuit development. *Neural Dev*. May 1 2018;13(1):7. doi:10.1186/s13064-018-0104-y
81. Allen NJ, Eroglu C. Cell Biology of Astrocyte-Synapse Interactions. Review. *Neuron*. Nov 1 2017;96(3):697-708. doi:10.1016/j.neuron.2017.09.056
82. Cahoy JD, Emery B, Kaushal A, et al. A transcriptome database for astrocytes, neurons, and oligodendrocytes: a new resource for understanding brain development and function. *J Neurosci*. Jan 2 2008;28(1):264-78. doi:10.1523/JNEUROSCI.4178-07.2008
83. Gennarini G, Bizzoca A, Picocci S, Puzzo D, Corsi P, Furley AJW. The role of Gpi-anchored axonal glycoproteins in neural development and neurological disorders. *Mol Cell Neurosci*. Jun 2017;81:49-63. doi:10.1016/j.mcn.2016.11.006
84. Traka M, Goutebroze L, Denisenko N, et al. Association of TAG-1 with Caspr2 is essential for the molecular organization of juxtaparanodal regions of myelinated fibers. *J Cell Biol*. Sep 15 2003;162(6):1161-72. doi:10.1083/jcb.200305078
85. Pinatel D, Hivert B, Saint-Martin M, et al. The Kv1-associated molecules TAG-1 and Caspr2 are selectively targeted to the axon initial segment in hippocampal neurons. *J Cell Sci*. Jul 1 2017;130(13):2209-2220. doi:10.1242/jcs.202267
86. Horresh I, Poliak S, Grant S, Bredt D, Rasband MN, Peles E. Multiple molecular interactions determine the clustering of Caspr2 and Kv1 channels in myelinated axons. *J Neurosci*. Dec 24 2008;28(52):14213-22. doi:10.1523/JNEUROSCI.3398-08.2008
87. Ramanathan S, Tseng M, Davies AJ, et al. Leucine-Rich Glioma-Inactivated 1 versus Contactin-Associated Protein-like 2 Antibody Neuropathic Pain: Clinical and Biological Comparisons. *Ann Neurol*. Oct 2021;90(4):683-690. doi:10.1002/ana.26189
88. Raasakka A, Kursula P. The myelin membrane-associated enzyme 2',3'-cyclic nucleotide 3'-phosphodiesterase: on a highway to structure and function. *Neurosci Bull*. Dec 2014;30(6):956-966. doi:10.1007/s12264-013-1437-5
89. Dakoji S, Tomita S, Karimzadegan S, Nicoll RA, Bredt DS. Interaction of transmembrane AMPA receptor regulatory proteins with multiple membrane associated guanylate kinases. *Neuropharmacology*. Nov 2003;45(6):849-56. doi:10.1016/s0028-3908(03)00267-3
90. Shanks NF, Savas JN, Maruo T, et al. Differences in AMPA and kainate receptor interactomes facilitate identification of AMPA receptor auxiliary subunit GSG1L. *Cell Rep*. Jun 28 2012;1(6):590-8. doi:10.1016/j.celrep.2012.05.004

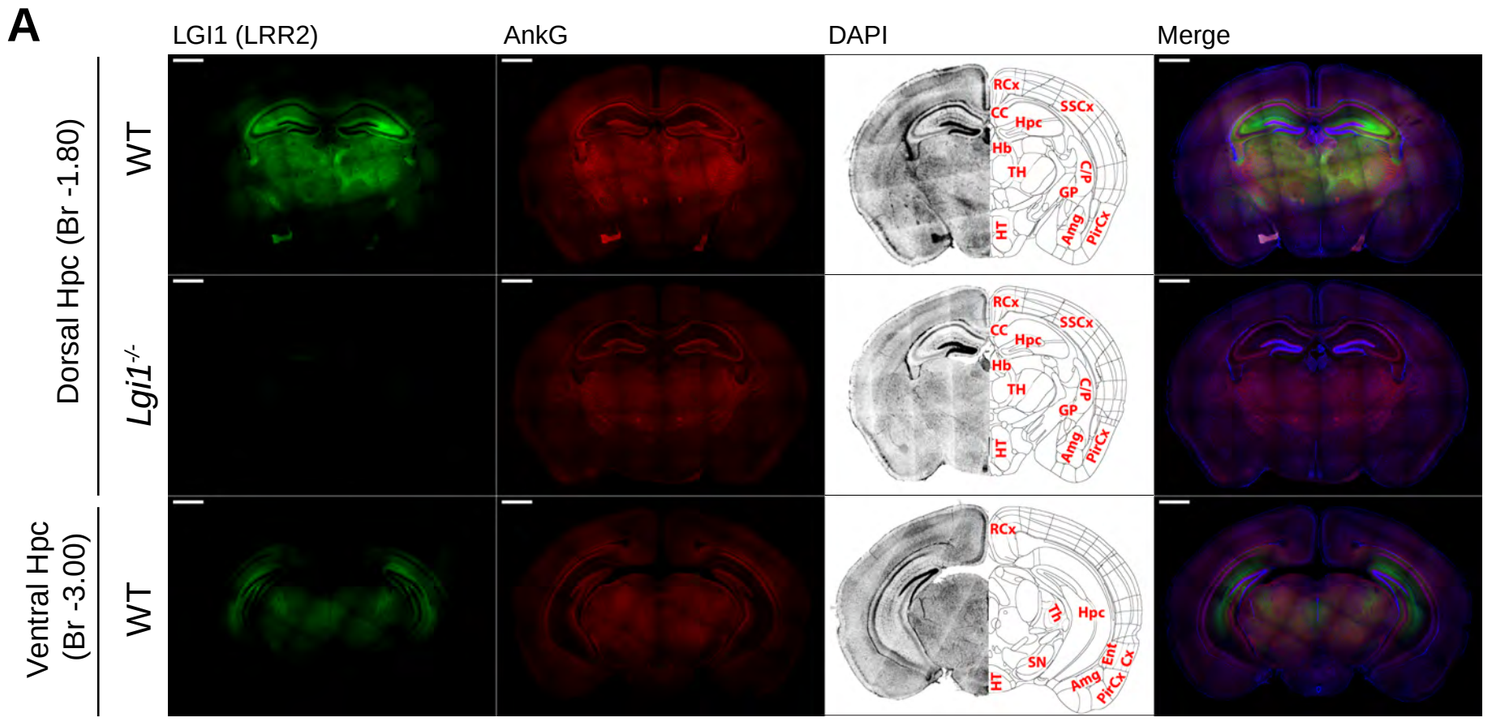
A
LGI1 (LRR2)
AnkG
DAPI
Merge
Dorsal Hpc (Br -1.80)
Ventral Hpc (Br -3.00)
WT
Lgi1-/-
WT
RCx
CC
Hpc
SSCx
Hb
TH
CP
GP
HT
Amg
PirCx
RCx
Hpc
TH
SN
HT
Amg
Ent
PirCx Cx

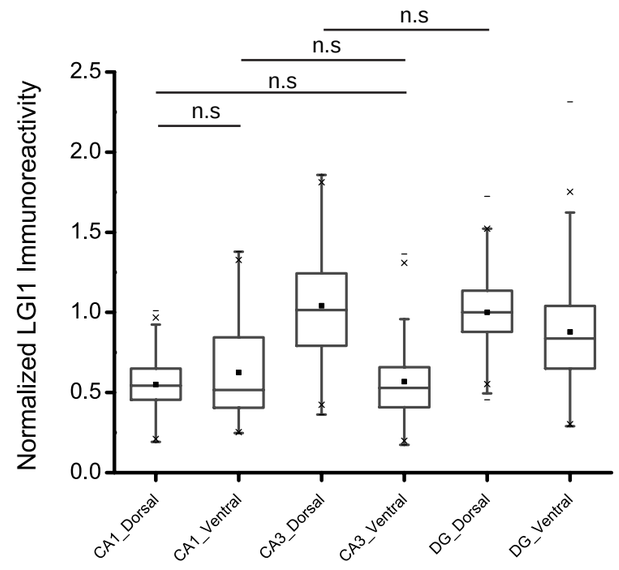
B
Normalized LGI1 Immunoreactivity
2.5
2.0
1.5
1.0
0.5
0.0
n.s
n.s
n.s
n.s
CA1_Dorsal
CA1_Ventral
CA3_Dorsal
CA3_Ventral
DG_Dorsal
DG_Ventral

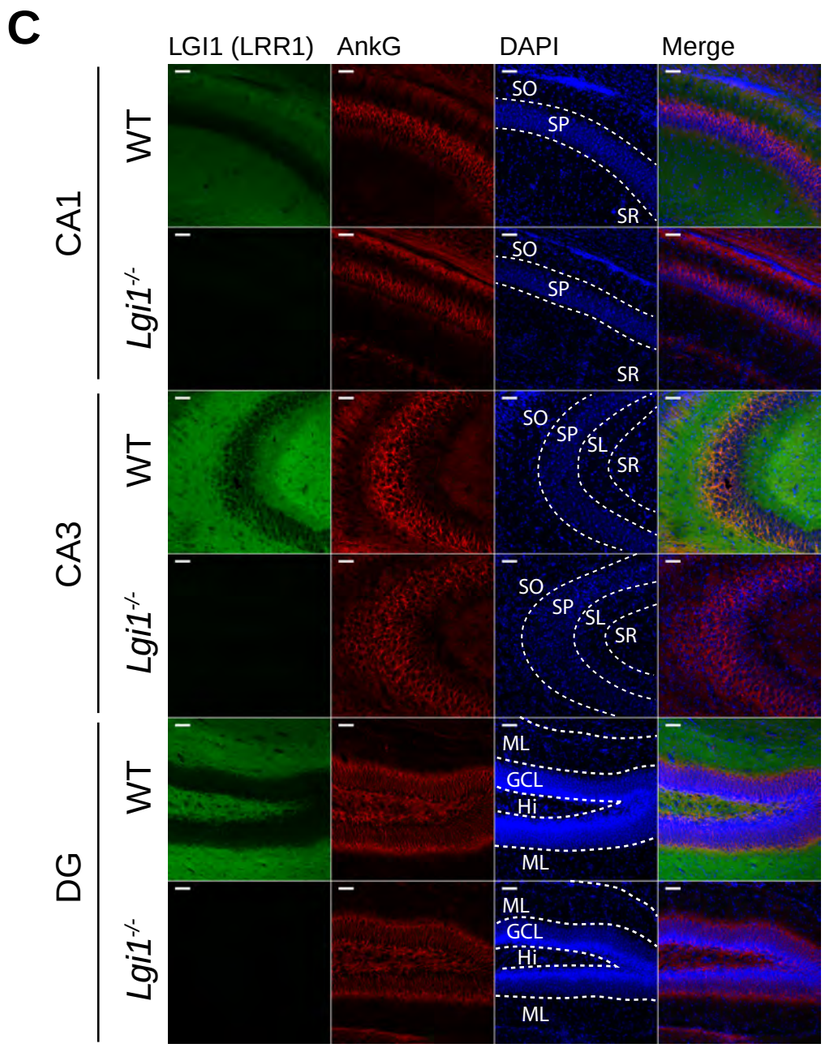
C
LGI1 (LRR1)
AnkG
DAPI
Merge
CA1
CA3
DG
WT
Lgi1-/-
WT
Lgi1-/-
WT
Lgi1-/-
SO
SP
SR
SL
ML
GCL
Hi

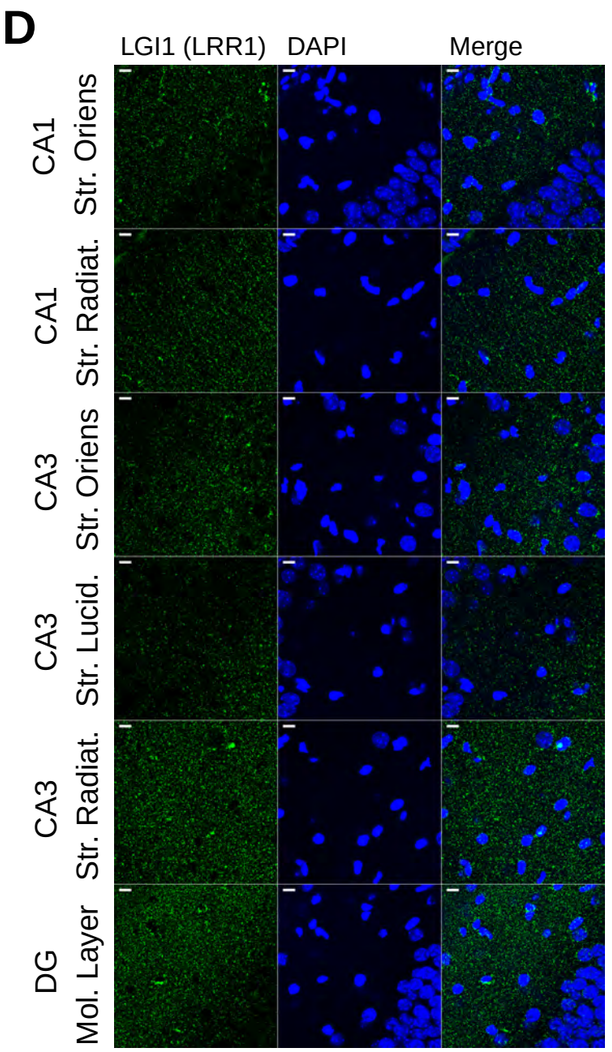
D
LGI1 (LRR1)
DAPI
Merge
CA1 Str. Oriens
CA1 Str. Radiat.
CA3 Str. Oriens
CA3 Str. Lucid.
CA3 Str. Radiat.
DG Mol. Layer

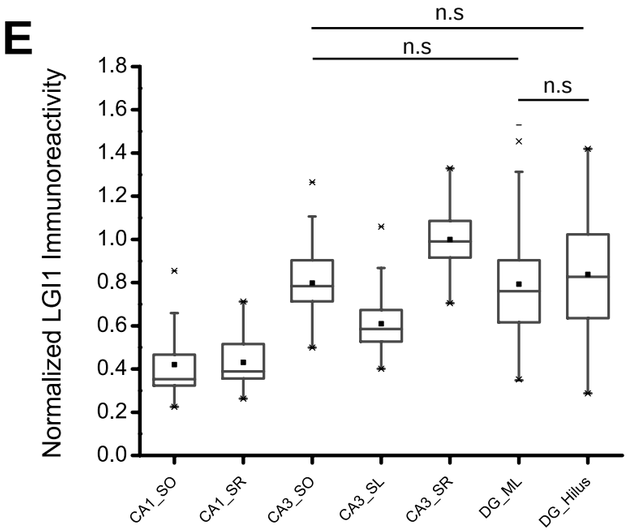
E
Immunoreactivity
1.8
1.6
1.4
1.2
1.0
0.8
0.6
0.4
0.2
0.0
n.s
n.s
n.s
CA1_SO
CA1_SR
CA3_SO
CA3_SL
CA3_SR
DG_ML
DG_Hilus

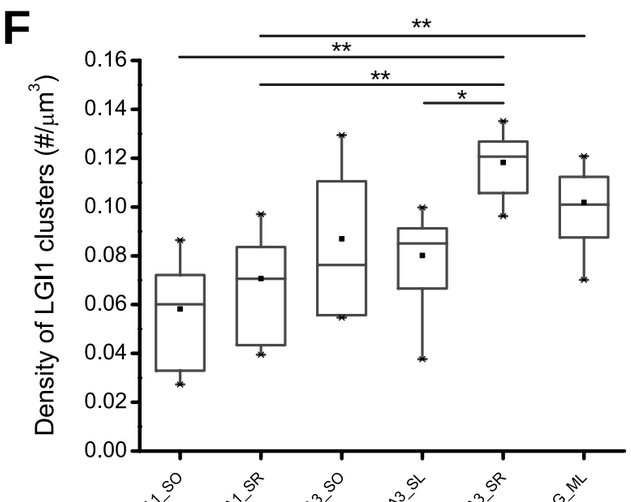
F
Density of LGI1 clusters (#/µm3)
0.16
0.14
0.12
0.10
0.08
0.06
0.04
0.02
0.00
**
**
**
*
CA1_SO
CA1_SR
CA3_SO
CA3_SL
CA3_SR
DG_ML

A

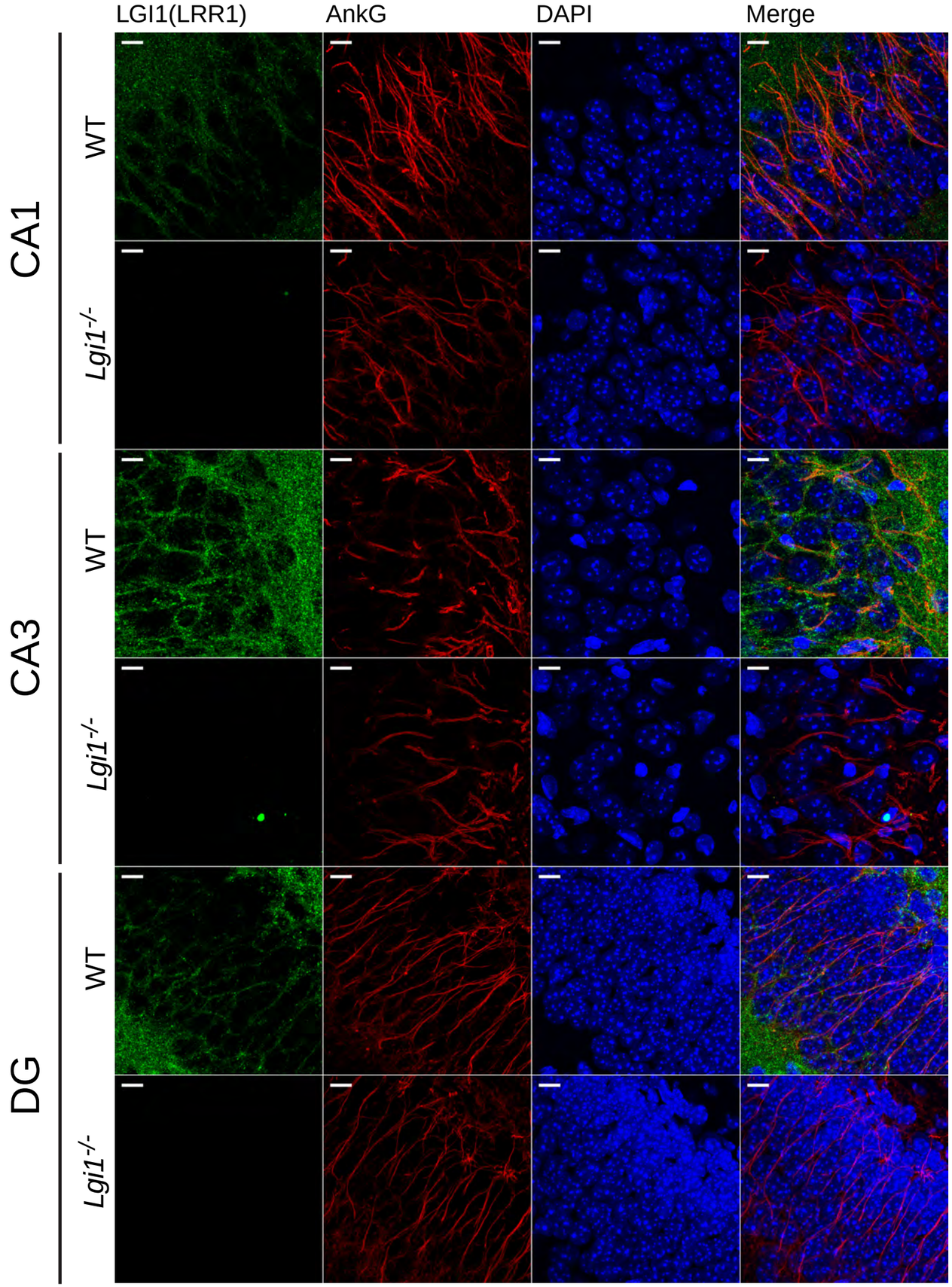
LGI1(LRR1)
AnkG
DAPI
Merge
CA1
CA3
DG
WT
Lgi1-/-

B

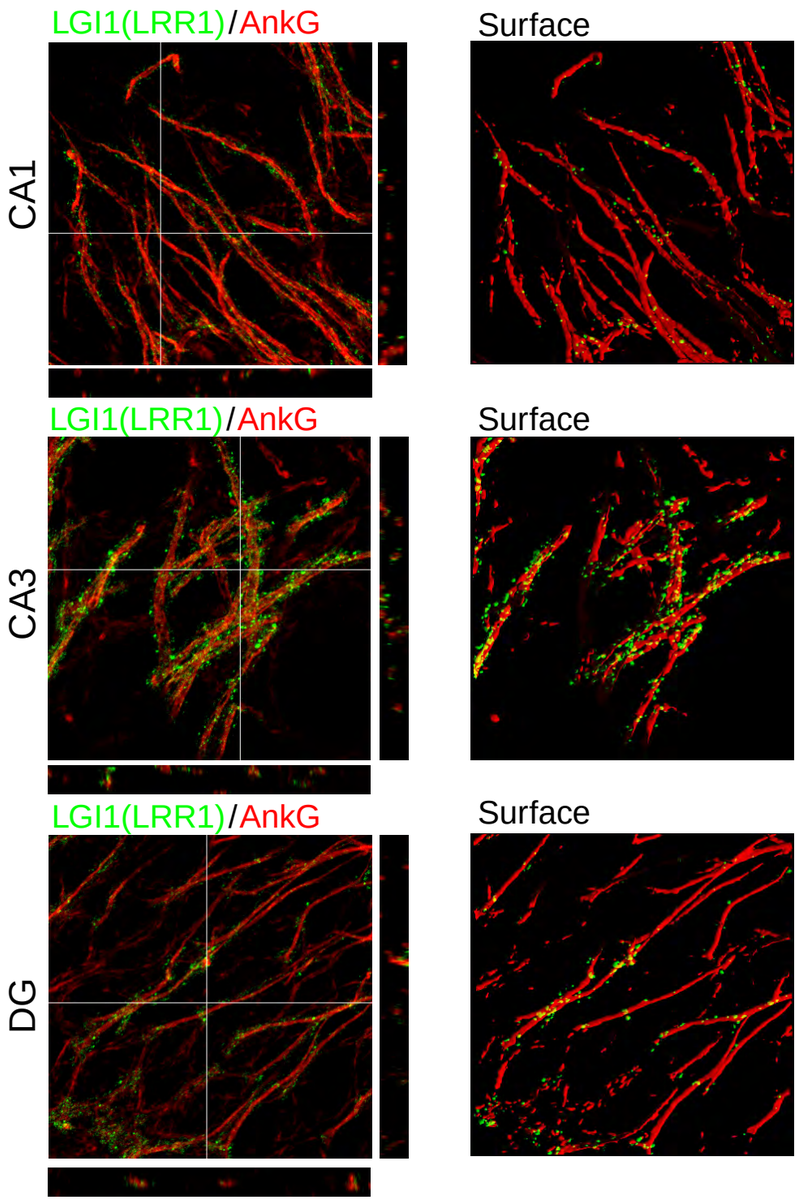
LGI1(LRR1)/AnkG
Surface
CA1
CA3
DG

C

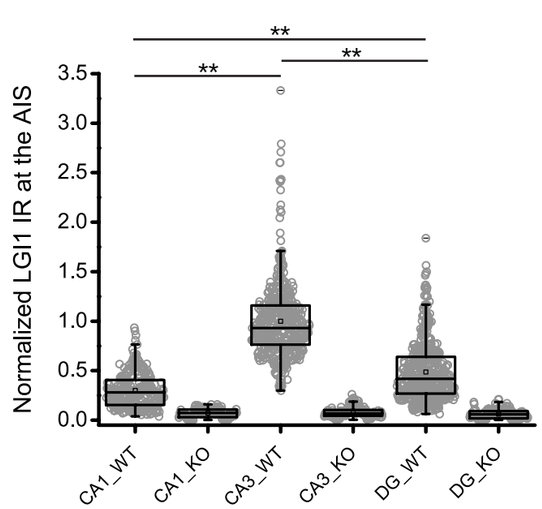
Normalized LGI1 IR at the AIS
3.5
3.0
2.5
2.0
1.5
1.0
0.5
0.0
**
**
**
CA1_WT
CA1_KO
CA3_WT
CA3_KO
DG_WT
DG_KO

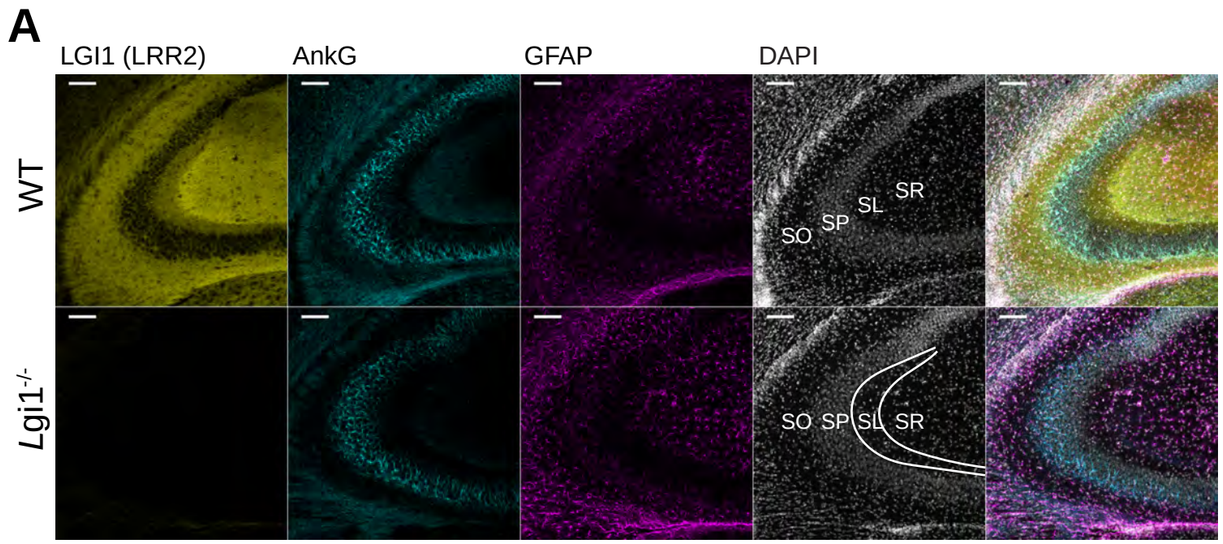
A
LGI1 (LRR2)
AnkG
GFAP
DAPI
WT
Lgi1-/-
SO
SP
SL
SR

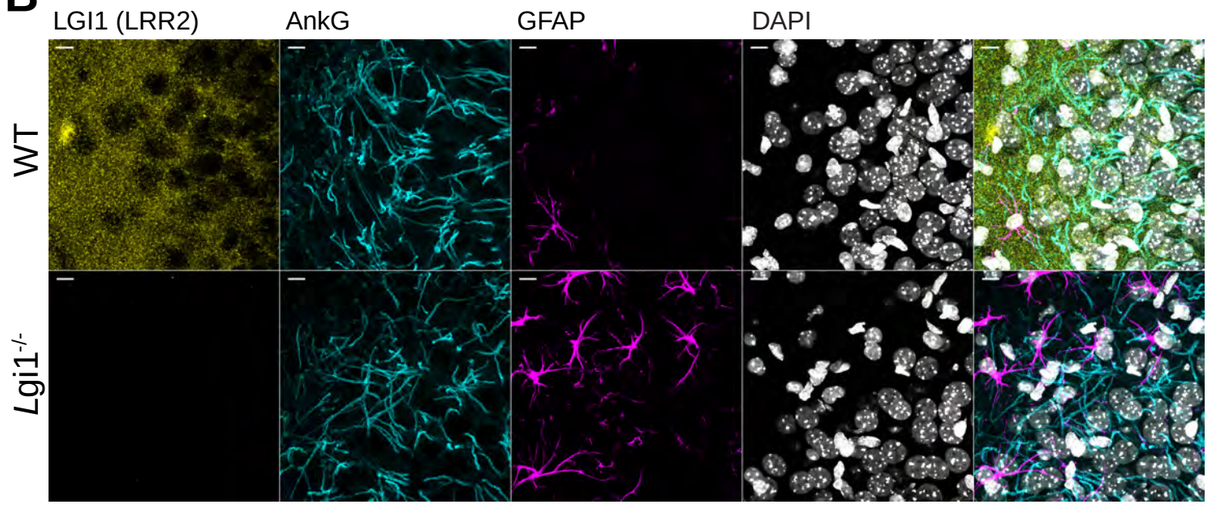
B
LGI1 (LRR2)
AnkG
GFAP
DAPI
WT
Lgi1-/-

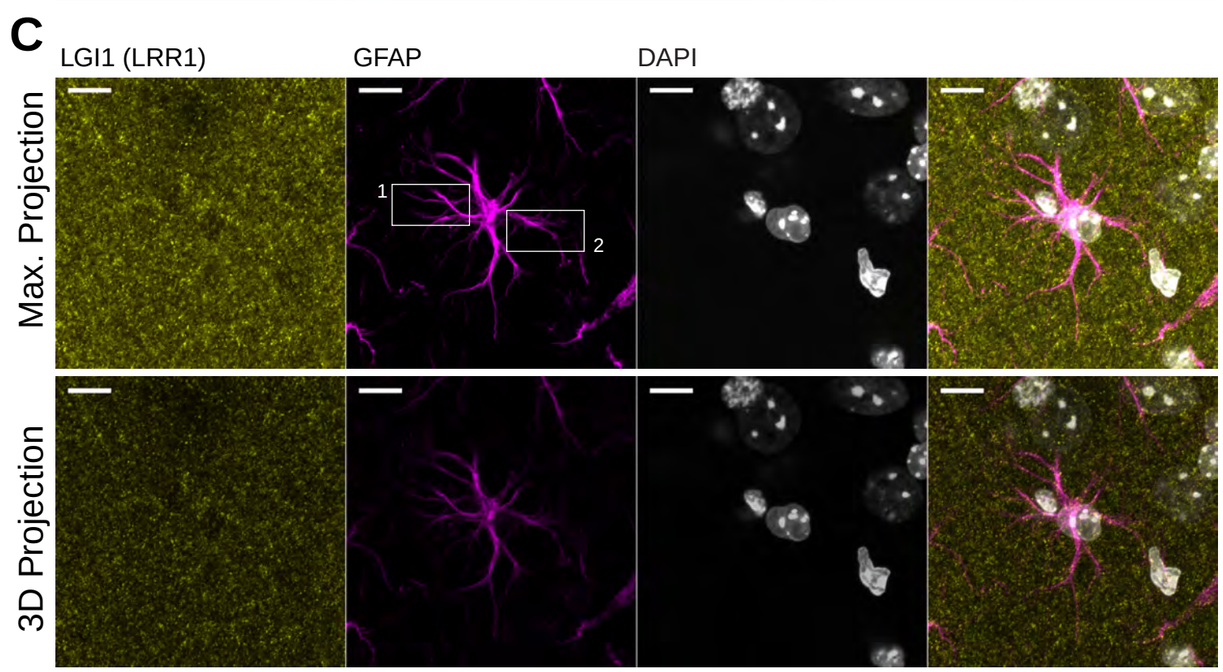
C
LGI1 (LRR1)
GFAP
DAPI
Full Z-Stack
Max. Projection
3D Projection
1
2

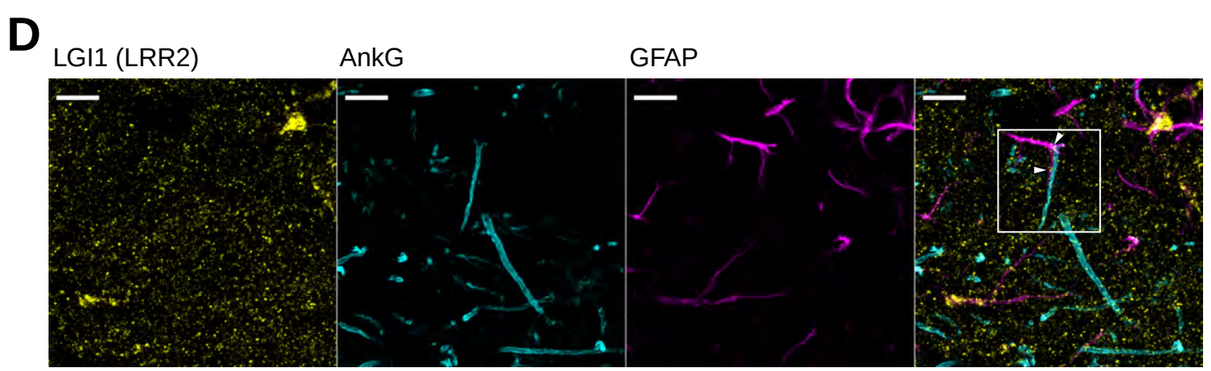
D
LGI1 (LRR2)
AnkG
GFAP

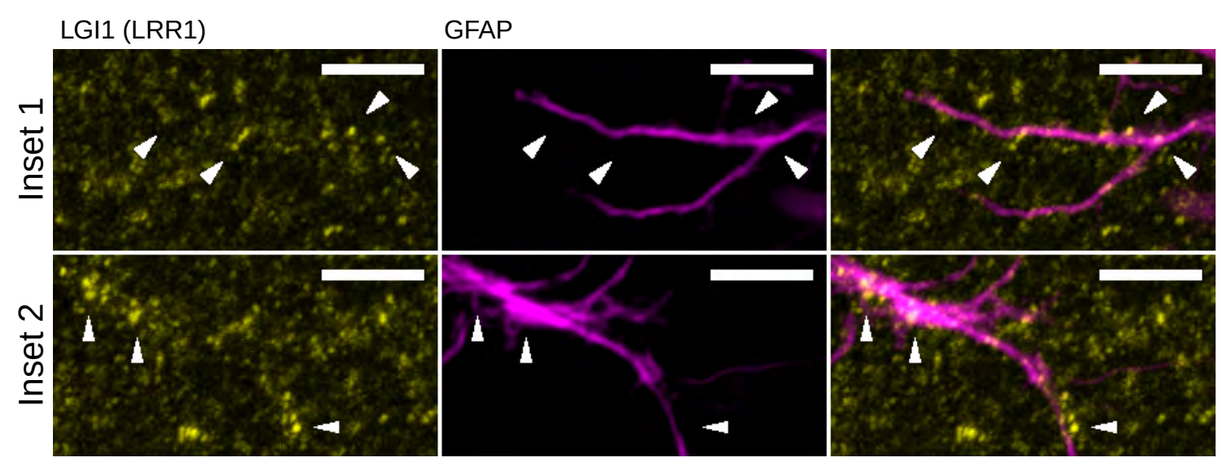
Reduced Z-Stack
LGI1 (LRR1)
GFAP
Inset 1
Inset 2

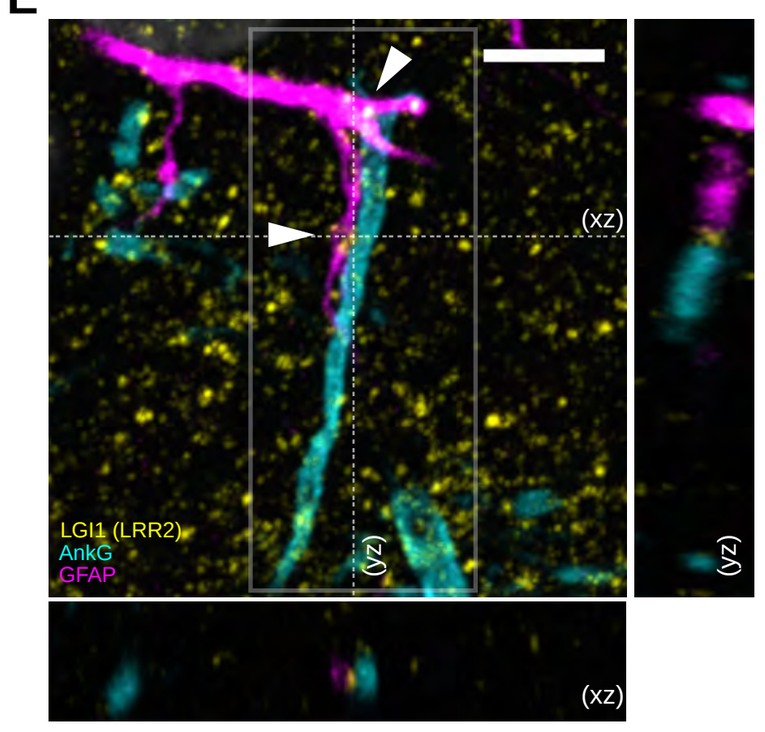
E
(xz)
(yz)
(yz)
(xz)
LGI1 (LRR2)
AnkG
GFAP

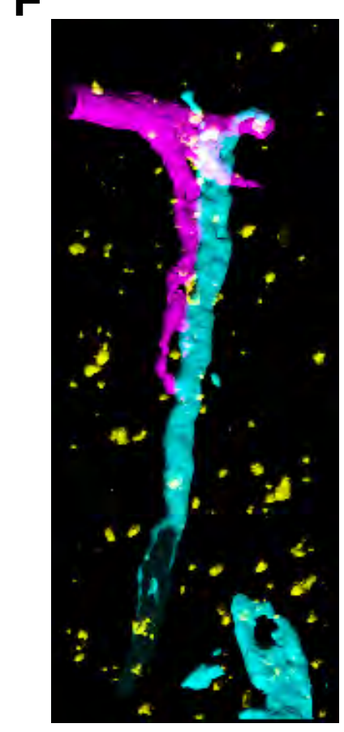
F

Fig.4

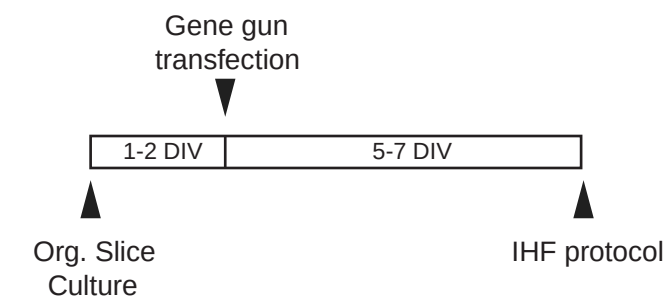
A
Gene gun transfection
1-2 DIV
5-7 DIV
Org. Slice Culture
IHF protocol

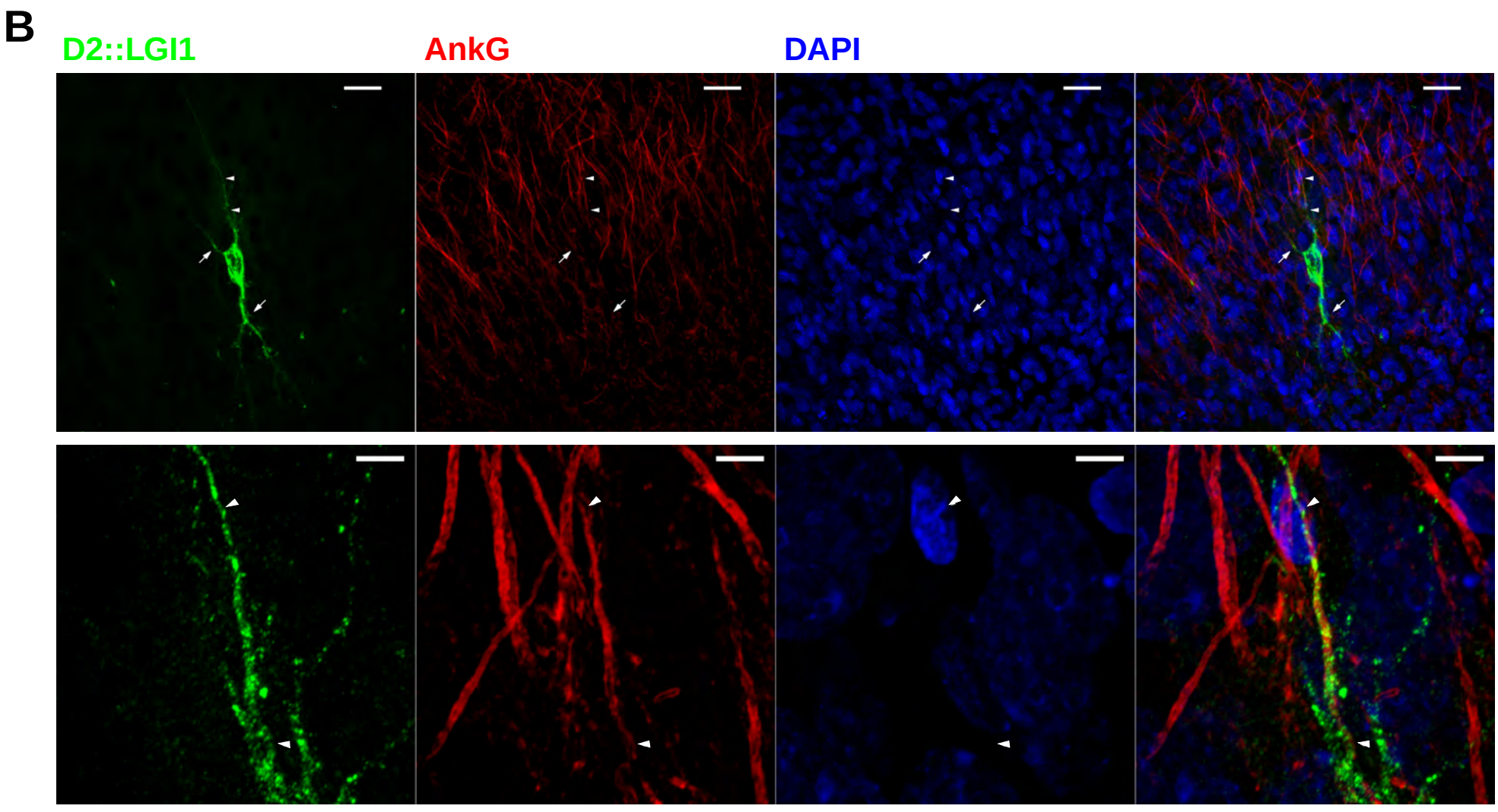
B
D2::LGI1
AnkG
DAPI

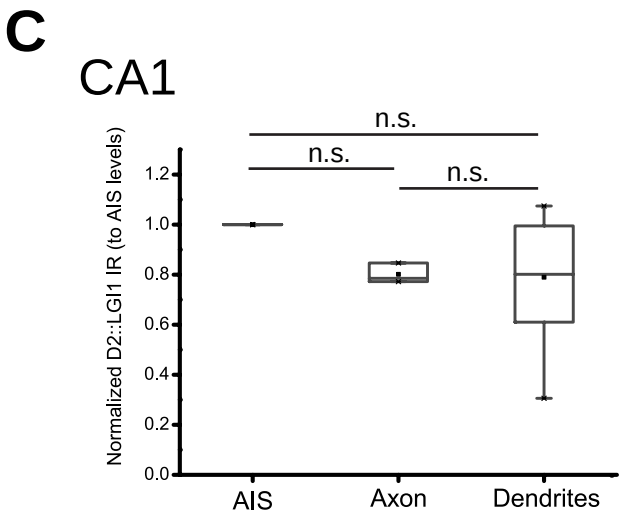
C
CA1
n.s.
n.s.
n.s.
Normalized D2::LGI1 IR (to AIS levels)
AIS
Axon
Dendrites

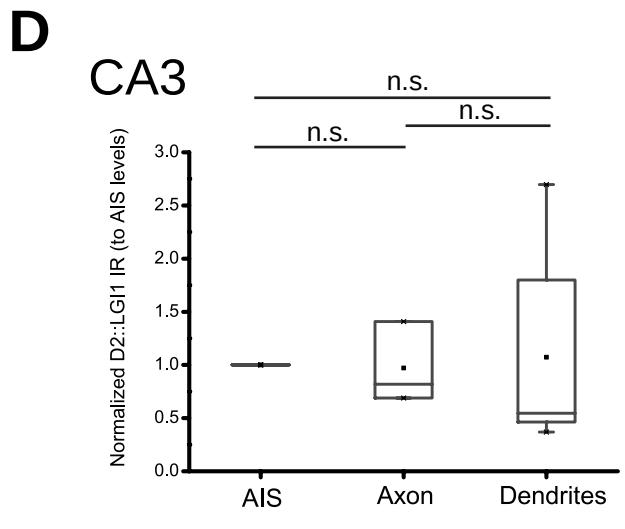
D
CA3
n.s.
n.s.
n.s.
Normalized D2::LGI1 IR (to AIS levels)
AIS
Axon
Dendrites

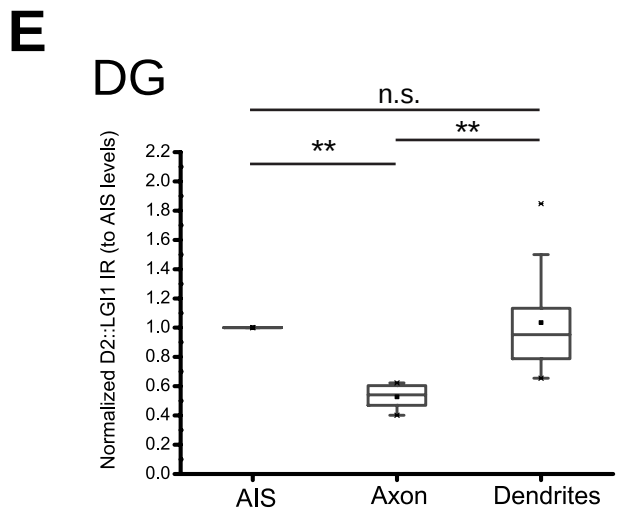
E
DG
n.s.
**
**
Normalized D2::LGI1 IR (to AIS levels)
AIS
Axon
Dendrites

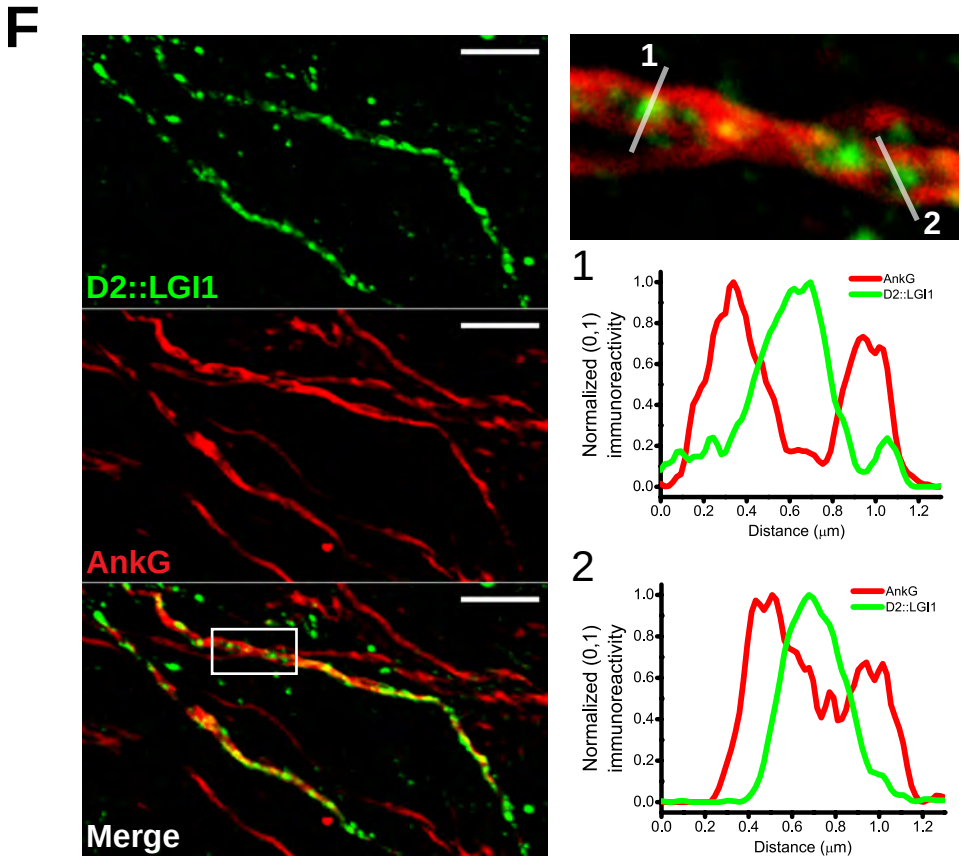
F
D2::LGI1
AnkG
Merge
1
2
Normalized (0,1) immunoreactivity
AnkG
D2::LGI1
Distance (μm)

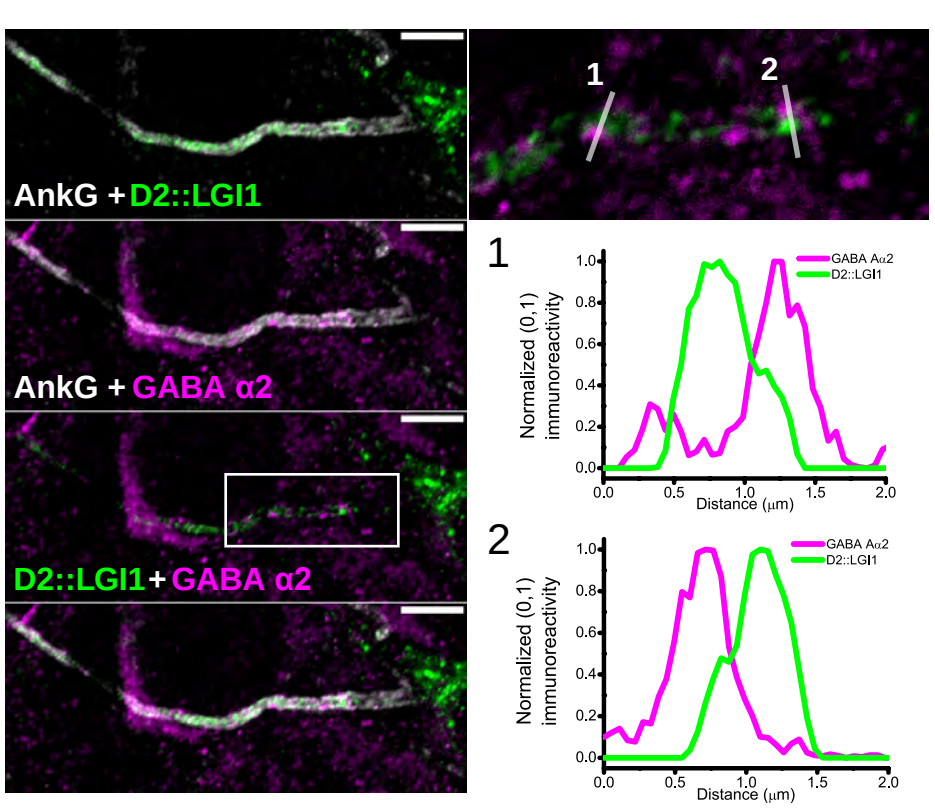
G
AnkG + D2::LGI1
AnkG + GABA α2
D2::LGI1 + GABA α2
1
2
Normalized (0,1) immunoreactivity
GABA Aα2
D2::LGI1
Distance (μm)

Fig.5

A

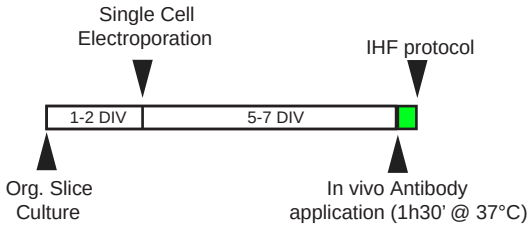
Single Cell
Electroporation
IHF protocol
1-2 DIV
5-7 DIV
Org. Slice
Culture
In vivo Antibody
application (1h30' @ 37°C)

B

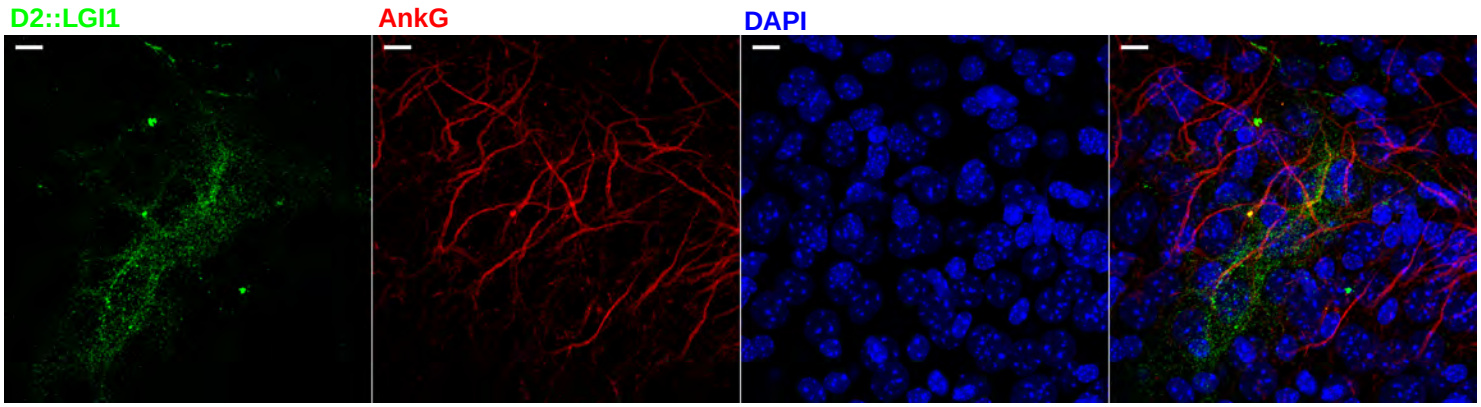
D2::LGI1
AnkG
DAPI

C

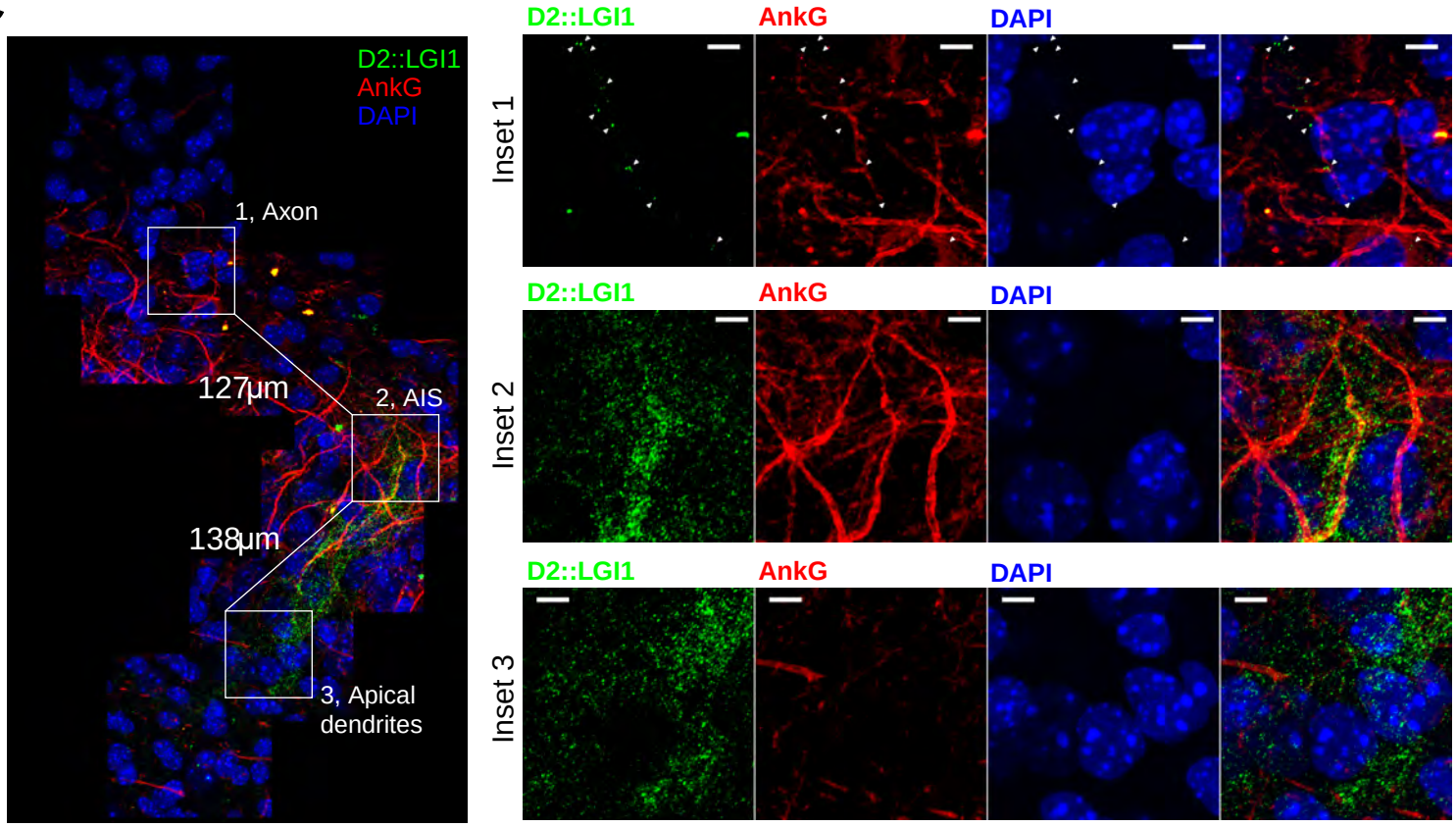
D2::LGI1
AnkG
DAPI
1, Axon
127µm
2, AIS
138µm
3, Apical
dendrites
Inset 1
Inset 2
Inset 3

Fig.6

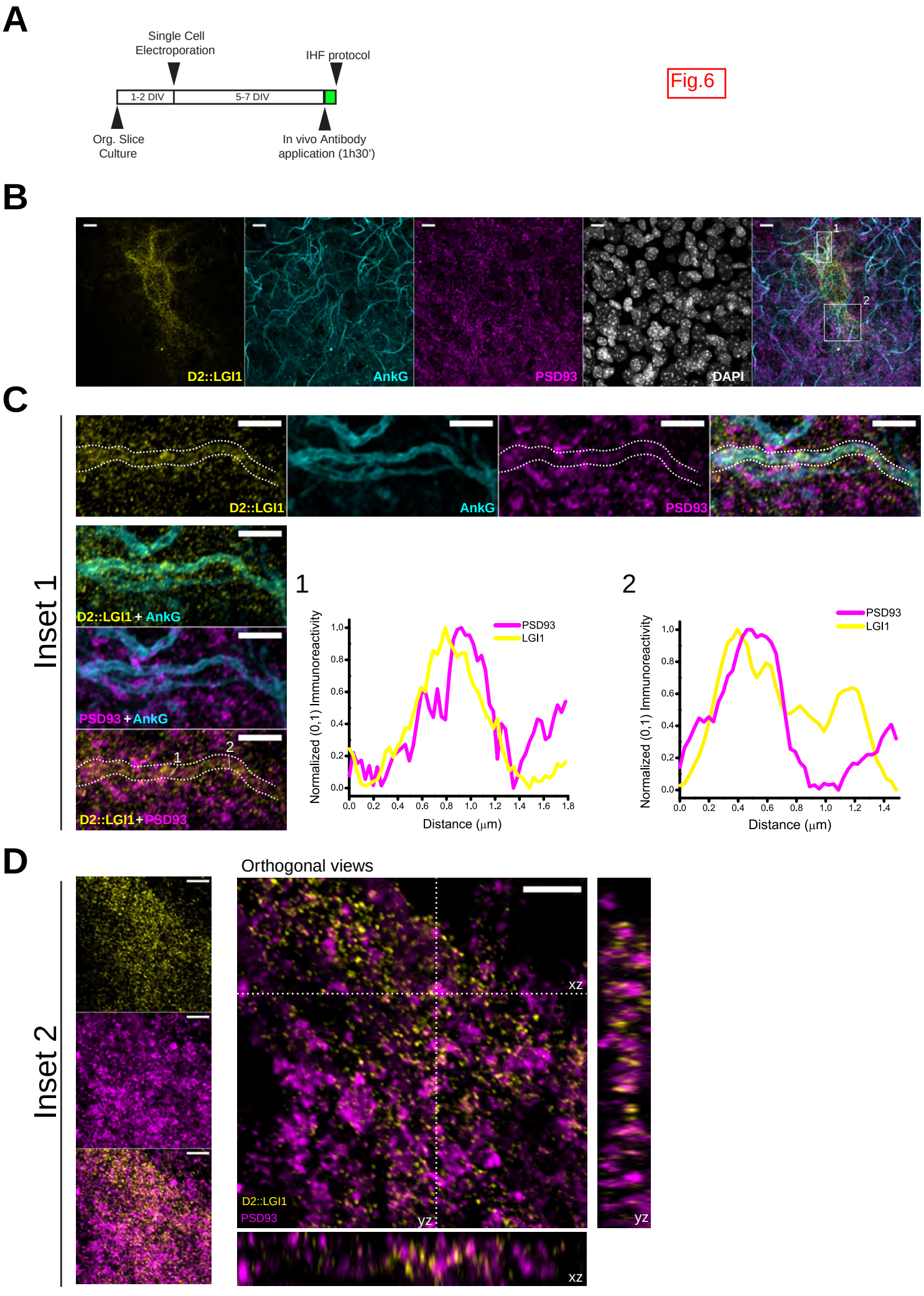
A
Single Cell Electroporation
IHF protocol
1-2 DIV
5-7 DIV
Org. Slice Culture
In vivo Antibody application (1h30')
B
D2::LGI1
AnkG
PSD93
DAPI
1
2
C
Inset 1
D2::LGI1
AnkG
PSD93
D2::LGI1 + AnkG
PSD93 + AnkG
D2::LGI1 + PSD93
1
2
Normalized (0,1) Immunoreactivity
PSD93
LGI1
Distance (μm)
D
Inset 2
Orthogonal views
xz
yz
D2::LGI1
PSD93

Fig.7

A

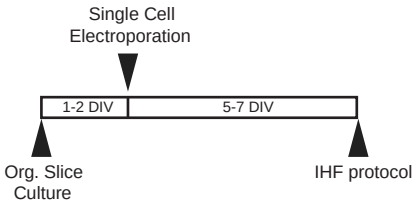

B

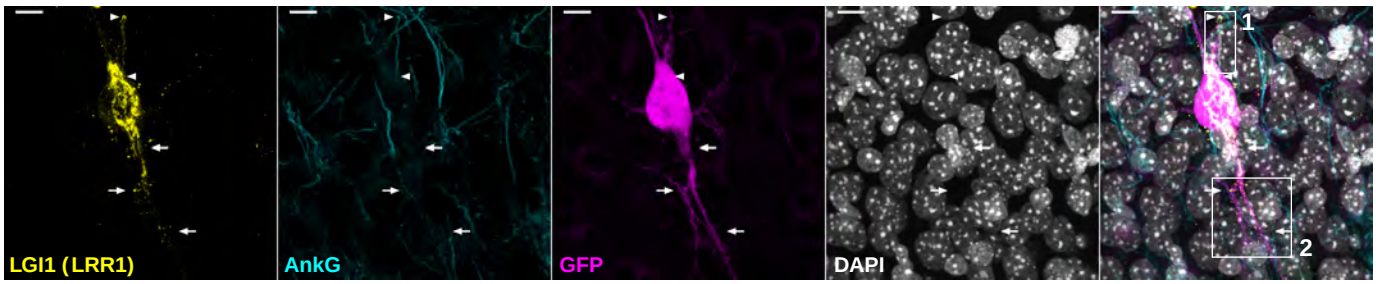

C

Inset 1

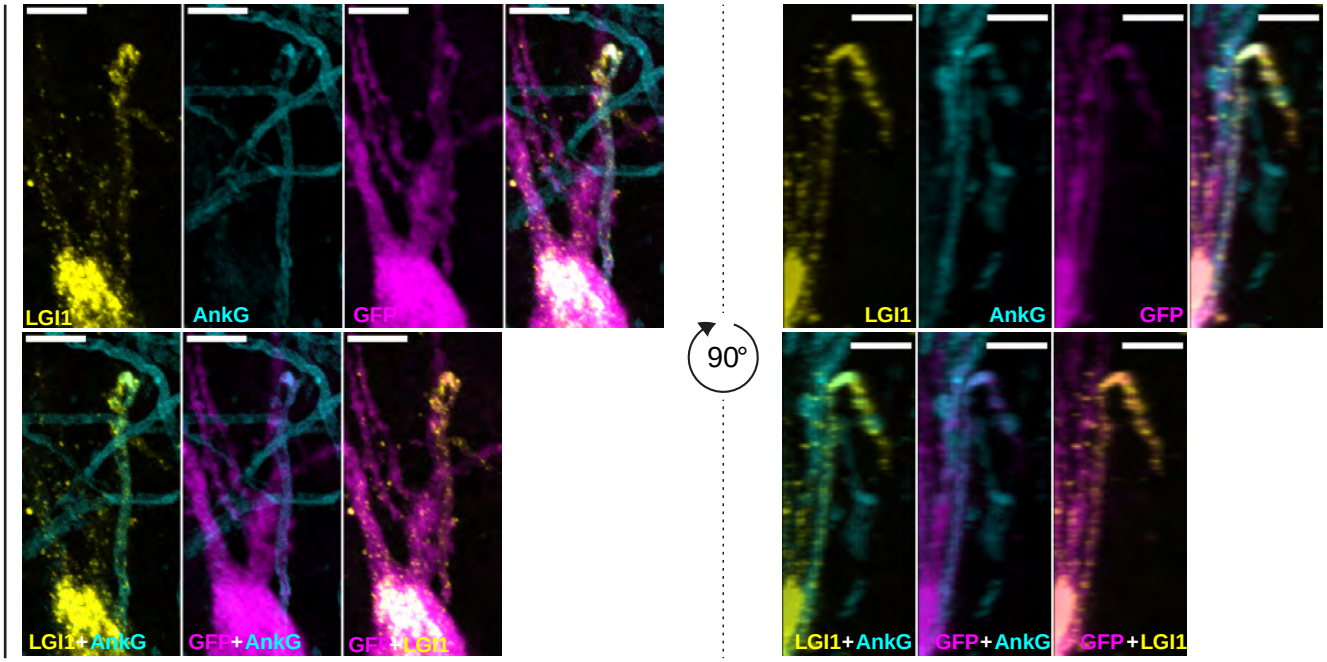

D

Inset 2

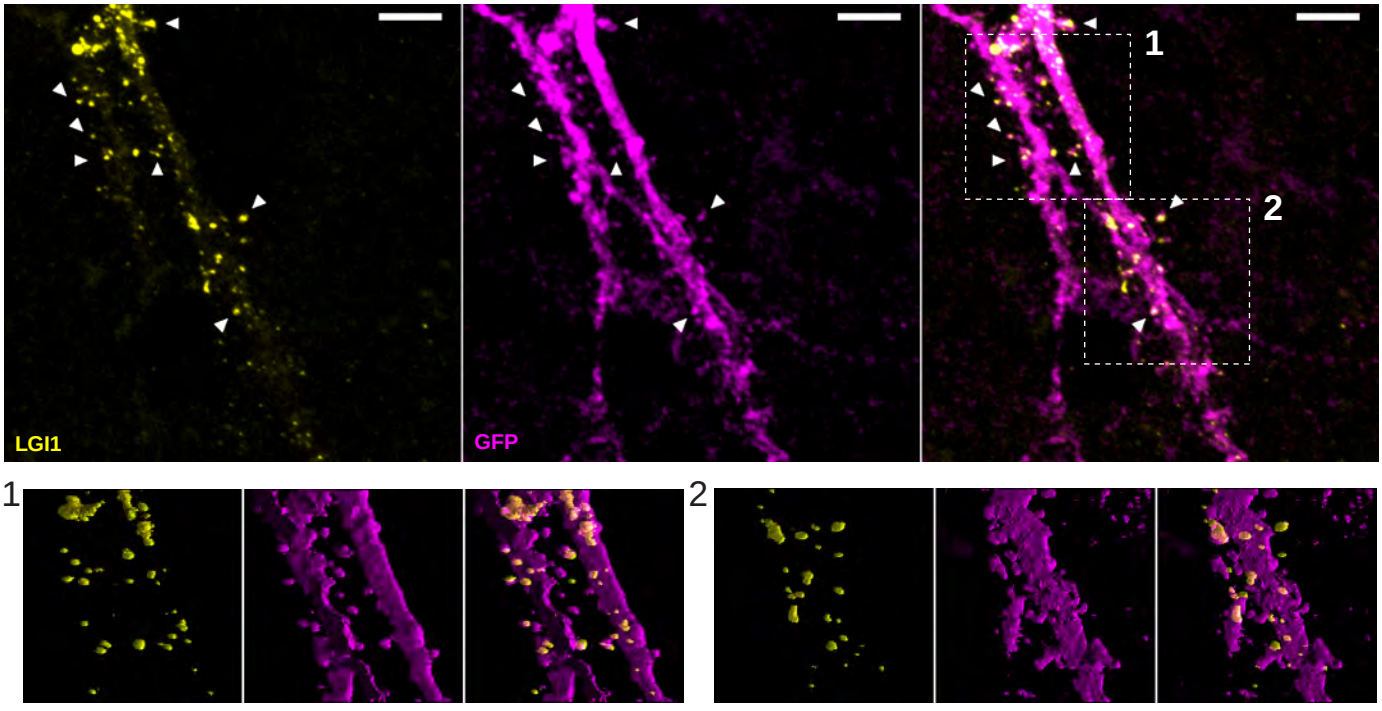

Fig.8

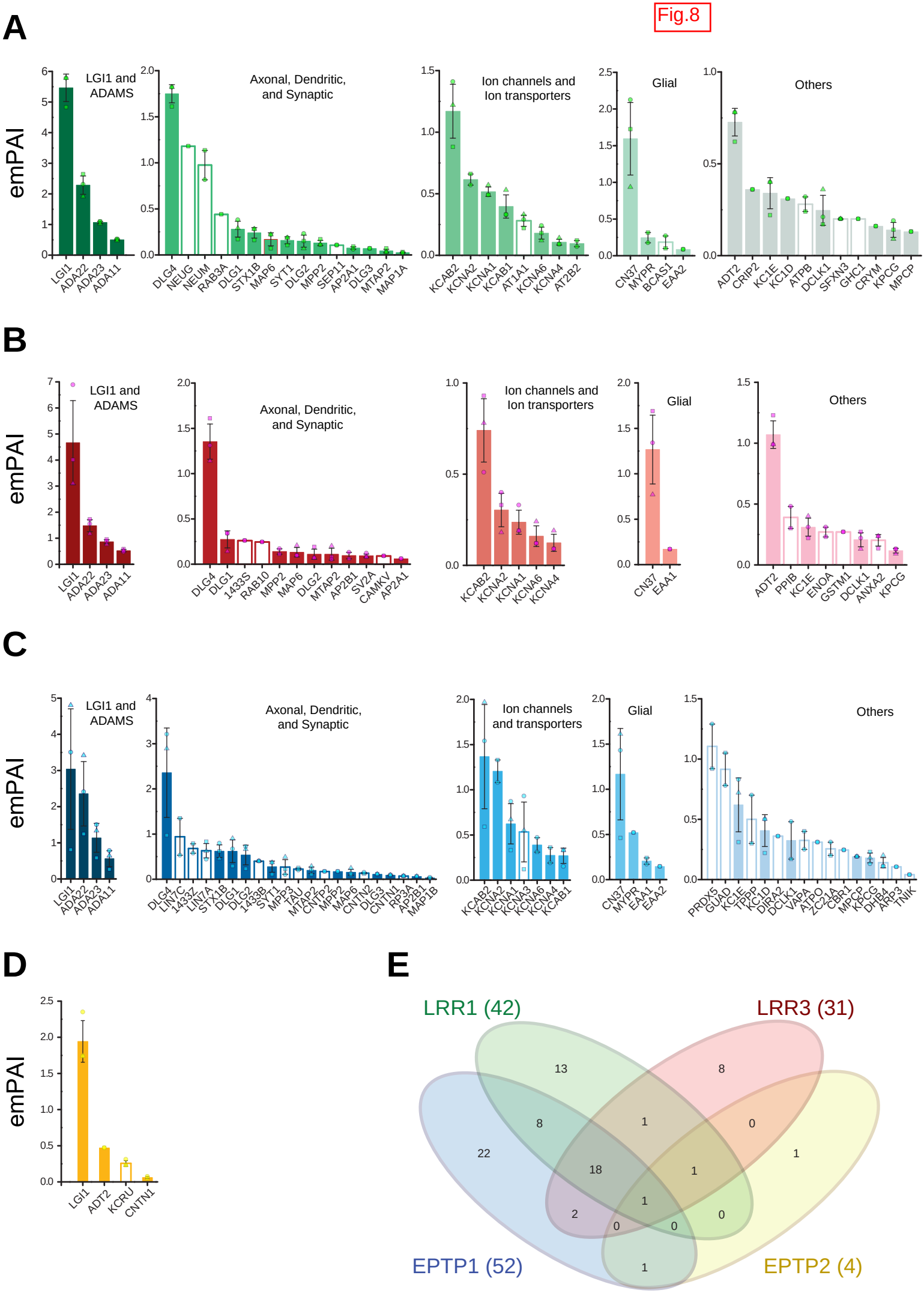
A
emPAI
LGI1 and ADAMS
LGI1 ADA22 ADA23 ADA11
Axonal, Dendritic, and Synaptic
DLG4 NEUG NEUM RAB3A DLG1 STX1B MAP6 SYT1 DLG2 MPP2 SEP11 AP2A1 DLG3 MTAP2 MAP1A
Ion channels and Ion transporters
KCAB2 KCNA2 KCNA1 KCAB1 AT1A1 KCNA6 KCNA4 AT2B2
Glial
CN37 MYPR BCAS1 EAA2
Others
ADT2 CRIP2 KC1E KC1D ATPB DCLK1 SFXN3 GHC1 CRYM KPCG MPCP
B
emPAI
LGI1 and ADAMS
LGI1 ADA22 ADA23 ADA11
Axonal, Dendritic, and Synaptic
DLG4 DLG1 1433S RAB10 MPP2 MAP6 DLG2 MTAP2 AP2B1 SV2A CAMKV AP2A1
Ion channels and Ion transporters
KCAB2 KCNA2 KCNA1 KCNA6 KCNA4
Glial
CN37 EAA1
Others
ADT2 PPIB KC1E ENOA GSTM1 DCLK1 ANXA2 KPCG
C
emPAI
LGI1 and ADAMS
LGI1 ADA22 ADA23 ADA11
Axonal, Dendritic, and Synaptic
DLG4 LIN7C 1433Z LIN7A STX1B DLG1 DLG2 1433B SYT1 MPP3 TAU MTAP2 CNTNP2 MPP2 MAP6 CNTN2 DLG3 CNTN1 RP3A AP2B1 MAP1B
Ion channels and transporters
KCAB2 KCNA2 KCNA1 KCNA3 KCNA6 KCNA4 KCAB1
Glial
CN37 MYPR EAA1 EAA2
Others
PRDX5 GUAD KC1E TPPP KC1D DIRA2 DCLK1 VAPA ATPO ZC21A CBR1 MPCP KPCG DHB4 ARP3 TNIK
D
emPAI
LGI1 ADT2 KCRU CNTN1
E
LRR1 (42)
LRR3 (31)
EPTP1 (52)
EPTP2 (4)
13
8
8
1
0
22
18
1
1
2
0
0
0
1

Electronic supplementary material

Patient-derived antibodies reveal the subcellular distribution and heterogeneous interactome of LGI1

Jorge Ramirez-Franco[1*], Kévin Debreux[1*], Johanna Extremet[1], Yves Maulet[1], Maya Belghazi[2], Claude Villard[2], Marion Sangiardi[1], Fahamoe Youssouf[1], Lara El Far[1], Christian Lévêque[1], Claire Debarnot[3], Pascale Marchot[3], Sofija Paneva[4], Dominique Debanne[1], Michael Russier[1], Michael Seagar[1], Sarosh R Irani[4,5] & Oussama El Far[1]

[1]UMR 1072, INSERM, Unité de Neurobiologie des canaux Ioniques et de la Synapse, (UNIS) Aix-Marseille Université, 13015 Marseille, France

[2]Aix-Marseille Univ, CNRS, Institute of Neurophysiopathology (INP), PINT, PFNT, 13385 Marseille cedex 5, France.

[3]Lab 'Architecture et Fonction des Macromolécules Biologiques (AFMB)', CNRS, Aix-Marseille Université, 13288 Marseille cedex 09, France.

[4]Oxford Autoimmune Neurology Group, Nuffield Department of Clinical Neurosciences, John Radcliffe Hospital, University of Oxford, Oxford, UK

[5]Department of Neurology, Oxford University Hospitals, Oxford, UK

*These authors contributed equally to this work

Correspondence to: Oussama El Far
Aix-Marseille University, INSERM,
UNIS, UMR_S 1072
51 Bvd Pierre Dramard
13015 Marseille
E-mail: oussama.el-far@inserm.fr

Contributions

OEF conceived the study, supervised the entire project, the experimental design, data interpretation and manuscript preparation. OEF and JRF designed the study, analysed and interpreted the data. JRF performed immunofluorescence experiments on slices, images treatments and analysis. SP performed immunofluorescence experiments on HEK cells and

corresponding images treatments. JRF performed Excel-based mass spectrometry analysis. LEF performed Python-based scripts for mass spectrometry analysis. JE performed brain slicing, organotypic cultures and single cell electroporation experiments. KD performed immunoprecipitation experiments and participated in immunofluorescence experiments and data analysis. JRF, KD and JE took care of mice breeding and availability of $Lgi1^{-/-}$ animals. MB and CV performed mass spectrometry experiments. CD and PM generated His-tagged LGI1 expressing viral particles, transfected cultured Sf9/21 cells and provided filtered conditioned culture medium. YM purified His-tagged recombinant LGI1. CL performed SPR experiments. DD and MR supervised the work of JE. SI provided human monoclonal anti LGI1 antibodies from limbic encephalitis patients. YM, YF and MS performed expression plasmids preparation and preliminary expression tests of recombinant constructs in heterologous systems. MS and CL contributed to the design of the study. OEF and JRF wrote the original draft of the manuscript. OEF and JRF prepared the figures. All authors edited and reviewed the manuscript.

Supplementary Material and Methods

Plasmids

pIND-IRES-EGFP comprises the Tet inducible promoter region and the entire expression cassette under the control of the ubiquitin promoter. The 473 bp Tet inducible promoter of pINDUCER11 was amplified with the forward (CAATTCAGTCGACT**GGATCC**TTTACC) and reverse (GATCGA**GCGGCCGC**CAGTGTGATGGATATCTGCAGAATTCAGGCTGGATCGGTCCCG) primers (underlined are overlap sequences with pINDUCER11), digested with BamHI and NotI (in bold) and inserted into pcDNA3.1 pre-digested with BglII/NotI. The resulting plasmid was digested with DraIII and ligated with MluI adaptors, then digested with BstBI and ligated with PstI adaptors. This 3539 bp vector fragment was ligated with the 4003 bp MluI/PstI fragment of pINDUCER11, yielding pIND-IRES-EGFP vector (7556 bp).

pIND-LGI1-IRES-EGFP was constructed as follows: the LGI1 sequence was obtained from pCDNA3.1-FLAG-LGI1 [7] (a generous gift from Stephanie Baulac). LGI1 sequence was PCR-amplified and modified by nested PCR, introducing an optimized Kozak consensus sequence in 5' and removing the FLAG tag. The signal peptide region was amplified with the forward (GGTACCGAGCTCGGACGAATTCCACCATGGAATCAGAAAGCAGCAGAAGG) and reverse (GGCATTTTGGCTTCGCTGGTTTCTTCCCCTCAGTCAGC) primers (underlined are overlaps with the LGI1 signal peptide coding sequence). The secretory LGI1 sequence was amplified with the forward (GCTGACTGAGGGGAAGAAACCAGCGAAGCCAAAATGCC) and reverse BGHR (TAGAAGGCACAGTCGAGG) primers (underlined is overlapping region with the LGI1 coding sequence). Both amplification products were mixed in equimolar amounts and amplified with the external (GGTACCGAGCTCGGACGAATTCCACCATGGAATCAGAAAGCAGCAGAAGG) and BGHR (TAGAAGGCACAGTCGAGG) primers. The resulting 1775 bp LGI1 insert was digested with EcoRI / NotI and ligated into the same sites of pIND-IRES-EGFP vector.

pIND-ΔIRES-Dendra2-LGI1: pIND-ΔIRES (6204 bp) lacking the IRES-EGFP module, was first obtained by AscI / PacI digestion of pIND-IRES-EGFP, blunting and re-ligation. Dendra2 coding sequence was inserted downstream of LGI1 signal-peptide coding sequence. It was obtained by PCR from pDendra2-LifeAct7 (Addgene #54694) and cloned by the SLIC method [2] using the forward CTGACTGAGGGGAAGAAGATGAACACCCCGGGAATTAAC and reverse primers TTTGGCTTCGCTGGTGAACCTCCAGACCACACCTGGCTGG (underlined are overlaps with LGI1 sequence).

Antibodies

Rabbit (386003, RRID: AB_2661876) and guinea pig (386005, RRID: AB_2737033) anti-ankyrinG (AnkG) and rabbit anti-GFP (132003, RRID: AB_1834147) were from Synaptic Systems. Mouse anti-synaptophysin 171B5 was a generous gift from Dr. S. Fujita, Mitsubishi Kasei Institute, Japan. Mouse anti-GFAP (75-240, RRID: AB_10672299) and mouse anti PSD-

93 (75-057, RRID: AB_2277296) were from Antibodies Incorporated. Rabbit anti-DENDRA2 (ABIN361314, RRID: AB_10789591) was from Antibodies-Online. Alexa coupled 488-goat anti-human and anti-rabbit, 594-goat anti-mouse, anti-rabbit and anti-mouse, 647-goat anti-mouse and anti-guinea pig were from Jackson ImmunoResearch.

Immunohistofluorescence of fixed brains

P14-P16 C57BL/6 wild-type mice or *Lgi1*$^{-/-}$ littermates of either sex were deeply euthanized with a Ketamine-Xylazine mix (100mg/Kg and 10mg/Kg Xylazine respectively), and transcardially perfused respectively with PBS and ice-cold 4% paraformaldehyde in PBS. Brains were removed and subsequently post-fixed overnight at 4°C in the same fixative solution. Coronal forebrain and rostral mid-brain slices were obtained by using a 7000SMZ-2 VIBROTOME (Campden Instruments) and collected as 50 μm floating sections. Slices were blocked for 90 min at room temperature (RT) in blocking solution made of PBS containing 0.3% Triton X-100 (SIGMA) and 5% Normal Goat Serum (NGS, Vector laboratories). Sections were incubated overnight (O/N) at 4°C with primary antibodies in PBS containing 0.3% Triton X-100 and 1% NGS in PBS. The following antibodies were used for immunofluorescence of fixed brains: human monoclonal anti-LGI1 (LRR1, LRR2 and LRR3) [6] at 12.8 µg/mL, 7.5 µg/mL and 6.7 µg/mL respectively, rabbit anti-AnkG (1:500), guinea pig anti-AnkG (1:500), mouse anti-synaptophysin, mouse anti-GFAP (1:400), mouse anti-PSD-93 (1:500). Afterwards, sections were washed three times (15 min each) in PBS containing 0.3% Triton X-100 and then incubated with the appropriate secondary antibodies (1:200) (2h, RT) in PBS containing 0.3% Triton X-100 and 1% NGS. Finally, sections were washed three times in a solution containing 0.3% Triton X-100 in PBS, incubated with DAPI (1.5 µg/mL; Sigma-Aldrich) for 10 min, washed one last time in PBS and mounted in Vectashield (Vector laboratories). Slides were kept at 4°C until use. Images were acquired on a Zeiss LSM-780 Confocal scanning microscope. All experiments involving WT and *lgi1*$^{-/-}$ comparisons were performed in parallel and the same acquisition settings were applied to both genotypes.

Hippocampal slice cultures and transfection of hippocampal neurons

Young Wistar rats (P7-P8) or mice (P7-P10) of either sex, were decapitated, the hippocampi were removed, and individual slices were collected (350µm) and placed on Millicell membranes (Merck-Millipore) inserted into 35mm Petri dishes containing 1mL of culture medium. The culture medium contained (in mL) 25 MEM, 12.5 HBSS, 12.5 horse serum, 0.5 penicillin (10,000U/mL), 0.5 streptomycin (10mg/mL), 0.8 glucose (1M), 0.1 ascorbic acid (1mg/mL), 0.4 HEPES (1M, pH 7.4), 0.5 B27, and 8.95 milli-Q H_2O. For rat organotypic slices, 5 µM Ara-C was added to the slices starting at 1DIV to limit glial proliferation and removed at 3 DIV. For Gene Gun (Helios Gene Gun, Bio-Rad) transfection, Gene Gun bullets were prepared following the manufacturer's instructions using 1-µm gold micro-carriers and a gold (mg) / cDNA (µg) ratio of 6/25. DIV 2-3 cultures were shot (1 µg DNA per bullet) at 120 psi. Single cell electroporation of CA3 pyramidal cells was performed at DIV 4-5 with an Axoporator 800A (Molecular Devices). Borosilicate pipettes (7-10 MΩ) were filled with the following solution (in mM): K-gluconate 120, KCl 20, HEPES 10, EGTA 0.5, $MgCl_2$ 2, Na_2ATP 2, and NaGTP 0.3 (pH 7.4). Plasmids were diluted to a final concentration of 33 ng/µl in the pipette solution. Slices were placed in an extracellular solution containing (in mM): 125 NaCl, 26 $NaHCO_3$, 3 $CaCl_2$, 2.5 KCl, 2 $MgCl_2$, 0.8 NaH_2PO_4, and 10 D-glucose, continuously bubbled with 95% O_2–5% CO_2. A loose-seal (25-40 MΩ) was formed between the pipette and the selected cell and then a train of -12 V pulses (pulse width: 0.5 ms, frequency: 50 Hz) was delivered for 500ms. When indicated, doxycycline (300 ng/mL) was added to the culture medium to induce protein expression under the control of Tet-on regulatory elements. The use of single cell electroporation technique in a *Lgi1*$^{-/-}$ background presents three main advantages, i) it limits the signal of a non-engineered version of LGI1 to a single neuron in a native environment, ii) it further validates the specificity of the monoclonal antibody (LRR1) iii) it

provides an opportunity to co-express a soluble GFP to trace neuronal morphology and to follow the distribution of LGI1 clusters throughout the transfected neuronal processes.

Immunofluorescence of organotypic slices

Organotypic slices were rinsed in PBS at 37°C and immediately immersed in ice-cold 4% paraformaldehyde in PBS. Slices were fixed at 4°C for 15 minutes and subsequently incubated in PBS containing 50 mM NH_4Cl (15 min, RT) in order to quench the remaining free aldehyde groups. Afterwards, the Millicell membrane containing the slices was cut with a scalpel, and the slices were blocked (O/N, 4°C) in PBS containing 0.5% Triton X-100 and 10% NGS. Then, slices were incubated with the primary antibodies (24h, 4°C) in a solution containing 0.5% Triton X-100 and 2% NGS in PBS. The following antibodies were used in these experiments: human monoclonal anti-LGI1 (LRR1, 12.8 µg/mL), rabbit anti-DENDRA2 (1:200), rabbit anti-GFP (1:500), guinea pig anti-AnkG (1:500), mouse anti-PSD93 (1:500). Afterwards, sections were washed three times (20min each) in PBS containing 0.5% Triton X-100 and then incubated with the appropriate secondary antibodies (1:200) (2h, RT) in PBS containing 0.3% Triton X-100 and 1% NGS. Finally, sections were washed three times (20min each) in a PBS solution containing 0.5% Triton X-100, incubated with DAPI (1.5 µg/mL; Sigma-Aldrich) for 10 min, washed one last time in PBS and mounted in Vectashield (Vector laboratories). Slides were kept at 4°C until use.

Immunofluorescence on HEK cells

Transfection of HEK cells and characterization of EPTP1 and 2 specificity were performed as described in [6].

Image analysis

For the quantification of the expression levels of LGI1 in forebrain and hippocampal regions, maximal projections of z-stacks consisting of 3 optical slices acquired with a 10x objective were

used. Several ROIs of the same size were drawn in different brain regions and the average grey value immunoreactivities were normalized to the overall hippocampal signal (for different brain region comparisons), to dorsal CA3 (for the analysis of the dorso-ventral pattern of expression), or to CA3 Stratum Radiatum (for comparisons within the dorsal hippocampus). The mentioned regions were chosen for normalization as they showed the highest immunoreactivity for LGI1 for each type of comparison. For the analysis of the density of LGI1 clusters, 63x images were acquired as z-stacks and the LGI1 signal was used to detect 3D objects with the 3D objects counter plugin [1]. Clusters' density was expressed as the number of LGI1 clusters/μm^3. For the analysis of LGI1 expression at the AIS, several ImageJ plugins were used in combination in a custom-written ImageJ macro. Briefly, z-stacks of 10 to 20 optical slices were acquired with a 63x objective in the different hippocampal subregions (CA1, CA3 and DG), and AnkG signal was used to detect 3D objects with the 3D objects counter plugin [1]. The objects were then added to the 3D ROI manager [5] and a 3D binary mask was created. The ROIs in this binary mask were processed with binary operators (Dilate and Fill holes) and the selection mask was over-imposed to the LGI1 z-stacks. The LGI1 signal ascribable to the AIS was quantified as average grey values with the 3D ROI manager, and compared between different hippocampal regions. For visual clarity in Fig. 3, LGI1 signal not corresponding to the AISs was erased using the inverse of selection for the previously described 3D mask. Then, maximal projections of 10 optical slices z-stacks were rendered and presented along with the orthogonal views of each maximal projection. VolumeJ was used to render volumetric reconstructions. For colocalization analysis, z-stacks of 10 optical slices were background subtracted and analyzed using the Intensity Correlation Analysis (ICA) plugin [3]. Colocalization values were expressed as Manders' overlapping coefficients (MOC) since the Ch1:Ch2 pixel ratio was ~1 [4].

Mass spectrometry analysis and data processing

Immunoprecipitated proteins were concentrated on a stacking gel that was cut into small pieces, rinsed three times with 50% acetonitrile in water, reduced with DTT, alkylated with

iodoacetamide and submitted for tryptic digestion overnight at 37°C in 25 mM ammonium bicarbonate. Peptides were extracted three times with a mixture of 50% acetonitrile and 0.1% formic acid then dried using a speedvac.

After resuspension with 2% acetonitrile and 0.1% formic acid mixture, samples were analyzed by mass spectrometry using a hybrid Q-Orbitrap mass spectrometer (Q-Exactive, Thermo Fisher Scientific, United States) coupled to a nanoliquid chromatography (LC) Dionex RSLC Ultimate 3000 system (Thermo Fisher Scientific, United States). Samples were trapped with a C18 PepMap 300 trap column (300 µm × 5 mm, C18, 5 µm, 300 Å) and desalted with 0.1% formic acid in water for 3 min at a flow rate of 20 µl/min. Peptide separation was performed on an Acclaim PepMap RSLC capillary column (75 µm × 15 cm, nanoViper C18, 2 µm, 100 Å) at a flow rate of 300 nl/min. The analytical gradient was run with various percentages of acetonitrile and 0.1% formic acid in the following manner: (1) 2.5–25% for 57 min, (2) 25–50% for 6 min, (3) 50-90% for 1 min, and (4) 90% for 10 min. MS spectra were acquired at a resolution of 35,000 within a mass range of 400–1,800 m/z. Ion accumulation was set at a maximum injection time of 100 ms. Fragmentation spectra of the 10 most abundant peaks (Top10 method) were acquired with high-energy collision dissociation (HCD) at a normalized collision energy of 27%.

All raw data files generated by MS were processed to generate mgf files and searched against the Swissprot database (Swissprot version june 2019, (560,118 sequence), with the taxonomy mus musculus, using the MASCOT software (www.matrixscience.com, version 2.3). Search parameters were as follows: mass tolerance: 10 ppm on parent ion and 0.02 Da on fragment ions, and a maximum of two missed tryptic cleavages. Methionine oxidation as well as carbamidomethylation of cysteine were considered as variable modification. The database was searched in the decoy mode. The emPAIs were automatically calculated by the MASCOT algorithm. All samples were analyzed in triplicates. For each antibody, interactomes from wild type samples were subtracted from the background interactomes obtained from LGI1 knockout samples using Excel and homemade python scripts. Partner proteins were considered positive when the emPAIs from WT samples were above 3 compared to those from *Lgi1*$^{-/-}$ tissue.

Keratins, ribosomal proteins, transcription factors and immunoglobulins were excluded from the list of candidates. Candidate proteins were classified using the pantherdb web site (www.pantherdb.org).

1 Bolte S, Cordelieres FP (2006) A guided tour into subcellular colocalization analysis in light microscopy. J Microsc 224: 213-232 Doi 10.1111/j.1365-2818.2006.01706.x

2 Li MZ, Elledge SJ (2012) SLIC: a method for sequence- and ligation-independent cloning. Methods Mol Biol 852: 51-59 Doi 10.1007/978-1-61779-564-0_5

3 Li Q, Lau A, Morris TJ, Guo L, Fordyce CB, Stanley EF (2004) A syntaxin 1, Galpha(o), and N-type calcium channel complex at a presynaptic nerve terminal: analysis by quantitative immunocolocalization. J Neurosci 24: 4070-4081 Doi 10.1523/JNEUROSCI.0346-04.2004

4 Manders EMM, Verbeek FJ, Aten JA (1993) Measurement of co-localization of objects in dual-colour confocal images. J Microsc 169: 375-382 Doi 10.1111/j.1365-2818.1993.tb03313.x

5 Ollion J, Cochennec J, Loll F, Escude C, Boudier T (2013) TANGO: a generic tool for high-throughput 3D image analysis for studying nuclear organization. Bioinformatics 29: 1840-1841 Doi 10.1093/bioinformatics/btt276

6 Ramberger M, Berretta A, Tan JMM, Sun B, Michael S, Yeo T, Theorell J, Bashford-Rogers R, Paneva S, O'Dowd Vet al (2020) Distinctive binding properties of human monoclonal LGI1 autoantibodies determine pathogenic mechanisms. Brain : a journal of neurology 143: 1731-1745 Doi 10.1093/brain/awaa104

7 Senechal KR, Thaller C, Noebels JL (2005) ADPEAF mutations reduce levels of secreted LGI1, a putative tumor suppressor protein linked to epilepsy. Hum Mol Genet 14: 1613-1620 Doi 10.1093/hmg/ddi169

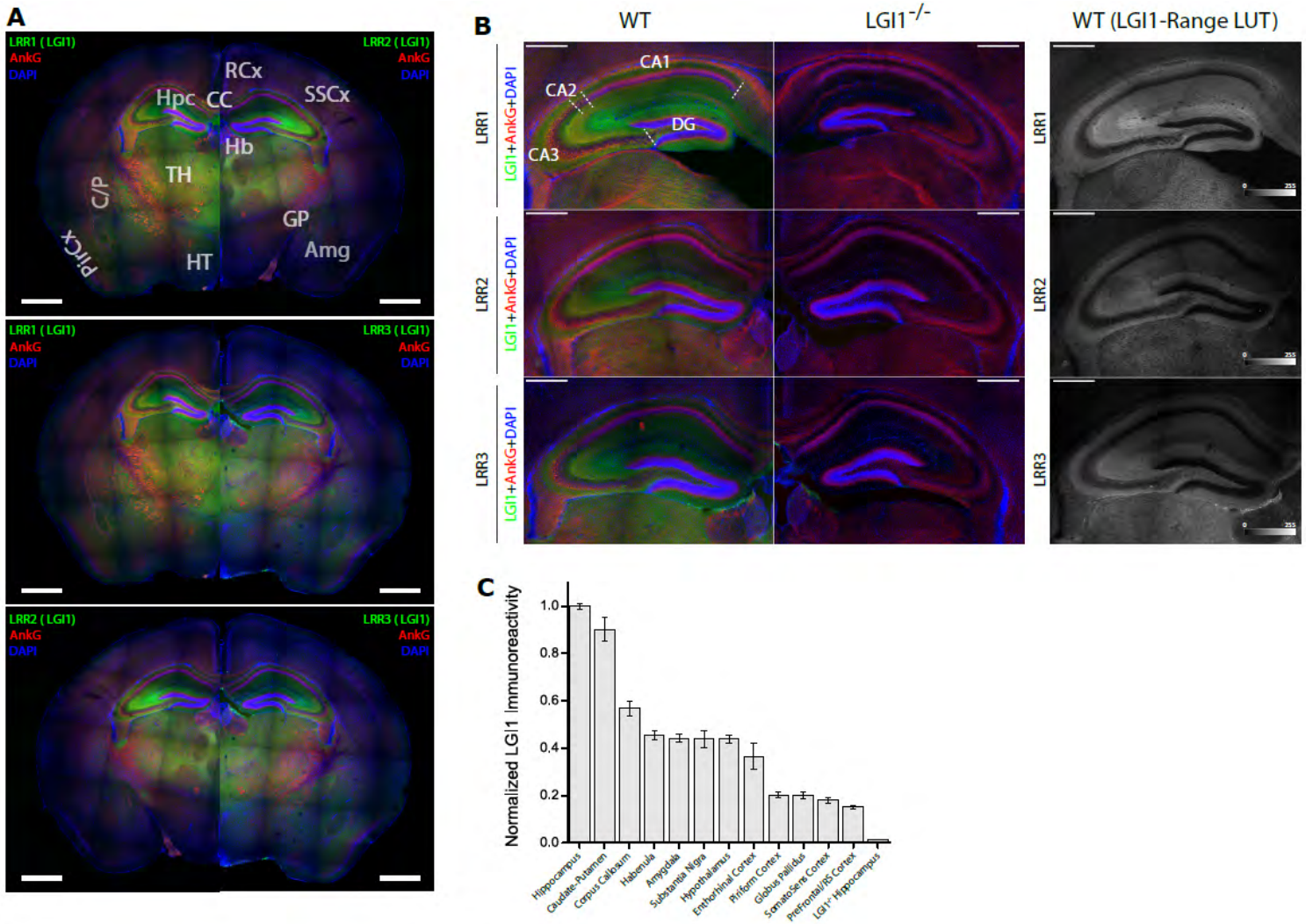

Supplementary Fig. 1 Validation and characterization of human monoclonal anti-LGI1 antibodies in the mouse brain. (**A**) Paired comparison of the immunoreactivity pattern of different antiobies in the mouse hippocampus showing LRR1 vs. LRR2 (top panels), LRR1 vs. LRR3 (middle panels), and LRR2 vs. LRR3 (bottom panels). The LGI1 signal is always shown in green. Slices were counter-stained with AnkG (red) and DAPI (blue). Scale bar = 1 mm. (**B)** Antibody validation showing a complete absence of immunostaining in the LGI1$^{-/-}$ hippocampus for LRR1 (top panels), LRR2 (middle panels) and LRR3 (bottom panels). In the right column, a range-color look-up table has been assigned to the LGI1 signal of each one of the antibodies to visually compare their immunostaining patterns. Scale bar = 0.5 mm. (**C**) Comparison of normalized immunoreactivity levels of LGI1 in different prosencephalic and mesencephalic structures. Columns and error bars show mean ± SEM. n = 4 independent experiments (WT vs *Lgi1*$^{-/-}$; LRR1 n = 1; LRR2 n = 2; LRR3 n = 1). n Hippocampus = 90 ROIs, n Amygdala = 90 ROIs; n Corpus callosum = 65 ROIs; n Caudate/Putamen = 55 ROIs; n Globus Pallidus = 30 ROIs; n Substantia nigra = 60 ROIs; n Habenula = 60 ROIs; n Hypothalamus = 95 ROIs; n Entorhinal cortex = 25 ROIs, n Piriform Cortex= 110 ROIs; n Prefrontal cortex = 160 ROIs; n Somatosensory Cortex = 95 ROIs; n *Lgi1*$^{-/-}$ hippocampus = 135 ROIs. Data obtained with different antibodies were normalized to WT hippocampal levels in each experiment, and pooled thereafter

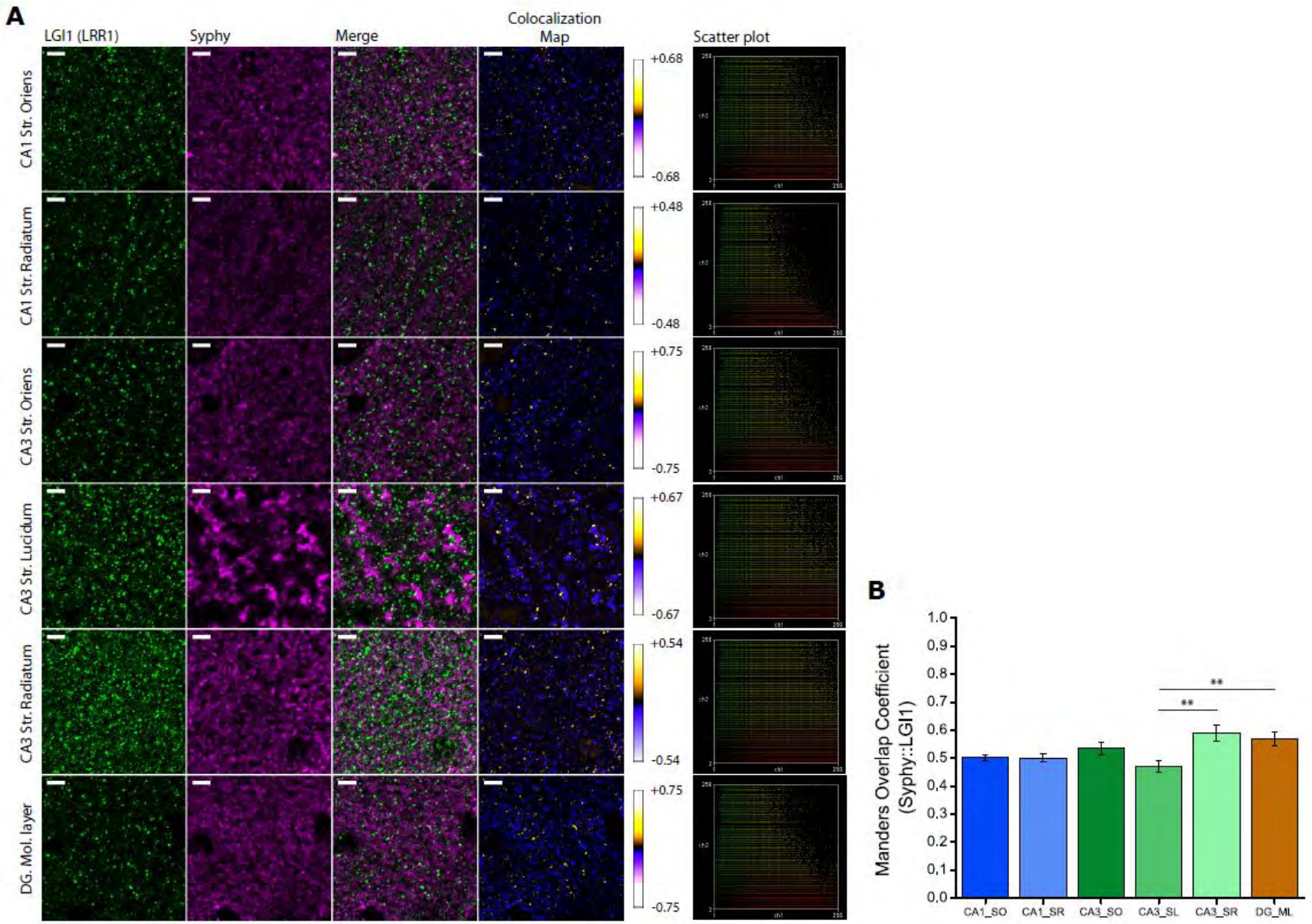

Supplementary Fig. 2 LGI1 partially colocalizes with the presynaptic marker synaptophysin in the hippocampus. (**A**) High-magnification pictures of LGI1 (green, LRR1) and synaptophysin (magenta) in the different hippocampal strata. Colocalization maps are shown (right columns) with their respective colocalization index values. Scatter-plots illustrate partial colocalization in all the analysed regions. Scale bar = 5 µm. (**B**) Manders' Overlapping coefficients for LGI1::synaptophysin colocalization in the different regions analyzed. Columns and error bars show mean ± SEM. *n* = 2 independent experiments (WT; LRR1 *n* = 1; LRR2 *n* = 1). For the sake of clarity only significant comparisons are shown. **p*<0.05; ***p*<0.01. Any other comparison is non-significant. *n* CA1 Str. Oriens = 8 Fields of view; ROIs; *n* CA1 Str. Radiatum = 8 Fields of view; *n* CA3 Str. Oriens = 8 Fields of view; *n* CA3 Str. Lucidum = 8 Fields of view; *n* CA3 Str. Radiatum = 8 Fields of view; *n* DG Molecular Layer = 8 Fields of view

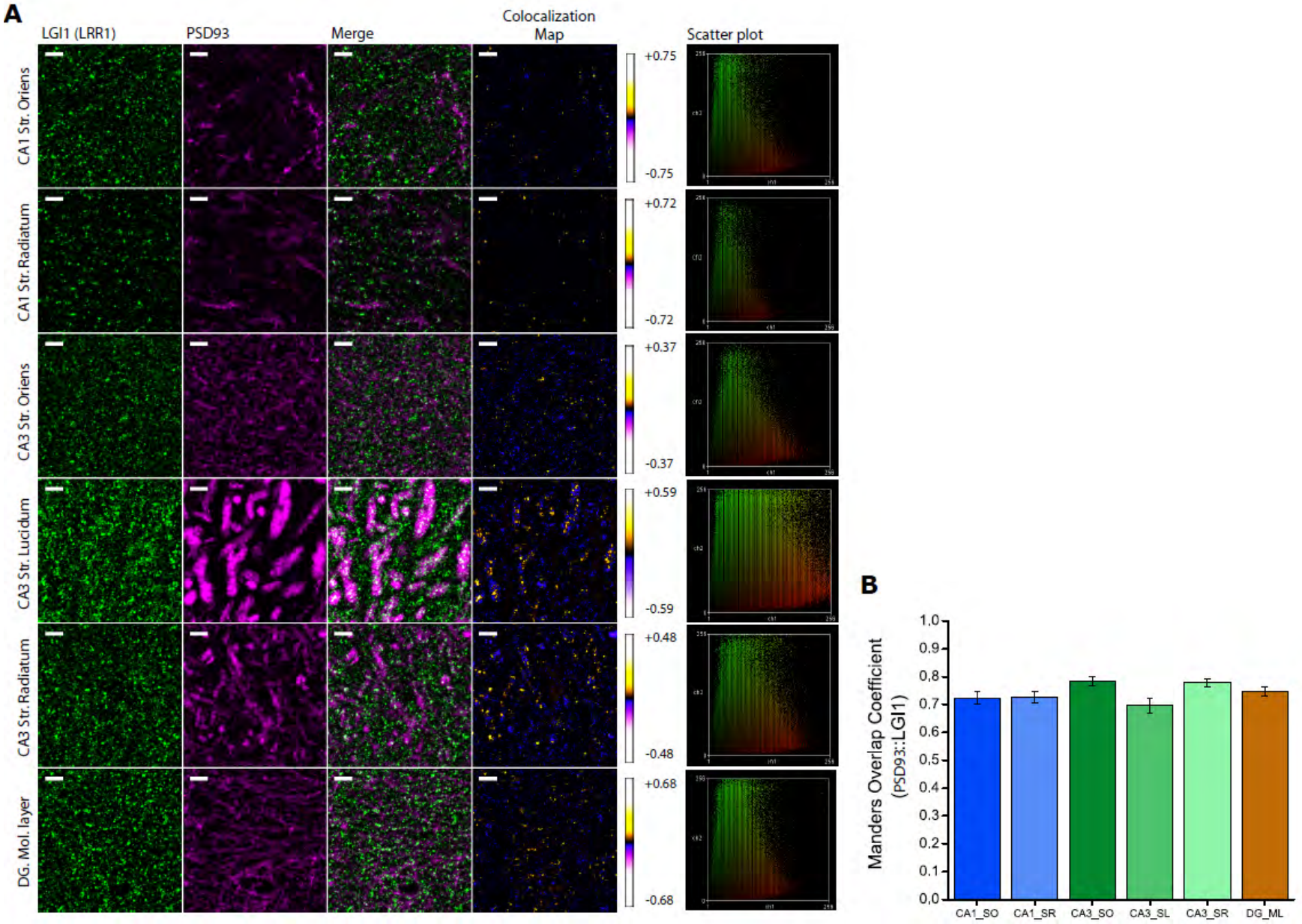

Supplementary Fig. 3 LGI1 partially colocalizes with the postsynaptic marker PSD93 in the hippocampus. (**A**) High-magnification pictures of LGI1 (green, LRR1) and PSD93 (magenta) in the different hippocampal strata. Colocalization maps are shown (right columns) with their respective colocalization index values. Scatter-plots illustrate partial colocalization in all the analysed regions. Scale bar = 5 µm. (**B**) Manders' Overlapping coefficients for LGI1::PSD93 colocalization in the different regions analyzed. Columns and error bars show mean ± SEM. *n* = 2 independent experiments (WT; LRR1 *n* = 1; LRR2 *n* = 1). *n* CA1 Str. Oriens = 8 Fields of view; ROIs; *n* CA1 Str. Radiatum = 8 Fields of view; *n* CA3 Str. Oriens=8 Fields of view; *n* CA3 Str. Lucidum = 8 Fields of view; *n* CA3 Str. Radiatum = 8 Fields of view; *n* DG Molecular Layer = 8 Fields of view

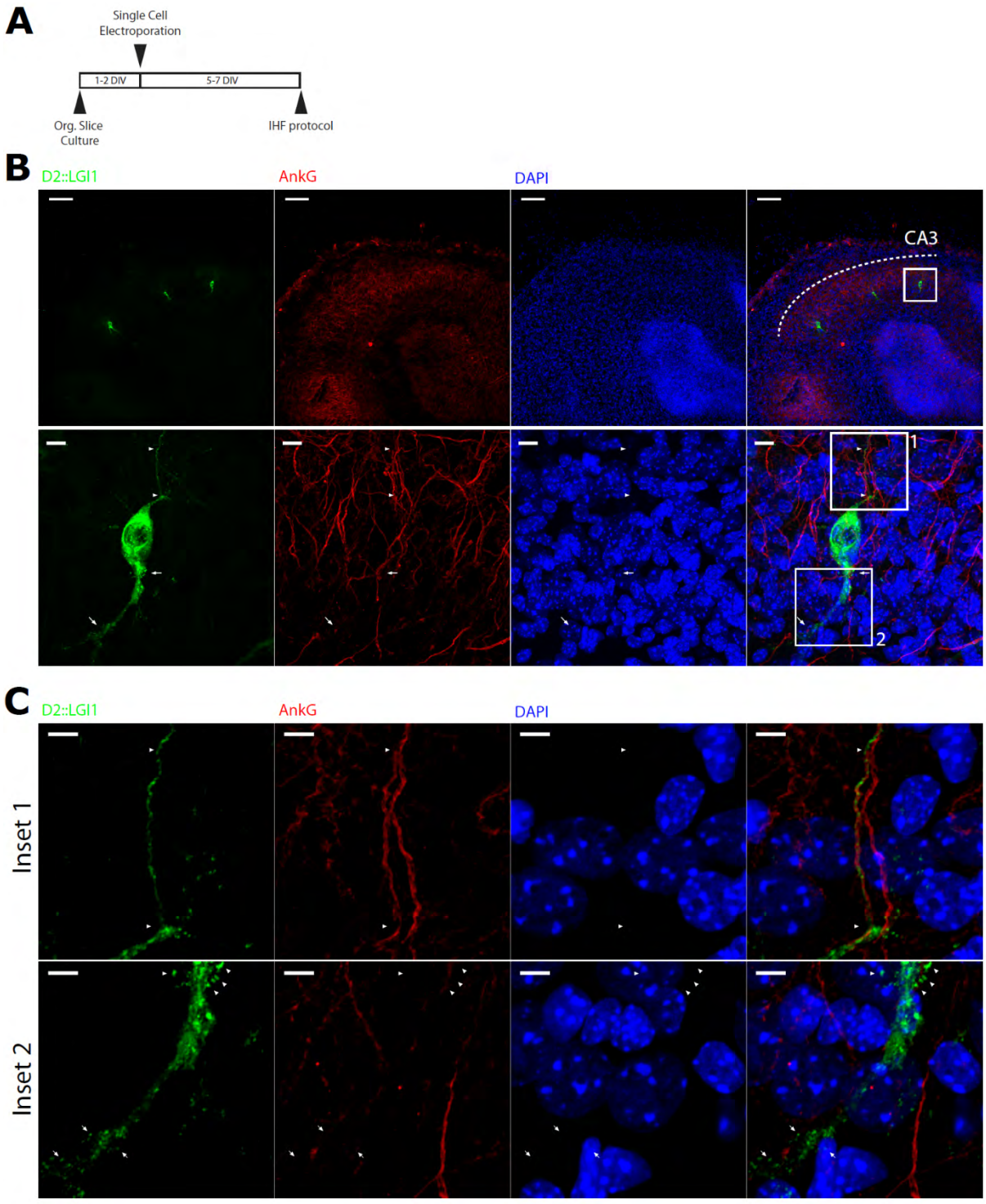

Supplementary Fig. 4 Subcellular distribution of DENDRA2::LGI1 studied by single cell electroporation and immunohistofluorescence in CA3 pyramidal neurons of mouse organotypic slices. (**A**) Schematic of the experimental protocol used for single cell electroporation and immunostaining. (**B**) Low-magnification picture of three individual CA3 pyramidal neurons electroporated with DENDRa2::LGI1 and immunostained with anti-DENDRA2 (green), anti-AnkG (red), and DAPI (blue). Scale bar = 100 µm (top panels). Detail of the inset outlined in the top panels showing DENDRA2::LGI1 expression in the AIS (arrowheads) and in the apical dendrites (arrows). Scale bar = 10 µm (bottom panels). **C** details of the insets 1 and 2 in (**B**). In the top panels, arrowheads point towards the AIS. In the bottom panels, arrowheads point towards thorny excrescences of the proximal apical dendrites. Arrows indicate the distal apical dendrite. Images are representative of 8 CA3 pyramidal neurons from 2 independent cultures. Scale bars = 5 µm

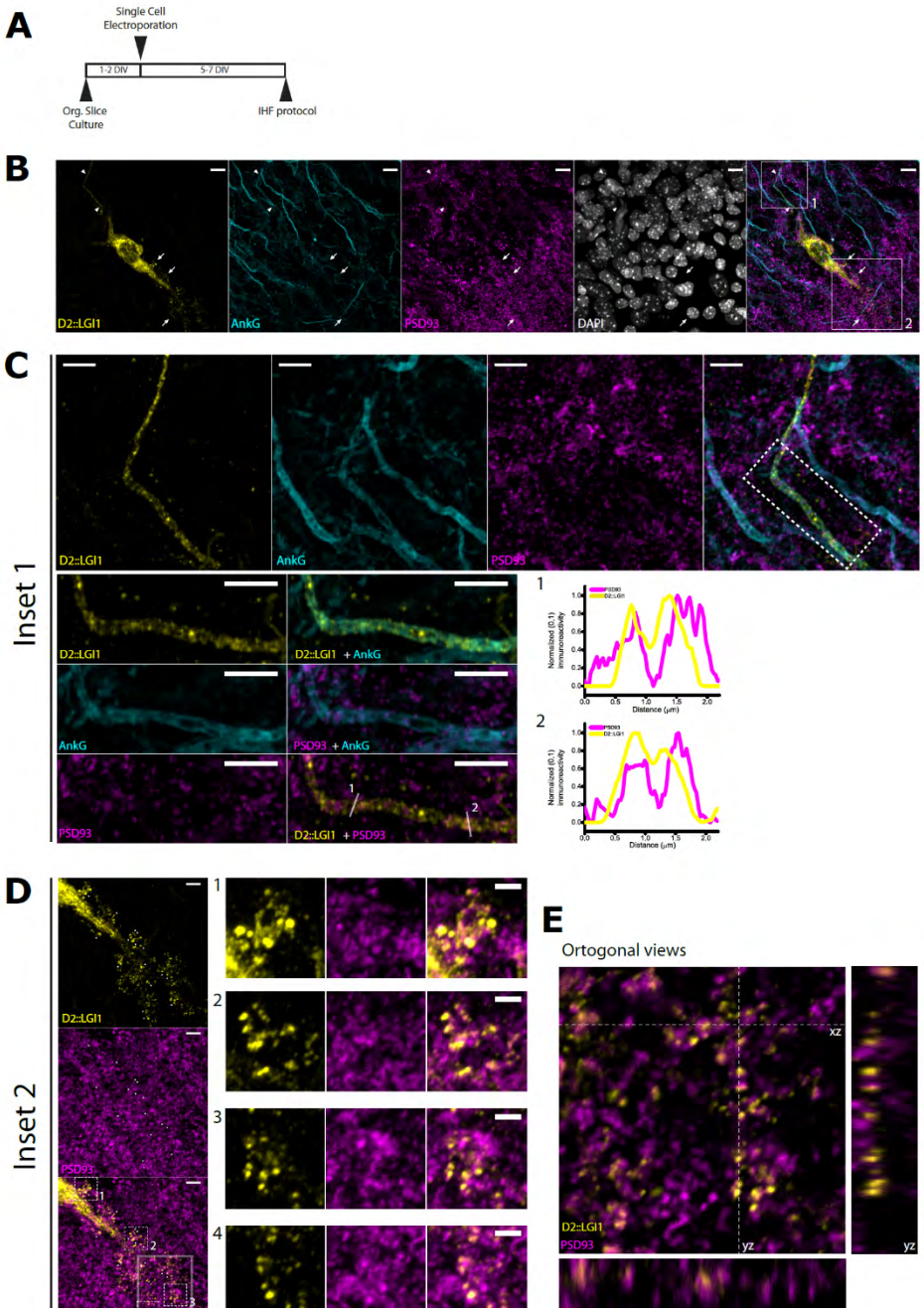

Supplementary Fig. 5 DENDRA2::LGI1 colocalizes with AnkG and PSD93 after single cell electroporation in mouse hippocampal slices. (**A**) Schematic of the experimental protocol used for single cell electroporation and immunostaining. (**B**) Low-magnification picture of one individual CA3 pyramidal neuron electroporated with DENDRA2::LGI1 and immunostained with anti-DENDRA2 (yellow), anti-AnkG (cyan), anti-PSD93 (magenta), and DAPI (gray). Arrowheads indicate the Axonal Initial Segment. Arrows indicate thorny excrescences and the basal dendrite. Scale bar = 10 µm. **C** High magnification detail of the region (inset 1) outlined in (**B**) showing prominent expression of DENDRA2::LGI1 within the axonal initial segment (top panels), and colocalization of DENDRA::LGI1 clusters with PSD93 at the AIS. The boxed region in the top panels is shown in the bottom left panels. The line traces in the bottom right panels (1 and 2) correspond to the lines depicted in the left panel. Scale bar = 5 µm. (**D**) High magnification detail of the region (inset 2) outlined in (**B**) showing expression of DENDRA2::LGI1 at the thorny excrescences and the basal dendrite (left). Scale bar = 5 µm. Insets 1, 2, 3, and 4 (dashed lines) are depicted in the adjacent panels (right). Scale bar = 2 µm. **E** Orthogonal views of the region boxed (solid line) in (**D**) showing co-localization of DENDRA2::LGI1 with PSD93. Scale bar = 2 µm

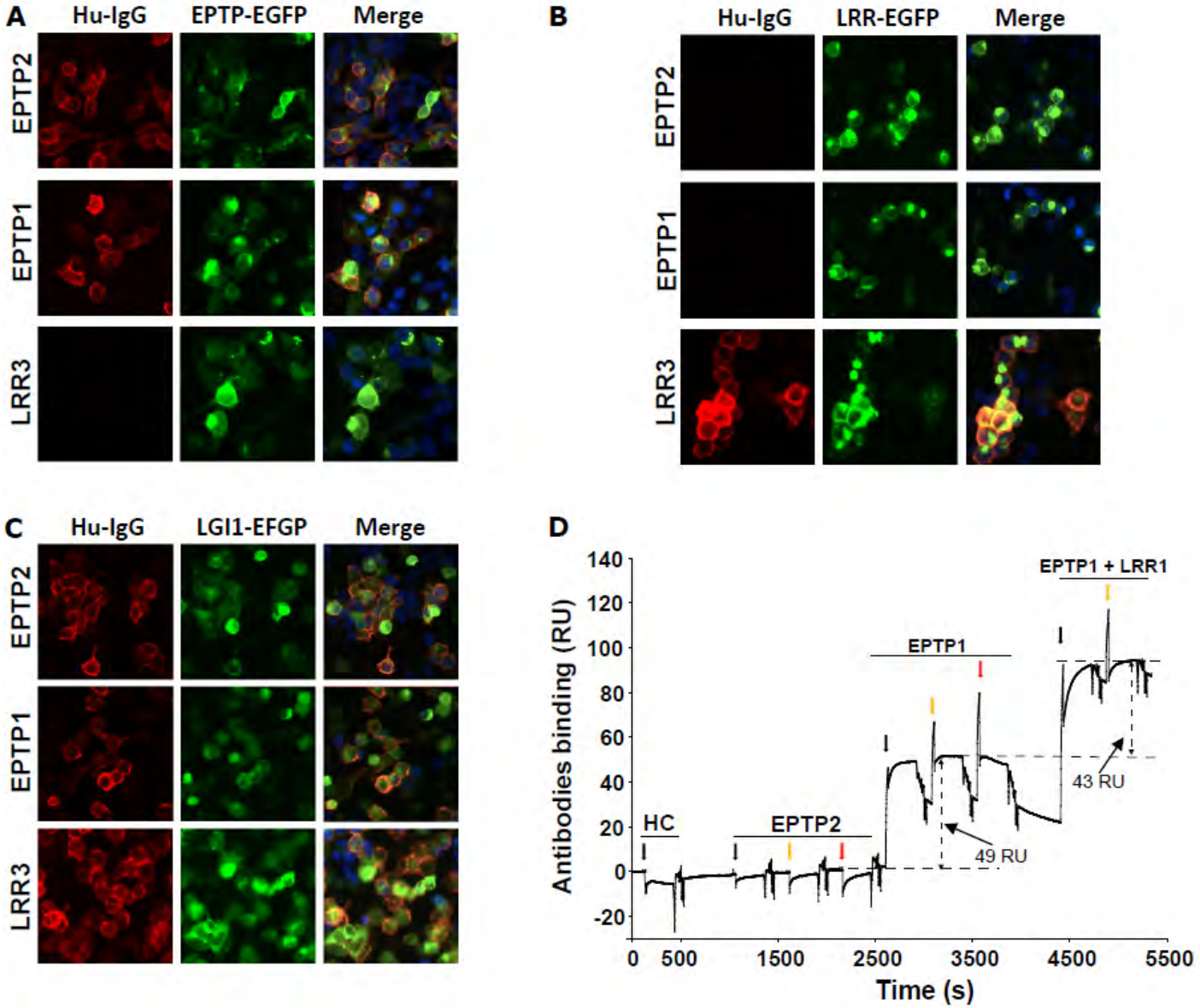

Supplementary Fig. 6 Characterisation of the anti-EPTP antibodies. Membrane tethered LGI1-EPTP (**A**) LGI1-LRR (**B**) or LGI1 (**C**) intracellularly fused to EGFP (EPTP-EGFP, LRR-EGFP, LGI1-EGFP respectively) were transfected into HEK293T cells and EPTP1, EPTP2 or LRR3 were applied to these live cells. Human IgG (Hu-IgG) binding is shown in red and EGFP fluorescence is shown in green. (**D**) 1-2 fmoles of LGI1 were captured on covalently immobilized EPTP2. Human control IgG (HC), EPTP2, EPTP1 and a mixture of EPTP1 and LRR1 were successively injected during 300s at 100 nM (black arrows), 200 nM (orange arrows) and 400 nM (red arrows). Horizontal dashed lines indicate the plateau level for each IgG. EPTP2 did not bind LGI1 indicating the absence of LGI1 multimeric forms. EPTP1 and LRR1 epitopes were similarly accessible leading to an increment of 49 and 43 RU respectively. Results are representative of 3 independent experiments.

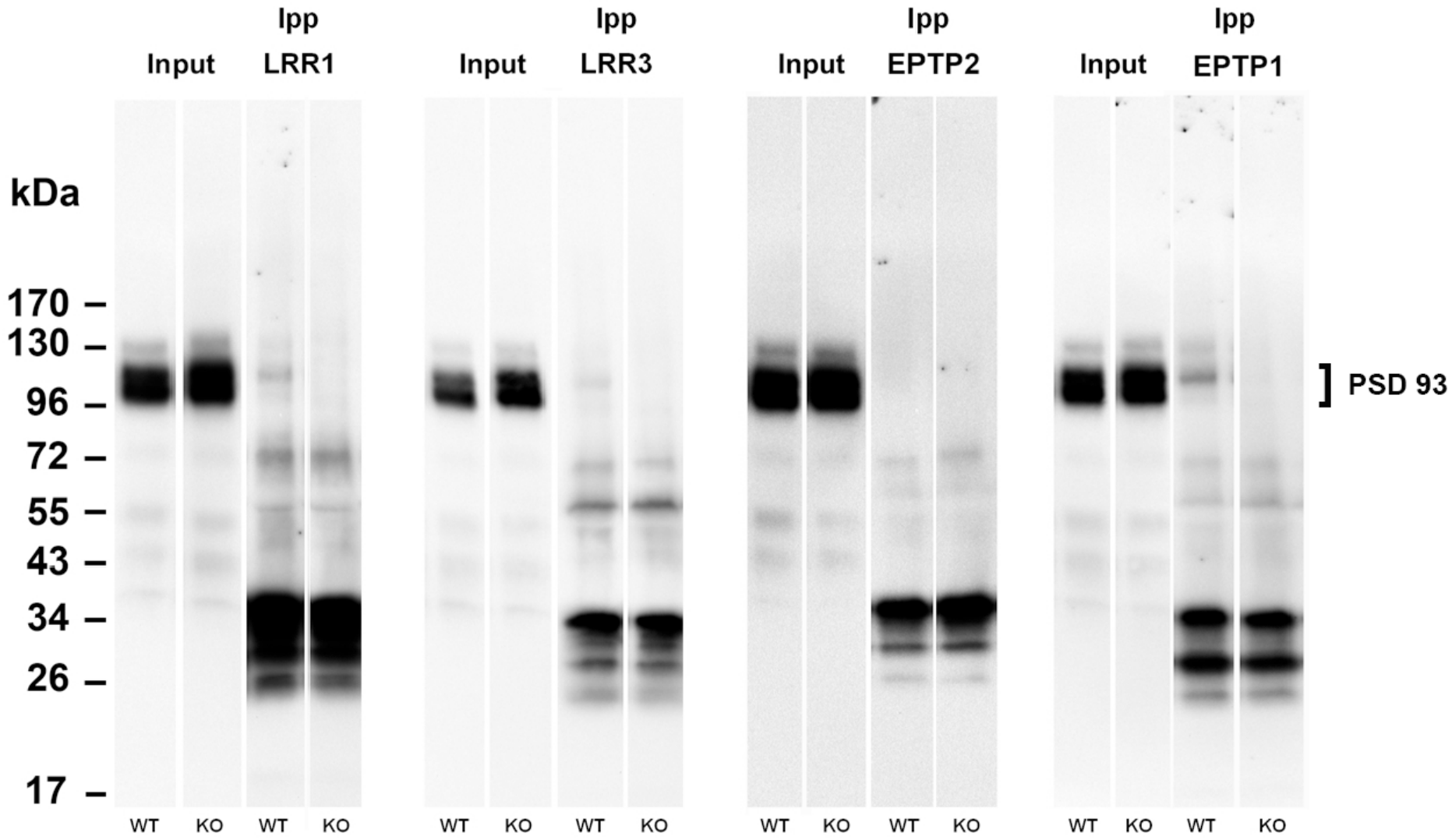

Supplementary Fig. 7 Specificity of PSD93 immunoprecipitation. Immunoprecipitations by LRR1, LRR3, EPTP2 and EPTP1 from wild type and *Lgi1*$^{-/-}$ samples were analysed by western blot using anti PSD93 antibodies. Bands between 26 and 34 kDa denote cross-reactivity of the secondary antibody with light chains of immunoprecipitating antibodies.

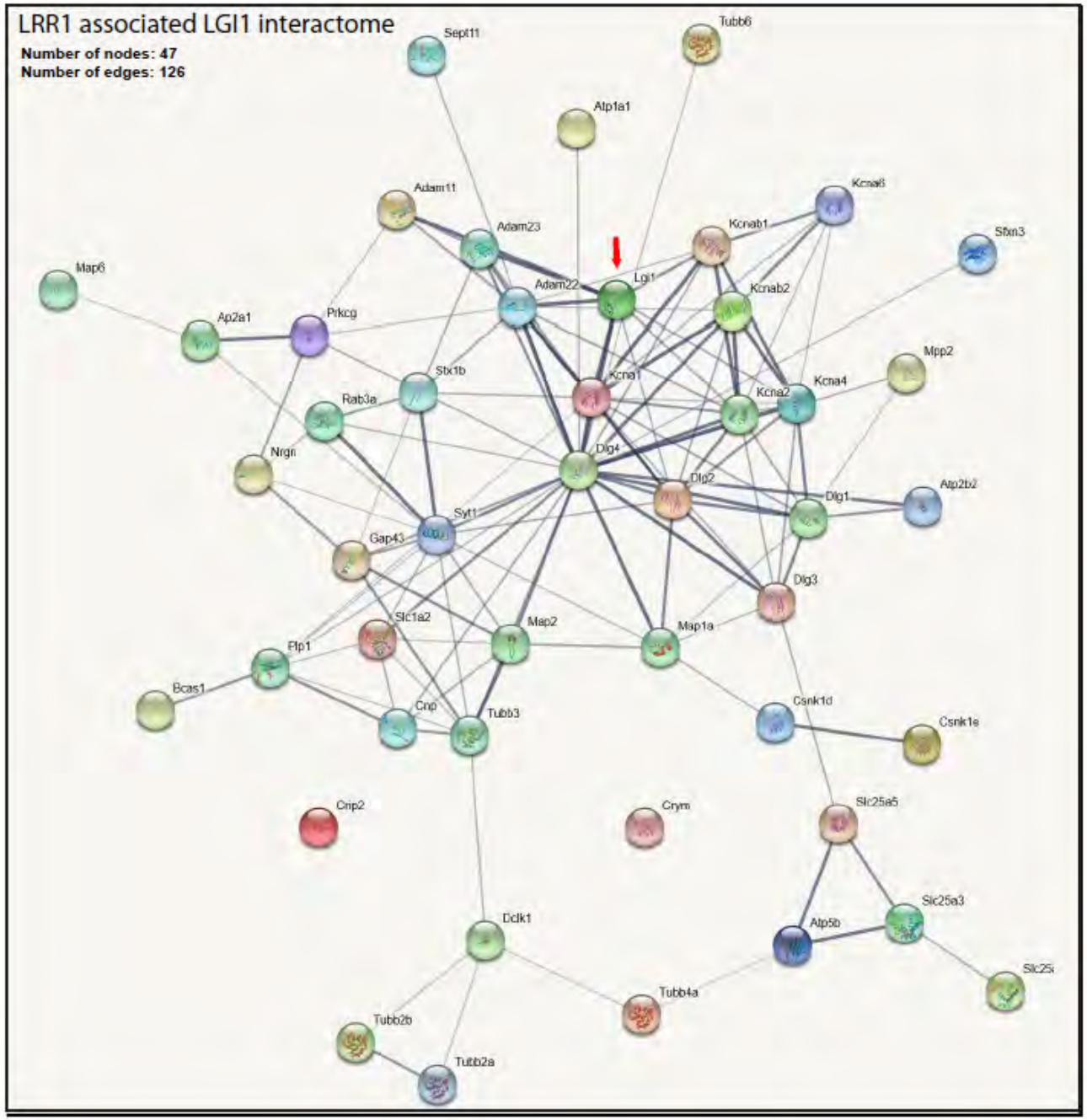

Supplementary Fig. 8 String Map of the LGI1 interactome associated with LRR1. Edge thicknesses indicate the strength of the data support

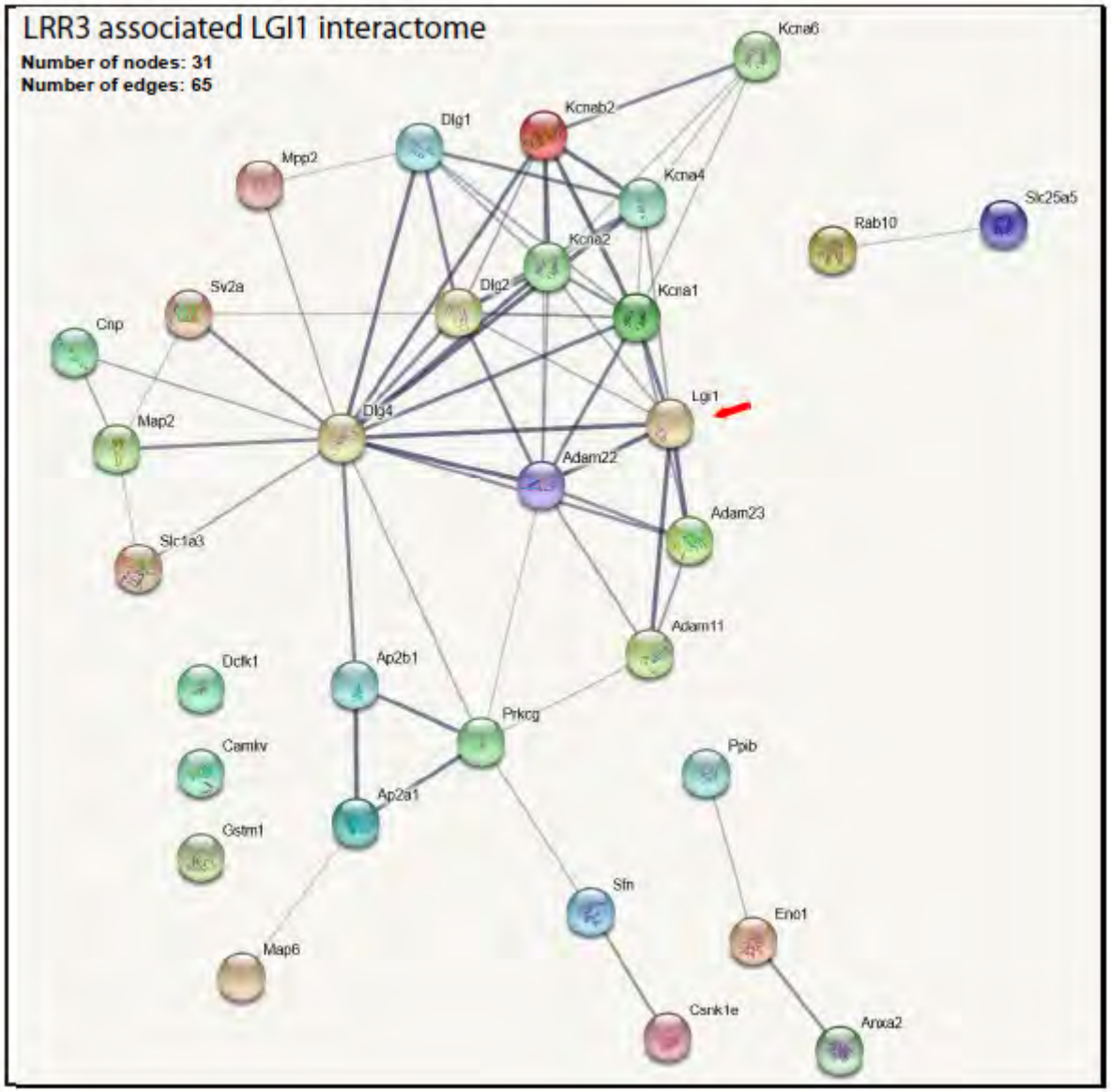

Supplementary Fig. 9 String Map of the LGI1 interactome associated with LRR3. Edge thicknesses indicate the strength of the data support

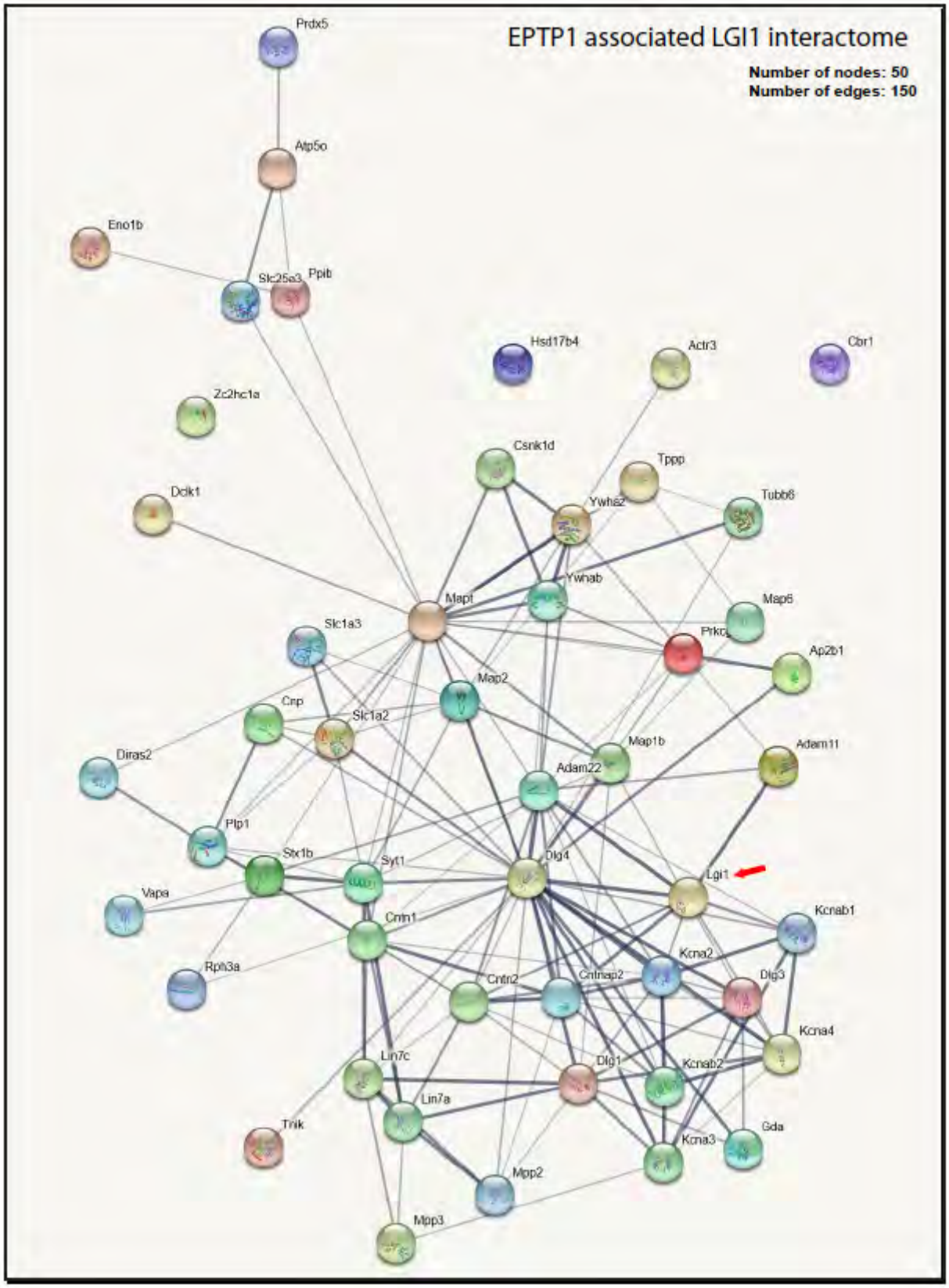

Supplementary Fig. 10 String Map of the LGI1 interactome associated with EPTP1. Edge thicknesses indicate the strength of the data support

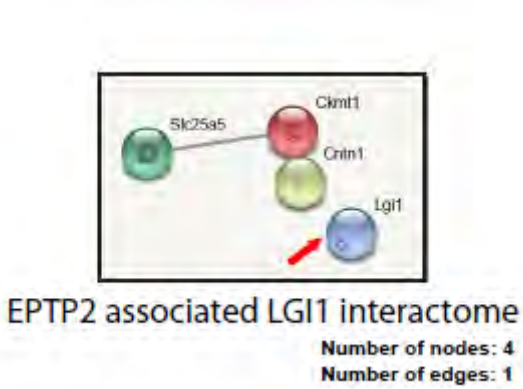

Supplementary Fig. 11 String Map of the LGI1 interactome associated with EPTP2. Edge thicknesses indicate the strength of the data support

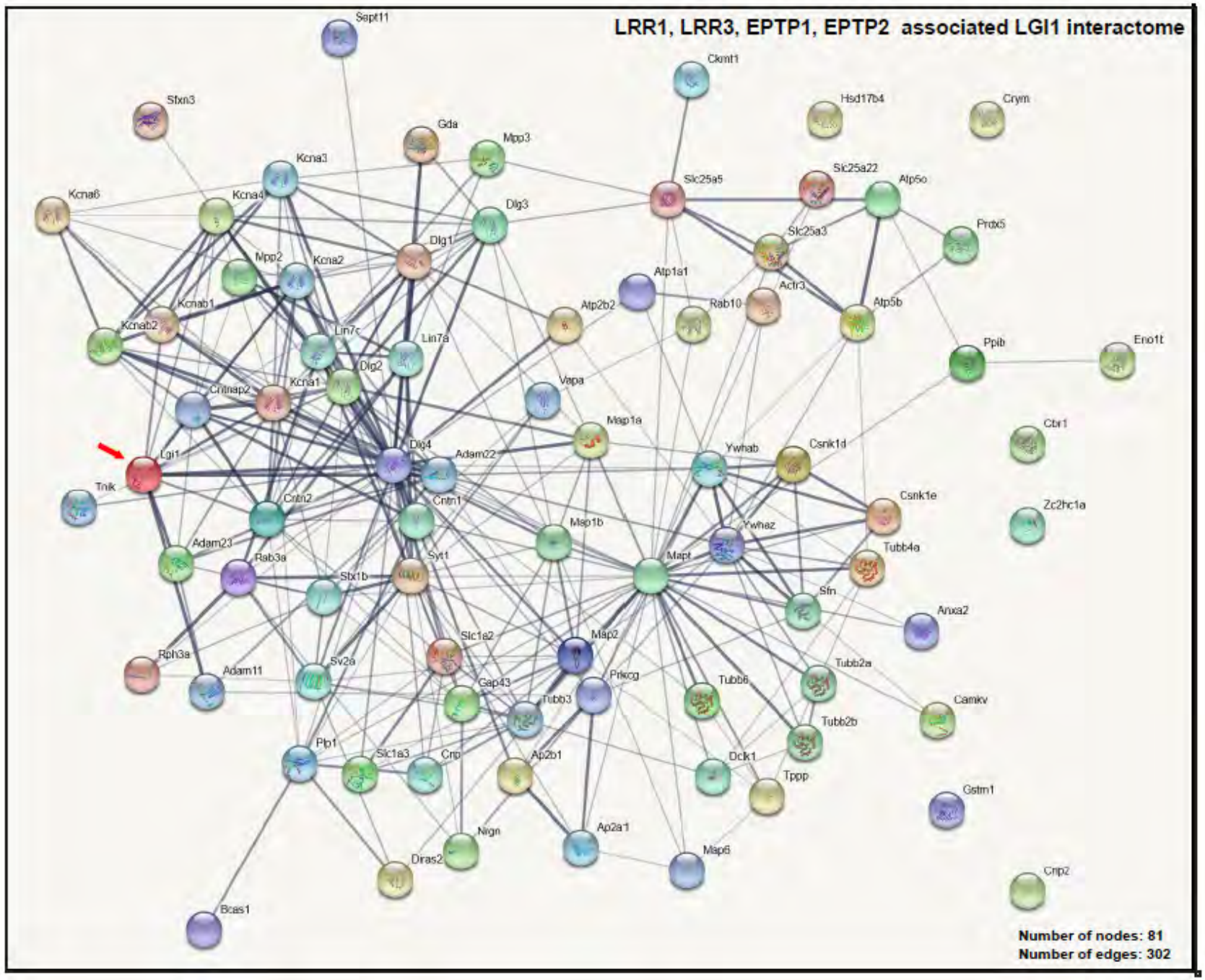

Supplementary Fig. 12 String Map of the LGI1 interactome associated with LRR1, LRR3, EPTP1 & EPTP2. Edge thicknesses indicate the strength of the data support

Spreadsheet. LGI1 partners immunoprecipitated by recombinant monoclonal antibodies derived from patients with LGI1-dependent limbic encephalitis.

Partner proteins immunoprecipitated by each anti-LGI1 are listed in the following 4 figures . Partners were considered as significantly present in experimental points if the emPAI ratio of the partner in the experimental point is superior to 3 compared to, when present, the emPAI in control *Lgi1*$^{-/-}$ controls. Scores and emPAIs from control *Lgi1*$^{-/-}$ control points are already subtracted (filtered) from the reported scores and emPAIs in the associated sheets. Keratin, immunoglobulins, ribosomal proteins and transcription factors were excluded from the analysis

Identifier (LGI1 partners by LRR1 ipp)	Score filtered	emPAI filtered	Score StdDev filtered	emPAI StdDev filtered	Occurrence in the triplicates (N times)	StdError Score filtered	StdError emPAI filtered	Description
TBB2B (#)	1902.167	24.04167	210.8496041	1.67348605	3	121.734076	0.96618762	Tubulin beta-2B chain OS=Mus musculus OX=10090 GN=Tubb2b PE=1 SV=1
TBB2A (*) (#)	1539.167	20.84333	244.232585	1.69234223	3	141.007749	0.97707424	Tubulin beta-2A chain OS=Mus musculus OX=10090 GN=Tubb2a PE=1 SV=1
TBB3 (*) (#)	980	13.065	23	1.7	2	16.263456	1.20208153	Tubulin beta-3 chain OS=Mus musculus OX=10090 GN=Tubb3 PE=1 SV=1
TBB4A (*) (#)	1155.167	9.721667	199.2273966	1.69001644	3	115.023991	0.97573144	Tubulin beta-4A chain OS=Mus musculus OX=10090 GN=Tubb4a PE=1 SV=3
LGI1	2105	5.463333	208.2994639	0.44783429	3	120.261752	0.25855725	Leucine-rich glioma-inactivated protein 1 OS=Mus musculus OX=10090 GN=Lgi1 PE=1 SV=1
TBB6 (#)	1200.667	4.486667	44.78342948	0.33469721	3	25.8557251	0.19323752	Tubulin beta-6 chain OS=Mus musculus OX=10090 GN=Tubb6 PE=1 SV=1
ADA22	1105.333	2.286667	119.2765228	0.29847762	3	68.8643325	0.17232613	Disintegrin and metalloproteinase domain-containing protein 22 OS=Mus musculus OX=10090 GN=Adam22 PE=1 SV=2
DLG4 (*)	819.3333	1.75	102.6980472	0.09899495	3	59.2927452	0.05715476	Disks large homolog 4 OS=Mus musculus OX=10090 GN=Dlg4 PE=1 SV=1
CN37 (*) (#)	360	1.595	88.73556221	0.49443571	3	51.2315007	0.28546259	2',3'-cyclic-nucleotide 3'-phosphodiesterase OS=Mus musculus OX=10090 GN=Cnp PE=1 SV=3
NEUG	47.5	1.18	2.5	0	2	1.76776695	0	Neurogranin OS=Mus musculus OX=10090 GN=Nrgn PE=1 SV=1
KCAB2 (#)	211.8333	1.17	34.7403064	0.21924112	3	20.0573253	0.12657892	Voltage-gated potassium channel subunit beta-2 OS=Mus musculus OX=10090 GN=Kcnab2 PE=1 SV=1
ADA23 (#)	694.6667	1.066667	37.81827894	0.03299832	3	21.8343935	0.01905159	Disintegrin and metalloproteinase domain-containing protein 23 OS=Mus musculus OX=10090 GN=Adam23 PE=1 SV=1
NEUM (*) (#)	141.5	0.975	54.5	0.16	2	38.5373196	0.11313708	Neuromodulin OS=Mus musculus OX=10090 GN=Gap43 PE=1 SV=1
ADT2 (*)	155.6667	0.726667	27.64456949	0.07542472	3	15.9605996	0.04354648	ADP/ATP translocase 2 OS=Mus musculus OX=10090 GN=Slc25a5 PE=1 SV=3
KCNA2 (#)	198	0.615	39	0.045	2	27.5771645	0.03181981	Potassium voltage-gated channel subfamily A member 2 OS=Mus musculus OX=10090 GN=Kcna2 PE=1 SV=1
KCNA1 (#)	160.6667	0.516667	22.60285134	0.03771236	3	13.0497623	0.02177324	Potassium voltage-gated channel subfamily A member 1 OS=Mus musculus OX=10090 GN=Kcna1 PE=1 SV=1
ADA11	469.3333	0.503333	16.21384868	0.02357023	3	9.3610699	0.01360828	Disintegrin and metalloproteinase domain-containing protein 11 OS=Mus musculus OX=10090 GN=Adam11 PE=1 SV=2
RAB3A (#)	75	0.44	4	0	2	2.82842712	0	Ras-related protein Rab-3A OS=Mus musculus OX=10090 GN=Rab3a PE=1 SV=1
KCAB1	134.6667	0.396667	36.16013766	0.0942809	3	20.8770652	0.05443311	Voltage-gated potassium channel subunit beta-1 OS=Mus musculus OX=10090 GN=Kcnab1 PE=1 SV=2
CRIP2	62.5	0.36	4.5	0	2	3.18198052	0	Cysteine-rich protein 2 OS=Mus musculus OX=10090 GN=Crip2 PE=1 SV=1
KC1E	98.66667	0.34	18.97952113	0.08485281	3	10.9578316	0.04898979	Casein kinase I isoform epsilon OS=Mus musculus OX=10090 GN=Csnk1e PE=1 SV=2
KC1D	80.5	0.31	15.5	0	2	10.9601551	0	Casein kinase I isoform delta OS=Mus musculus OX=10090 GN=Csnk1d PE=1 SV=2
AT1A1 (*)	257	0.28	38.99572626	0.04546061	3	22.5141931	0.02624669	Sodium/potassium-transporting ATPase subunit alpha-1 OS=Mus musculus OX=10090 GN=Atp1a1 PE=1 SV=1
DLG1	228.3333	0.28	30.94439457	0.08602325	3	17.8657545	0.04966555	Disks large homolog 1 OS=Mus musculus OX=10090 GN=Dlg1 PE=1 SV=1
ATPB (*)	94.5	0.28	9.5	0.04	2	6.71751442	0.02828427	ATP synthase subunit beta, mitochondrial OS=Mus musculus OX=10090 GN=Atp5f1b PE=1 SV=2
DCLK1	82	0.246667	30.43024811	0.08178563	3	17.5689119	0.04721895	Serine/threonine-protein kinase DCLK1 OS=Mus musculus OX=10090 GN=Dclk1 PE=1 SV=1
MYPR (Plp1) (*) (#)	59.5	0.245	18	0.07	2	12.7279221	0.04949747	Myelin proteolipid protein OS=Mus musculus OX=10090 GN=Plp1 PE=1 SV=2
STX1B (*)	75.83333	0.24	30.22508156	0.05656854	3	17.450459	0.03265986	Syntaxin-1B OS=Mus musculus OX=10090 GN=Stx1b PE=1 SV=1
SFXN3 (#)	42.66667	0.2	6.236095645	2.7756E-17	3	3.6004115	1.6025E-17	Sideroflexin-3 OS=Mus musculus OX=10090 GN=Sfxn3 PE=1 SV=1
GHC1	54.5	0.2	0.5	0	2	0.35355339	0	Mitochondrial glutamate carrier 1 OS=Mus musculus OX=10090 GN=Slc25a22 PE=1 SV=1
BCAS1 (#)	96.5	0.185	56.5	0.085	2	39.9515331	0.06010408	Breast carcinoma-amplified sequence 1 homolog OS=Mus musculus OX=10090 GN=Bcas1 PE=1 SV=3
KCNA6	64.66667	0.18	13.9124245	0.04898979	3	8.03234203	0.02828427	Potassium voltage-gated channel subfamily A member 6 OS=Mus musculus OX=10090 GN=Kcna6 PE=1 SV=1
MAP6 (#)	144	0.17	64.96665812	0.07071068	3	37.5085176	0.04082483	Microtubule-associated protein 6 OS=Mus musculus OX=10090 GN=Map6 PE=1 SV=2
CRYM	33	0.16	6	0	2	4.24264069	0	Ketimine reductase mu-crystallin OS=Mus musculus OX=10090 GN=Crym PE=1 SV=1
SYT1 (*) (#)	73.5	0.158333	24.12467616	0.03771236	3	13.9283883	0.02177324	Synaptotagmin-1 OS=Mus musculus OX=10090 GN=Syt1 PE=1 SV=1
DLG2	113	0.15	69.77583154	0.06531973	3	40.2850951	0.03771236	Disks large homolog 2 OS=Mus musculus OX=10090 GN=Dlg2 PE=1 SV=2
KPCG	37	0.14	8.041558721	0.04082483	3	4.64279609	0.02357023	Protein kinase C gamma type OS=Mus musculus OX=10090 GN=Prkcg PE=1 SV=1
MPCP	21	0.13	7.5	0	2	5.30330086	0	Phosphate carrier protein, mitochondrial OS=Mus musculus OX=10090 GN=Slc25a3 PE=1 SV=1
MPP2	53.66667	0.13	25.03774928	0.02828427	3	14.4555513	0.01632993	MAGUK p55 subfamily member 2 OS=Mus musculus OX=10090 GN=Mpp2 PE=1 SV=1
KCNA4	72	0.106667	13.1402689	0.02357023	3	7.58653778	0.01360828	Potassium voltage-gated channel subfamily A member 4 OS=Mus musculus OX=10090 GN=Kcna4 PE=1 SV=2
SEP11 (#)	45	0.105	16.5	0	2	11.6672619	0	Septin-11 OS=Mus musculus OX=10090 GN=Sept11 PE=1 SV=4
AT2B2	52	0.095	1.5	0.025	2	1.06066017	0.01767767	Plasma membrane calcium-transporting ATPase 2 OS=Mus musculus OX=10090 GN=Atp2b2 PE=1 SV=2
EAA2 (GLT-1)	50.5	0.085	16	0	2	11.3137085	0	Excitatory amino acid transporter 2 OS=Mus musculus OX=10090 GN=Slc1a2 PE=1 SV=1
AP2A1	55.5	0.075	6.5	0.015	2	4.59619408	0.0106066	AP-2 complex subunit alpha-1 OS=Mus musculus OX=10090 GN=Ap2a1 PE=1 SV=1
DLG3	87	0.07	8	0	2	5.65685425	0	Disks large homolog 3 OS=Mus musculus OX=10090 GN=Dlg3 PE=1 SV=1
MTAP2	51.66667	0.043333	18.78533707	0.01885618	3	10.8457194	0.01088662	Microtubule-associated protein 2 OS=Mus musculus OX=10090 GN=Map2 PE=1 SV=2
MAP1A*	43	0.025	16	0.005	2	11.3137085	0.00353553	Microtubule-associated protein 1A OS=Mus musculus OX=10090 GN=Map1a PE=1 SV=2

(*) Present in Lipid rafts proteome and (#) Present in myelin sheaths proteome

Identifier (LGI1 partners by LRR3 ipp)	Score filtered	Score StdDev filtered	emPAI filtered	emPAI StdDev filtered	Occurrence in the triplicates (N times)	StdError Score filtered	StdError emPAI filtered	Description
LGI1	1926.333	246.5932	4.666667	1.615433	3	142.3707	0.93267	Leucine-rich glioma-inactivated protein 1 OS=Mus musculus OX=10090 GN=Lgi1 PE=1 SV=1
ADA22	1004.333	149.7027	1.48	0.229928	3	86.43088	0.132749	Disintegrin and metalloproteinase domain-containing protein 22 OS=Mus musculus OX=10090 GN=Adam22 PE=1 SV=2
DLG4 (*)	651.6667	32.66327	1.353333	0.194308	3	18.85814	0.112184	Disks large homolog 4 OS=Mus musculus OX=10090 GN=Dlg4 PE=1 SV=1
CN37 (*) (#)	277.3333	68.17787	1.266667	0.379151	3	39.36251	0.218903	2',3'-cyclic-nucleotide 3'-phosphodiesterase OS=Mus musculus OX=10090 GN=Cnp PE=1 SV=3
ADT2 (*)	218.1667	22.69116	1.07	0.113137	3	13.10075	0.06532	ADP/ATP translocase 2 OS=Mus musculus OX=10090 GN=Slc25a5 PE=1 SV=3
ADA23 (#)	531.6667	72.92614	0.863333	0.078457	3	42.10393	0.045297	Disintegrin and metalloproteinase domain-containing protein 23 OS=Mus musculus OX=10090 GN=Adam23 PE=1 SV=1
KCAB2 (#)	146.6667	18.78534	0.74	0.173781	3	10.84572	0.100333	Voltage-gated potassium channel subunit beta-2 OS=Mus musculus OX=10090 GN=Kcnab2 PE=1 SV=1
ADA11	403.3333	4.109609	0.523333	0.044969	3	2.372684	0.025963	Disintegrin and metalloproteinase domain-containing protein 11 OS=Mus musculus OX=10090 GN=Adam11 PE=1 SV=2
PPIB	72.5	5.5	0.39	0.09	2	3.889087	0.06364	Peptidyl-prolyl cis-trans isomerase B OS=Mus musculus OX=10090 GN=Ppib PE=1 SV=2
KC1E	89	9.899495	0.31	0.073485	3	5.715476	0.042426	Casein kinase I isoform epsilon OS=Mus musculus OX=10090 GN=Csnk1e PE=1 SV=2
KCNA2 (#)	151.6667	60.17936	0.303333	0.091773	3	34.74457	0.052985	Potassium voltage-gated channel subfamily A member 2 OS=Mus musculus OX=10090 GN=Kcna2 PE=1 SV=1
DLG1	232.3333	53.08065	0.273333	0.094281	3	30.64613	0.054433	Disks large homolog 1 OS=Mus musculus OX=10090 GN=Dlg1 PE=1 SV=1
ENOA	111.5	28.5	0.27	0.04	2	20.15254	0.028284	Alpha-enolase OS=Mus musculus OX=10090 GN=Eno1 PE=1 SV=3
GSTM1 (#)	40.5	2.5	0.27	0	2	1.767767	0	Glutathione S-transferase Mu 1 OS=Mus musculus OX=10090 GN=Gstm1 PE=1 SV=2
1433S (Stratifin; Sfn)(#)	50.5	9.5	0.26	0	2	6.717514	0	14-3-3 protein sigma OS=Mus musculus OX=10090 GN=Sfn PE=1 SV=2
RAB10	35	5	0.245	0	2	3.535534	0	Ras-related protein Rab-10 OS=Mus musculus OX=10090 GN=Rab10 PE=1 SV=1
KCNA1 (#)	65.66667	17.01633	0.236667	0.065997	3	9.824384	0.038103	Potassium voltage-gated channel subfamily A member 1 OS=Mus musculus OX=10090 GN=Kcna1 PE=1 SV=1
DCLK1	122.8333	40.14418	0.206667	0.057927	3	23.17726	0.033444	Serine/threonine-protein kinase DCLK1 OS=Mus musculus OX=10090 GN=Dclk1 PE=1 SV=1
ANXA2 (#)	42.5	17.68238	0.201667	0.04714	3	10.20893	0.027217	Annexin A2 OS=Mus musculus OX=10090 GN=Anxa2 PE=1 SV=2
EAA1 (GLAST-1)	195.5	43.5	0.17	0	2	30.75914	0	Excitatory amino acid transporter 1 OS=Mus musculus OX=10090 GN=Slc1a3 PE=1 SV=2
KCNA6	68.33333	20.36882	0.16	0.056569	3	11.75994	0.03266	Potassium voltage-gated channel subfamily A member 6 OS=Mus musculus OX=10090 GN=Kcna6 PE=1 SV=1
MPP2	84	2	0.14	0.03	2	1.414214	0.021213	MAGUK p55 subfamily member 2 OS=Mus musculus OX=10090 GN=Mpp2 PE=1 SV=1
MAP6 (#)	113.8333	56.40528	0.131667	0.051854	3	32.5656	0.029938	Microtubule-associated protein 6 OS=Mus musculus OX=10090 GN=Map6 PE=1 SV=2
KCNA4	79.33333	26.63748	0.123333	0.04714	3	15.37916	0.027217	Potassium voltage-gated channel subfamily A member 4 OS=Mus musculus OX=10090 GN=Kcna4 PE=1 SV=2
KPCG	50	13.58921	0.116667	0.018856	3	7.845735	0.010887	Protein kinase C gamma type OS=Mus musculus OX=10090 GN=Prkcg PE=1 SV=1
DLG2	69.33333	21.92918	0.11	0.056569	3	12.66082	0.03266	Disks large homolog 2 OS=Mus musculus OX=10090 GN=Dlg2 PE=1 SV=2
MTAP2	123.5	86.16651	0.11	0.064807	3	49.74826	0.037417	Microtubule-associated protein 2 OS=Mus musculus OX=10090 GN=Map2 PE=1 SV=2
AP2B1	85	31	0.095	0.035	2	21.92031	0.024749	AP-2 complex subunit beta OS=Mus musculus OX=10090 GN=Ap2b1 PE=1 SV=1
SV2A	49.33333	8.498366	0.093333	0.018856	3	4.906534	0.010887	Synaptic vesicle glycoprotein 2A OS=Mus musculus OX=10090 GN=Sv2a PE=1 SV=1
CAMKV	30.5	2.5	0.09	0	2	1.767767	0	CaM kinase-like vesicle-associated protein OS=Mus musculus OX=10090 GN=Camkv PE=1 SV=2
AP2A1	43	6	0.06	0	2	4.242641	0	AP-2 complex subunit alpha-1 OS=Mus musculus OX=10090 GN=Ap2a1 PE=1 SV=1

(*) Present in Lipid rafts proteome and (#) Present in myelin sheaths proteome

Identifier (LGI1 partners by EPTP1 ipp)	Score filtered	emPAI filtered	Score StdDev filtered	emPAI StdDev filtered	Occurrence in the triplicates (N times)	StdError Score filtered	StdError emPAI filtered	Description
LGI1	1343.5	3.038333	257.5358	1.666	3	148.6883	0.961865	Leucine-rich glioma-inactivated protein 1 OS=Mus musculus OX=10090 GN=Lgi1 PE=1 SV=1
ADA22	1823	2.356667	544.0515	0.89078	3	314.1083	0.514292	Disintegrin and metalloproteinase domain-containing protein 22 OS=Mus musculus OX=10090 GN=Adam22 PE=1 SV=2
DLG4 (*)	1173	2.356667	392.334	0.989186	3	226.5142	0.571107	Disks large homolog 4 OS=Mus musculus OX=10090 GN=Dlg4 PE=1 SV=1
TBB6 (#)	600.5	2.255	94.5	0.105	2	66.82159	0.074246	Tubulin beta-6 chain OS=Mus musculus OX=10090 GN=Tubb6 PE=1 SV=1
KCAB2 (#)	276.3333	1.366667	62.76588	0.576561	3	36.2379	0.332877	Voltage-gated potassium channel subunit beta-2 OS=Mus musculus OX=10090 GN=Kcnab2 PE=1 SV=1
KCNA2 (#)	406.5	1.205	38.5	0.125	2	27.22361	0.088388	Potassium voltage-gated channel subfamily A member 2 OS=Mus musculus OX=10090 GN=Kcna2 PE=1 SV=1
CN37 (*) (#)	257.3333	1.166667	78.77535	0.505063	3	45.48097	0.291598	2',3'-cyclic-nucleotide 3'-phosphodiesterase OS=Mus musculus OX=10090 GN=Cnp PE=1 SV=3
ADA23 (#)	774.3333	1.136667	194.1157	0.399694	3	112.0727	0.230764	Disintegrin and metalloproteinase domain-containing protein 23 OS=Mus musculus OX=10090 GN=Adam23 PE=1 SV=1
PRDX5	158.5	1.105	5.5	0.185	2	3.889087	0.130815	Peroxiredoxin-5, mitochondrial OS=Mus musculus OX=10090 GN=Prdx5 PE=1 SV=2
LIN7C	145.5	0.94	21.5	0.41	2	15.2028	0.289914	Protein lin-7 homolog C OS=Mus musculus OX=10090 GN=Lin7c PE=1 SV=2
GUAD	260	0.915	13.5	0.135	2	9.545942	0.095459	Guanine deaminase OS=Mus musculus OX=10090 GN=Gda PE=1 SV=1
1433Z (Ywhaz) (#)	82	0.68	17.5	0.105	2	12.37437	0.074246	14-3-3 protein zeta/delta OS=Mus musculus OX=10090 GN=Ywhaz PE=1 SV=1
LIN7A	129	0.63	21.64871	0.159374	3	12.49889	0.092014	Protein lin-7 homolog A OS=Mus musculus OX=10090 GN=Lin7a PE=1 SV=2
KCNA1 (#)	218.6667	0.623333	94.98187	0.22291	3	54.83781	0.128697	Potassium voltage-gated channel subfamily A member 1 OS=Mus musculus OX=10090 GN=Kcna1 PE=1 SV=1
STX1B (*)	76.66667	0.621667	50.17525	0.138884	3	28.96869	0.080185	Syntaxin-1B OS=Mus musculus OX=10090 GN=Stx1b PE=1 SV=1
DLG1	379.3333	0.62	159.1317	0.251529	3	91.87471	0.14522	Disks large homolog 1 OS=Mus musculus OX=10090 GN=Dlg1 PE=1 SV=1
KC1E	217.3333	0.62	72.98554	0.223756	3	42.13822	0.129185	Casein kinase I isoform epsilon OS=Mus musculus OX=10090 GN=Csnk1e PE=1 SV=2
ADA11	496	0.56	221.5687	0.219697	3	127.9227	0.126842	Disintegrin and metalloproteinase domain-containing protein 11 OS=Mus musculus OX=10090 GN=Adam11 PE=1 SV=2
DLG2	350.6667	0.536667	180.3004	0.218225	3	104.0965	0.125992	Disks large homolog 2 OS=Mus musculus OX=10090 GN=Dlg2 PE=1 SV=2
KCNA3 (#)	159.3333	0.533333	86.92653	0.330891	3	50.18706	0.19104	Potassium voltage-gated channel subfamily A member 3 OS=Mus musculus OX=10090 GN=Kcna3 PE=1 SV=3
MYPR (Plp1) (*) (#)	129	0.52	9	0	2	6.363961	0	Myelin proteolipid protein OS=Mus musculus OX=10090 GN=Plp1 PE=1 SV=2
TPPP (#)	111.5	0.5	28.5	0.2	2	20.15254	0.141421	Tubulin polymerization-promoting protein OS=Mus musculus OX=10090 GN=Tppp PE=1 SV=1
KC1D	173.3333	0.406667	76.65652	0.131993	3	44.25766	0.076206	Casein kinase I isoform delta OS=Mus musculus OX=10090 GN=Csnk1d PE=1 SV=2
1433B (Ywhab) (*) (#)	121.6667	0.4	7.408704	5.55E-17	3	4.277417	3.2E-17	14-3-3 protein beta/alpha OS=Mus musculus OX=10090 GN=Ywhab PE=1 SV=3
KCNA6	154.5	0.39	23.5	0.08	2	16.61701	0.056569	Potassium voltage-gated channel subfamily A member 6 OS=Mus musculus OX=10090 GN=Kcna6 PE=1 SV=1
DIRA2	102	0.36	28	0	2	19.79899	0	GTP-binding protein Di-Ras2 OS=Mus musculus OX=10090 GN=Diras2 PE=1 SV=1
DCLK1	174	0.325	47	0.155	2	33.23402	0.109602	Serine/threonine-protein kinase DCLK1 OS=Mus musculus OX=10090 GN=Dclk1 PE=1 SV=1
VAPA	77.5	0.325	8.5	0.075	2	6.010408	0.053033	Vesicle-associated membrane protein-associated protein A OS=Mus musculus OX=10090 GN=Vapa PE=1 SV=2
ATPO	101	0.31	1	0	2	0.707107	0	ATP synthase subunit O, mitochondrial OS=Mus musculus OX=10090 GN=Atp5po PE=1 SV=1
SYT1 (*)	89.33333	0.278333	48.05784	0.122565	3	27.7462	0.070763	Synaptotagmin-1 OS=Mus musculus OX=10090 GN=Syt1 PE=1 SV=1
KCNA4	150.5	0.275	48.5	0.085	2	34.29468	0.060104	Potassium voltage-gated channel subfamily A member 4 OS=Mus musculus OX=10090 GN=Kcna4 PE=1 SV=2
MPP3	131	0.27	38.40139	0.163095	3	22.17105	0.094163	MAGUK p55 subfamily member 3 OS=Mus musculus OX=10090 GN=Mpp3 PE=1 SV=2
KCAB1	81.66667	0.27	35.64953	0.084853	3	20.58226	0.04899	Voltage-gated potassium channel subunit beta-1 OS=Mus musculus OX=10090 GN=Kcnab1 PE=1 SV=2
ZC21A	43.5	0.255	13.5	0.055	2	9.545942	0.038891	Zinc finger C2HC domain-containing protein 1A OS=Mus musculus OX=10090 GN=Zc2hc1a PE=1 SV=1
CBR1	77.5	0.245	7	0	2	4.949747	0	Carbonyl reductase [NADPH] 1 OS=Mus musculus OX=10090 GN=Cbr1 PE=1 SV=3
TAU	103	0.225	39	0.025	2	27.57716	0.017678	Microtubule-associated protein tau OS=Mus musculus OX=10090 GN=Mapt PE=1 SV=3
EAA1	166	0.205	20	0.035	2	14.14214	0.024749	Excitatory amino acid transporter 1 OS=Mus musculus OX=10090 GN=Slc1a3 PE=1 SV=2
MTAP2	342.5	0.198333	172.7503	0.073636	3	99.73743	0.042514	Microtubule-associated protein 2 OS=Mus musculus OX=10090 GN=Map2 PE=1 SV=2
MPCP	37.5	0.19	11.77568	2.78E-17	3	6.798693	1.6E-17	Phosphate carrier protein, mitochondrial OS=Mus musculus OX=10090 GN=Slc25a3 PE=1 SV=1
KPCG	109	0.18	13.92839	0.040825	3	8.041559	0.02357	Protein kinase C gamma type OS=Mus musculus OX=10090 GN=Prkcg PE=1 SV=1
CNTNAP2 (Caspr2)	219	0.17	22	0	2	15.55635	0	Contactin-associated protein-like 2 OS=Mus musculus OX=10090 GN=Cntnap2 PE=1 SV=2
MPP2	95.5	0.17	7.5	0	2	5.303301	0	MAGUK p55 subfamily member 2 OS=Mus musculus OX=10090 GN=Mpp2 PE=1 SV=1
MAP6 (#)	183.8333	0.155	91.54355	0.064807	3	52.8527	0.037417	Microtubule-associated protein 6 OS=Mus musculus OX=10090 GN=Map6 PE=1 SV=2
EAA2 (GLT-1)	68.5	0.145	21	0	2	14.84924	0	Excitatory amino acid transporter 2 OS=Mus musculus OX=10090 GN=Slc1a2 PE=1 SV=1
DHB4	76.5	0.14	45.97826	0.042426	3	26.54556	0.024495	Peroxisomal multifunctional enzyme type 2 OS=Mus musculus OX=10090 GN=Hsd17b4 PE=1 SV=3
CNTN2 (TAG1) (*)	229	0.135	18	0.015	2	12.72792	0.010607	Contactin-2 OS=Mus musculus OX=10090 GN=Cntn2 PE=1 SV=2
DLG3	114	0.11	37.49667	0	3	21.64871	0	Disks large homolog 3 OS=Mus musculus OX=10090 GN=Dlg3 PE=1 SV=1
ARP3	44.5	0.105	8.5	0	2	6.010408	0	Actin-related protein 3 OS=Mus musculus OX=10090 GN=Actr3 PE=1 SV=3
CNTN1 Contactin-1 (*) (#)	59.66667	0.09	9.285592	1.39E-17	3	5.361039	8.01E-18	Contactin-1 OS=Mus musculus OX=10090 GN=Cntn1 PE=1 SV=1
RP3A	49.33333	0.07	10.07748	0	3	5.818234	0	Rabphilin-3A OS=Mus musculus OX=10090 GN=Rph3a PE=1 SV=2
AP2B1	41	0.06	16.51262	0	3	9.533566	0	AP-2 complex subunit beta OS=Mus musculus OX=10090 GN=Ap2b1 PE=1 SV=1
TNIK	94.5	0.04	7.5	0	2	5.303301	0	Traf2 and NCK-interacting protein kinase OS=Mus musculus OX=10090 GN=Tnik PE=1 SV=2
MAP1B (#)	79.5	0.03	32.5	0.01	2	22.98097	0.007071	Microtubule-associated protein 1B OS=Mus musculus OX=10090 GN=Map1b PE=1 SV=2

(*) Present in Lipid rafts proteome and (#) Present in myelin sheaths proteome

Identifier (LGI1 partners by EPTP2 ipp)	Score filtered	emPAI filtered	Score StdDev filtered	emPAI StdDev filtered	Occurrence in the triplicates (N times)	StdError Score filtered	StdError emPAI filtered	description
LGI1	774.6667	1.943333	193.1516	0.287557	3	111.5162	0.166021	Leucine-rich glioma-inactivated protein 1 OS=Mus musculus OX=10090 GN=Lgi1 PE=1 SV=1
ADT2 (*)	98.5	0.47	16.5	0	2	11.66726	0	ADP/ATP translocase 2 OS=Mus musculus OX=10090 GN=Slc25a5 PE=1 SV=3
KCRU	107.6667	0.256667	57.51715	0.037712	3	33.20754	0.021773	Creatine kinase U-type, mitochondrial OS=Mus musculus OX=10090 GN=Ckmt1 PE=1 SV=1
CNTN1 (Contactin-1) (*) (#)	61.5	0.06	33	0.015	2	23.33452	0.010607	Contactin-1 OS=Mus musculus OX=10090 GN=Cntn1 PE=1 SV=1

(*) Present in Lipid rafts proteome and (#) Present in myelin sheaths proteome

Supplementary Table 1. LGI1 partners specific to each IgG

Antibody	Gene Symbol	Description
LRR1	AT1A1 (*)	Sodium/potassium-transporting ATPase subunit alpha-1
	AT2B2	Plasma membrane calcium-transporting ATPase 2
	ATPB (*)	ATP synthase subunit beta, mitochondrial
	BCAS1 (#)	Breast carcinoma-amplified sequence 1 homolog
	CRIP2	Cysteine-rich protein 2
	CRYM	Ketimine reductase mu-crystallin
	GHC1	Mitochondrial glutamate carrier 1
	MAP1A (*)	Microtubule-associated protein 1
	NEUG	Neurogranin
	NEUM (*) (#)	Neuromodulin
	RAB3A (#)	Ras-related protein Rab-3A
	SEP11 (#)	Septin-11
	SFXN3 (#)	Sideroflexin-3
LRR3	1433S (#)	14-3-3 protein sigma
	ANXA2 (#)	Annexin A2
	CAMKV	CaM kinase-like vesicle-associated protein
	ENOA	Alpha-enolase
	GSTM1 (#)	Glutathione S-transferase Mu 1
	PPIB	Peptidyl-prolyl cis-trans isomerase B
	RAB10	Ras-related protein Rab-10
	SV2A	Synaptic vesicle glycoprotein 2A
EPTP1	1433B (*) (#)	14-3-3 protein beta/alpha
	1433Z (#)	14-3-3 protein zeta/delta
	ARP3	Actin-related protein 3
	ATPO	ATP synthase subunit O, mitochondrial
	CBR1	Carbonyl reductase [NADPH] 1
	CNTN2 (*)	Contactin-2
	CNTNAP2	Contactin-associated protein-like 2
	DHB4	Peroxisomal multifunctional enzyme type 2
	DIRA2	GTP-binding protein Di-Ras2
	GUAD	Guanine deaminase
	KCNA3 (#)	Potassium voltage-gated channel subfamily A member 3
	LIN7A	Protein lin-7 homolog A
	LIN7C	Protein lin-7 homolog C
	MAP1B (#)	Microtubule-associated protein 1B
	MPP3	MAGUK p55 subfamily member 3
	PRDX5	Peroxiredoxin-5, mitochondrial
	RP3A	Rabphilin-3A
	TAU	Microtubule-associated protein tau
	TNIK	Traf2 and NCK-interacting protein kinase
	TPPP (#)	Tubulin polymerization-promoting protein
	VAPA	Vesicle-associated membrane protein-associated protein A
	ZC21A	Zinc finger C2HC domain-containing protein 1A
EPTP2	KCRU	Creatine kinase U-type, mitochondrial

(*) Present in lipid rafts proteome (#) Present in myelin sheaths proteome

Supplementary Table 2. LGI1 partners immunoprecipitated with two antibodies

Antibody	Gene Symbol	Description
LRR1 ∩ EPTP1	DLG3 (SAP102)	Disks large homolog 3
	EAA2	Excitatory amino acid transporter 2
	KC1D	Casein kinase I isoform delta
	KCAB1	Voltage-gated potassium channel subunit beta-1
	MPCP	Phosphate carrier protein, mitochondrial
	MYPR (*) (#)	Myelin proteolipid protein
	STX1B (*)	Syntaxin-1B
	SYT1 (*) (#)	Synaptotagmin-1
LRR3 ∩ EPTP1	AP2B1	AP-2 complex subunit beta
	EAA1	Excitatory amino acid transporter 1
LRR1 ∩ LRR3	AP2A1	AP-2 complex subunit alpha-1
EPTP2 ∩ EPTP1	CNTN1 ((*) (#)	Contactin-1

(*) Present in lipid rafts proteome (#) Present in myelin sheaths proteome

Supplementary Table 3.
LGI1 partners immunoprecipitated with three antibodies

Gene Symbol	Description
ADA11	Disintegrin and metalloproteinase domain-containing protein 11
ADA22	Disintegrin and metalloproteinase domain-containing protein 22
ADA23 (#)	Disintegrin and metalloproteinase domain-containing protein 23
CN37 (*) (#)	2',3'-cyclic-nucleotide 3'-phosphodiesterase
DCLK1	Serine/threonine-protein kinase DCLK1
DLG1 (SAP97)	Disks large homolog 1
DLG2 (PSD93)	Disks large homolog 2
DLG4 (PSD95) (*)	Disks large homolog 4
KC1E	Casein kinase I isoform epsilon
KCAB2 (#)	Voltage-gated potassium channel subunit beta-2
KCNA1 (#)	Potassium voltage-gated channel subfamily A member 1
KCNA2 (#)	Potassium voltage-gated channel subfamily A member 2
KCNA4	Potassium voltage-gated channel subfamily A member 4
KCNA6	Potassium voltage-gated channel subfamily A member 6
KPCG	Protein kinase C gamma type
MAP6 (#)	Microtubule-associated protein 6
MPP2	MAGUK p55 subfamily member 2
MTAP2	Microtubule-associated protein 2
ADT2 (*)	ADP/ATP translocase 2

(*) Present in Lipid rafts proteome (#) Present in myelin sheaths proteome